# COMPARING METHODOLOGIES OF MEASURING EVAPORATION FROM URBAN WATERSHEDS

SHISHIR HANDA

A THESIS SUBMITTED TO
THE FACULTY OF GRADUATE STUDIES
IN PARTIAL FULFILLMENT OF THE REQUIREMENTS
FOR THE DEGREE OF
MASTER OF SCIENCE

GRADUATE PROGRAM IN GEOGRAPHY
YORK UNIVERSITY
TORONTO, ONTARIO

November 2013

**Abstract**

For this research, evaporation was measured from two contrasting land cover types within the Humber River watershed over a two year period. Multi-level Bowen ratio energy balance (BREB) systems were used to collect hourly estimates of the surface latent heat flux and surface water budget. Results showed that despite similar rainfall receipt, the naturalized site evaporated 73.0% on average of precipitation back to the atmosphere. In contrast, the impervious site only evaporated 23.5% of precipitation.

The second part of the research explored the theory behind the complementary relationship (CR), based on Bouchet's (1963) hypothesis, between potential and real (or actual) evaporation. The experiment occurred at the naturalized flux site using traditional aerodynamic theory to derive hourly estimates of canopy and aerodynamic resistances in combination with estimates of true potential evaporation from a Class A evaporation pan in order to examine the behavior of the critical resistance.

**Dedication**

I dedicate this research endeavour to my mother, father and brother for always being there for me and giving me the love and care I needed to achieve my desired results.

**Acknowledgements**

I would like to first acknowledge my supervisor, Dr. Richard Bello for taking me on as his graduate student and teaching me about the complexity of water and the climate of the Greater Toronto Area. Similarly, I would like to acknowledge my supervisory committee member, Dr. Tarmo Remmel for the thoughtful guidance and insight he gave me during this time period as well as some financial support through his Natural Science and Engineering Research Council Discovery Grant.

My research endeavour could not have been possible without the support from York University's Faculty of Graduate Studies, York's Geography Department (Department Technician – Patrick Mojdehi) and the Toronto and Region Conservation Authority. This thesis hinged on the connection and collaboration between York University and Toronto and Region Conservation Authority. Also, Cole Engineering (Edward Graham) played a pivotal role in my ability to be accepted to a Mathematics of Information Technology and Complex Systems Accelerate internship, which helped to streamline my learning, professional development and quality of life with an additional source of income. Additionally, if it was not for Dr. Bello, I would not have been awarded the Ontario Graduate Scholarship in Science and Technology upon my graduate school entrance that supplemented my research funding costs.

The people from the Toronto and Region Conservation Authority that were instrumental in my research are Glenn MacMillian, Derek Smith, Greg Dilane, and Gil Amdurski. They helped guide and assist me whenever I needed help from the Toronto and Region Conservation Authority on varying levels.

Lastly, I would like to acknowledge all the students from York University who had a direct impact on my research starting with my field assistant Schiraz Ramjohn. He showed dedication as a volunteer and as a research assistant at YorkU. Other students that I will openly acknowledge are, in no particular order, Daphne So, Kristina Delidjakova and Zoe Davis.

## Table of Contents

## List of Tables

**List of Figures**

## List of Maps

**List of Variables and Constants**

$X_\phi = 1/\phi_M$

$Y_\phi = 1/\phi_V$

$\frac{z-d}{L} = \zeta$

Acceleration due to gravity 9.81 m $s^{-2}$, $g$

Actual storage, $C_{D_s}$

Aerodynamic resistance, $r_a$

Apparent potential evaporation, $Q_{EP*}$

Arid environmental conditions, $Ar$

Atmospheric pressure, $p$

Bouchet's index of aridity, $A$

Bowen ratio determined by Szilagyi and Josza 2008, $\beta_{SJ08}$

Bowen ratio, $\beta$

Canopy resistance, $r_c$

Change in depth, $\Delta z$

Change in sensible heat flux, $\delta Q_H$

Change in storage of the system, $\Delta S$

Change in temperature, $\Delta T$

Change in time, $\Delta t$

Change of saturation vapour pressure, $\delta e^*$

Change of temperature, $\delta T$

Change of the regional latent heat flux, $\delta Q_{ER}$

Class A evaporation pan water surface temperature, $T_{o_{pan}}$

Class A evaporation pan, $pan$

Class A pan evaporation, $ET_{pan}$

Latent heat flux of Class A evaporation pan, $Q_{E_{pan}}$

Condensation, $C$

Critical resistance, $r'$

Density of air, $\rho$

Dew point temperature, $T_d$

Difference between dry and wet bulb temperature at the surface, $\delta T_0$

Difference between dry and wet bulb temperature in the atmosphere, $\delta T_a$

Dimensionless stability parameter for heat during stable atmospheric conditions, $\phi_H = (1 + 5\zeta)$

Dimensionless stability parameter for heat during unstable atmospheric conditions, $\phi_H = (1 - 16\zeta)^{-0.5}$

Dimensionless stability parameter for momentum during stable atmospheric conditions, $\phi_M = (1 + 5\zeta)$

Dimensionless stability parameter for momentum during unstable atmospheric conditions, $\phi_M = (1 - 16\zeta)^{-0.25}$

Dimensionless stability parameter for water vapour during stable atmospheric conditions, $\phi_V = (1 + 5\zeta)$

Dimensionless stability parameter for water vapour during unstable atmospheric conditions, $\phi_V = (1 - 16\zeta)^{-0.5}$

Drainage rate, $D_s$

Drainage, $D$

Dry bulb temperature at the measurement height, $T_z$

Dry bulb temperature at the surface, $T_0$

Dry bulb temperature in the atmosphere, $T_a$

Eddy diffusivity of heat, $K_H$

Eddy diffusivity of water vapour , $K_V$

Emissivity of the surface, $\varepsilon$

Empirical drainage coefficient, $b_{D_s}$

Energy advected into the region by large scale air mass movement, $M$

Equilibrium evaporation, $Q_{EQ}$

Evaporation influenced only by energetic interactions, $Q_{E_{rad}}$

Evaporation, $E$

Evapotranspiration, $ET$

Friction velocity, $u^*$

Geometric mean height, $\hat{z}$

Ground heat flux, $Q_G$

Ground heat flux measured with the Bowen ratio energy balance system, $Q_{G_{BREB}}$

Ground heat flux of the Class A evaporation pan, $Q_{G_{pan}}$

Ground heat flux of the field site measured with Middleton CN3 heat plates, $Q_{G_{field}}$

Heat capacity of water, $c_w$

Heat transfer function of the pan, $f_{h_{pan}}$

Heat transfer variable, $f_h$

Height, $h$

Horizontal wind speed, $u$

Humid environmental conditions, $Hu$

Humidity deficit accounted by advection, $D_{z_A}$

Humidity deficit accounted by local interactions, $D_{z_L}$

Humidity, $q$

Hypothetical wet-bulb depression at the measurement height if the surface was wet, $D_{z_{Q_{EP0}}}$

Incoming longwave radiation, $L^{\downarrow}$

Incoming shortwave radiation, $K^{\downarrow}$

Inverse of the net longwave radiation, $B$

Isothermal resistance, $r_i$

Joules, $J$

Latent heat flux of the Class A evaporation pan, $Q_{E\,pan}$

Latent heat flux of the region, $Q_{ER}$

Latent heat of vaporization, $L_v$, $\lambda$

Maximum latent heat flux, $Q_{ER_{max}}$

Maximum potential evaporation, $Q_{EP_{max}}$

Maximum storage, $S$

Measurement height, $z$

Minimum evaporation influenced only the aerodynamic interactions, $Q_{E_{vent_{min}}}$

Minimum latent heat flux of the region, $Q_{ER_{min}}$

Minimum potential latent heat flux, $Q_{EP_{min}}$

Molecular weight of air, $M_A$

Molecular weight of water, $M_w$

Monin-Obukhov length, $L$

Net available energy, $Q_n$

Net longwave radiation, $L^*$

Net radiation, $Q^*$

Net radiation measured with Middleton CN1-1471, $Q^*_{CN1\ 1471}$

Net radiation measured with the Bowen ratio energy balance system, $Q^*_{BREB}$

Net radiation of the Class A evaporation pan, $Q^*_{pan}$

Net shortwave radiation, $K^*$

Oasis effect, $O_{Fx}$

Outgoing longwave radiation, $L^{\uparrow}$

Outgoing shortwave radiation, $K^{\uparrow}$

Pan coefficient, $\varrho$

Potential evaporation equilibrium temperature, $T_{eq}$

Potential Evapotranspiration, $Q_{EP}$

Potential temperature, $\theta$

Precipitation, $P$

Priestley-Taylor alpha value, $\alpha_{PT72}$

Psychrometric constant, $\gamma$

Radiant heat transfer coefficient, $f_{rh}$

Radius, $r$

Ratio of radiant heat transfer area to the evaporation surface area given by Morton 1965, $m_{M65}$

Ratio of sensible heat flux area to the evaporation surface area given by Morton 1965, $n_{M65}$

Ratio of the net shortwave radiation area to the evaporation surface area, $k$

Reflected fraction of incoming longwave radiation, $\alpha'$

Region of study, $R$

Relative humidity, $RH$

Richardson number, $Ri$

Runoff, $RO$

Saturation vapour pressure, $e^*$

Saturation vapour pressure at the equilibrium temperature, $e^*_{T_{eq}}$

Saturation vapour pressure at the surface, $e^*_{T_0}$

Saturation vapour pressure in the atmosphere, $e^*_{T_a}$

Saturation vapour pressure of the Class A evaporation pan surface, $e^*_{T_{o_{pan}}}$

Sensible heat flux of the Class A evaporation pan, $Q_{H_{pan}}$

Sensible heat flux of the region, $Q_H$

Slope of the saturation vapour pressure temperature curve, $\Delta$

Slope of the saturation vapour pressure temperature curve determined by Morton 1969, $\Delta_{M69}$

Specific of air at constant pressure, $c_p$

Stability parameter for momentum, $\Psi_m$

Stability parameter for water vapour, $\Psi_v$

Stefan-Boltzman constant of $5.67 \times 10^{-8}$ W m$^{-2}$ K$^{-4}$, $\sigma$

Sub-equilibrium evaporation, $Q_{EQ_{sub}}$

Supra-equilibrium evaporation, $Q_{EQ_{sup}}$

Surface Albedo, $\alpha$

Surface roughness, $z_0$

Temperature at the surface, $T_0$

Temperature of the atmosphere, $T_a$

Temperature, $T$

Vapour pressure at the dew point temperature, $e_{T_d}$

Vapour pressure deficit, $VPD$

Vapour transfer function of the pan, $f_{v_{pan}}$

Vapour transfer function of the region, $f_{v_R}$

Variable determined by Morton 1971 to assist better understanding the complementary relationship, $M_{71}$

Variable given by Morton 1968 to account for heat transfer through the bottom and wall of the Class A evaporation pan, $n_{M68}$

Variable replacement by Morton 1971 for the psychrometric constant, $\lambda_{71}$

Variable to account for changes in the radiant heat transfer coefficient to space with surface temperature, $b$

Vertical potential temperature gradient, $\Delta\theta$

Vertical vapour pressure gradient, $\Delta e$

View factor, $VF$

Virtual potential temperature, $\theta_v$

Volumetric soil moisture, $\theta_V$

von Kármán constant of 0.41, $\kappa$

Water flux of the Class A evaporation pan, $Q_W$

Wet bulb temperature at the measurement height, $T_z{}'$

Wet bulb temperature at the surface, $T_0{}'$

Wet bulb temperature in the atmosphere, $T_a{}'$

Wet equilibrium evaporation, $Q_{EP0}$

Wet-bulb depression at measurement height above the surface, $D_z$

Wet-bulb depression at the height of the critical resistance, $D_Z{}'$

Wet-bulb depression at the surface, $D_0$

Wind direction, $\rightleftharpoons$

Wind function, $f(u)$

Zero plane displacement height, $d$

## Chapter 1 Introduction

The hydrological cycle (HC) is a very complex system (Hendriks 2010: p. 3). The distribution and cycling of water through different environments on the Earth promotes or hinders the progression of biological life (Hendriks 2010: p. 3). Water is one of the most important abiotic components of life to facilitate biological activity, allowing for the development of trophic structures (Ye et al. 2011). The quantity and diversity of trophic structures helps to determine the vitality and health of ecosystems. This study will focus on evapotranspiration ($ET$) within the HC and methods of observation.

The overall goal of this thesis is to better understand the complexity of $ET$ for a watershed within the urban setting of Toronto, Canada. The first objective is accomplished by using different $ET$ monitoring systems over two years for contrasting surface types representing extremes in infiltration. From this data set, seasonal patterns in the surface energy and water balances will be developed. This will contribute to a better understanding of the factors controlling surface runoff, erosion and base flow within the Humber R. Watershed.

The second objective is the performance of evaporation pans will be evaluated for producing estimates of $ET$. An extension of existing theory on complementary evaporation will be tested to explore the potential for determining real evaporation from historical pan data. This would contribute to an understanding of how climate change may have been influencing the surface energy budgets.

$ET$ is a very important component of the HC because it transfers large quantities of mass and energy to the atmosphere. In fact, next to precipitation itself, it is the largest component of the HC (Bonan 2008: p. 192). This study will examine complementary relationship (CR) theory, first proposed by Bouchet (1963), to determine the physical interactions, relationships and control mechanisms between potential evaporation, as measured by the US National Weather Service (NWS) Class A evaporation pans (CAEP) ($Q_{E_{pan}}$) and the real or actual latent heat flux of a region ($Q_{ER}$). An understanding of the HC will be sought through use of the CR, with respect to the relationship between

potential $ET$ ($Q_{EP}$) and $Q_{ER}$. There is a possibility that the terms $Q_{EP}$ and $Q_{E_{pan}}$ may be identical, which will be discussed to greater extent in this thesis.

When $ET$ is present, water vapour ascends higher into the atmosphere and the exchange of energy and mass influence the movement of water vapour (Bonan 2008: p. 192). Wind generated through global circulation patterns move water vapour across different geographic areas than where the moisture originated (Bonan, 2008 p. 57). Better understanding the absolute quantity of $Q_{ER}$ from varying land surfaces and ecological regions can allow for greater understanding of weather systems and how different ecosystems influence hydrological interactions. As important as measurements of water loss from Earth's surface in the form of evapotranspiration might be, observations of accurate $Q_{ER}$ are difficult to obtain at hourly and daily time scales due to advanced technical requirements and sophisticated data analysis (Wessel and Rouse 1994). In urban environments, better understanding variations in $ET$ increases in importance because of the greater complexity the different urban surfaces pose in determining accurate quantities of water and energy from climatological and hydrological perspectives (Grimmond and Oke 1999).

In Canada, knowledge regarding the quantity of water available to the Canadian society, economy and ecosystems as well as the distribution of water across the landscape is gaining more importance as awareness to climate change increases (Peck et al. 2013a and 2013b). General attempts at quantifying all components of the water balance (WB) and achieving full account of the WB is attractive to policy makers, industry and scientists (Niedzialek and Ogden 2012) because a complete accounting of the WB provides greater insight of how land-use and climate change affect water resources over spatial and temporal scales. In theory, accounting for all processes of the WB should make assessment and decision making easier, which may give guidance to city planners and industry for long-term operational objectives and policies.

## 1.1 The Complementary Relationship and its Historical Development

### *1.1.1 Precursor to the Complementary Relationship and Evapotranspiration*

Continentally, $Q_{ER}$ consumes approximately 62% of precipitation ($P$) on an annual basis thereby making it the single largest water flow pathway of the HC (Budyko 1974; Lvovitch 1970; Lvovitch 1973; Baumgartner and Reichel 1975; Korzun et al. 1978). The other 38% of $P$ is directed into surface water processes such as stream flow, lake and groundwater recharge, affecting how societies, economies and ecosystems are shaped. From the perspective of global warming, a 5% increase of global temperature would negatively affect surface water availability from 38% to 34.9% of $P$ regimes, thereby changing socio-biological activities that are dependent upon the availability of surface water resources (Fairbridge 1990). This change of the HC would increase $Q_{ER}$ to 65.1% of $P$ consumption from the originally averaged value of 62%. However, these proportions are highly variable temporally and contain a great deal of uncertainty since long-term evaporation datasets are scarce in many regions of the world. Despite this they are highly desirable by many professionals who use water data in research and for practical applications.

There are other challenges associated with modelling accurate terrestrial $Q_{ER}$ values. Many meteorological stations worldwide do not measure gradients of temperature ($T$), humidity ($q$), wind speed ($u$), which are required to parameterize the flow of water upwards though the atmosphere. The lack of infrastructure at meteorological stations compounds the issue of accurate $Q_{ER}$ monitoring and dataset archiving (Whitfield 2012; Peck et al. 2013a), limiting the knowledge base related to understanding the complexity of $Q_{ER}$ interactions and gaining full closure of the WB.

Climate change has negatively impacted the availability of water resources from regions such as North America and changed atmospheric circulation patterns in Europe (Fung et al. 2011; Philipona 2013). The effects of warmer temperatures on water resources is not fully understood with respect to weather patterns but future projections indicate that drought and flood stricken areas will endure prolonged periods of catastrophic environmental disasters, which will be harder to predict due to the uncertainty of temperature change (Fung et al. 2011; Philipona 2013). Better

understanding how the HC is changing at multiple spatial and temporal scales will better assist to determine what course of action should be taken to avoid future human and ecosystem casualties and hardships.

There is the possibility that meteorological stations that are presently or have been outfitted with Class A evaporation pan (CAEP) systems could prove useful for estimating $ET$. CAEP are simple water monitoring tanks used during the ice-free period. Decreases in water level of the CAEP can be attributed to $ET$ in the absence of recorded rainfall. The simplicity of the CAEP is attractive and it has been in use at weather stations around the world for decades.

The evaporation from an open tank or pan, $Q_{E_{pan}}$ is termed potential evaporation as it expresses the maximum amount of water loss from a wet surface under prevailing energy and atmospheric conditions with an unlimited water supply. Pan evaporation would probably best mimic evaporation of a small, shallow pond. There have been published correction factors (Iruthayaraj and Morachan 1978) to account for local environmental conditions and configurations so that $Q_{E_{pan}}$ data may be used to resemble values of $Q_{ER}$ or real evaporation from the surrounding landscape. The use of pan correction coefficients seem reasonable because they depend on energy and wind influences controlling $Q_{E_{pan}}$, which must be accounted for in order to develop the corrections. Pan evaporation however, suffers from a more fundamental phenomenon known as the complementary evaporation. Bouchet (1963) described the CR as the decrease in real evaporation during periods of volumetric soil moisture ($\theta_V$) decreases, being accompanied by increases in $Q_{E_{pan}}$ evaporation in response to increasingly drier air. A decrease in local evaporation thereby facilitates an inverse or complementary relationship from freely evaporating surfaces during periods of moisture stress within the surrounding landscape.

### *1.1.2 R. J. Bouchet's Complementary Relationship*

The CR was developed based on the understanding of the system from an energy balance perspective. By avoiding accounting for thermal inertia of the environment

during long term cycling, the assessment would focus on a 24 hour period, thereby eliminating $T$ variations over lengthy time frames. Bouchet (1963) allowed that if the environmental system the CAEP was placed within does not experience the same climatic characteristics then lateral exchanges of energy to the walls of the CAEP will be present and must be analysed. The heat exchanges of the CAEP with the atmosphere are much different and can be attributed to air mass movement and may create an oasis effect. The movement of energy created by the oasis effect would create the limits of interaction of natural conditions when related to a CAEP with heterogeneous covers such as soil type, vegetation cover and $Q_{ER}$. Bouchet (1963) said the size of the system of interaction with the CAEP must account for all element of the study site and displayed this in a diagram. His study was completely published in French and translations have been made, including a reproduced graph as Figure 1.1.

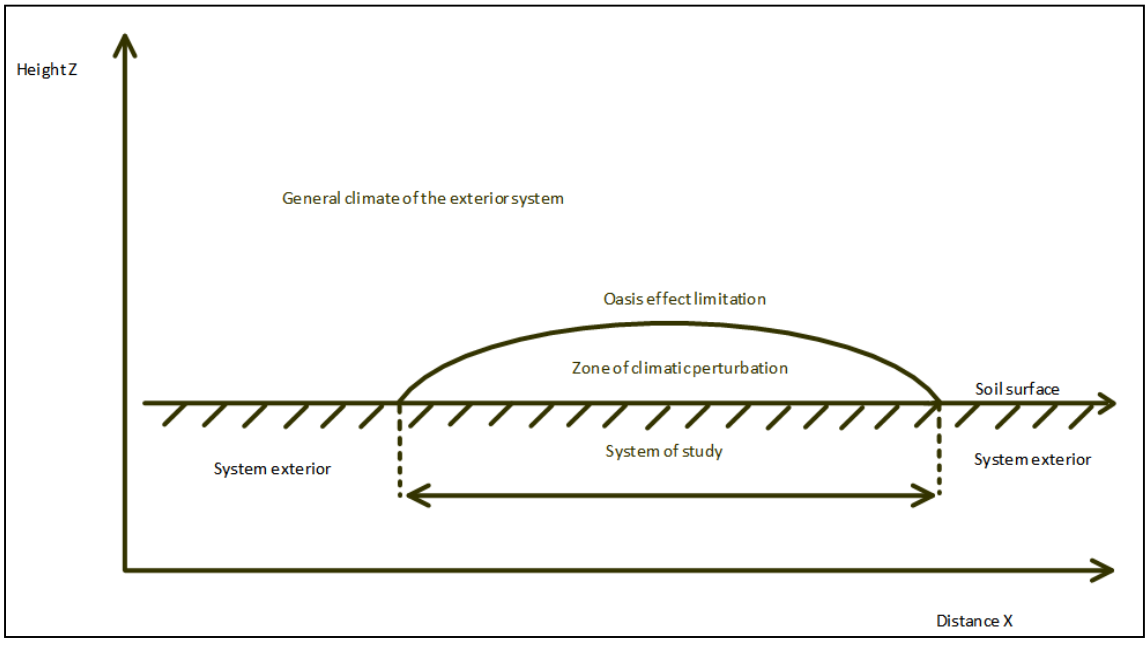


Figure 1.1. Diagram of ecological system of interaction for development of the complementary relationship. This is a replicate diagram of the original found in Bouchet (1963) with translated terms.

Bouchet (1963) argued the oasis effect will respond to disturbances of the system being studied, including the entire area with its boundaries that are being perturbed. Due

to this complexity of scale, the representation of the system is presented across a plane so the boundary layer thickness is small compared to the horizontal dimension. This understanding allowed for the observation of the system to be analyzed at specified scales, which were identified in a categorical chart given by Table 1.1. Therefore, a clearly defined geographic surface area should have an equally corresponding oasis effect, which indicates the lateral exchange of energy.

Table 1.1. Tabular organization of the complementary relationship oasis effects with their associated temporal, spatial and energetic scales. This chart has been translated from Bouchet (1963).

| **Energy Scale** | **Time scale** | **Distance scale** | **Corresponding oasis effect** |
|---|---|---|---|
| Molecular (1) | $10^{-9}$ second | | OF1 |
| Turbulent (2) | from 1 sec to minutes | several 100 meters | OF2 |
| Convection and associated movements (3) | from 10 minutes to hours | several km | OF3 |
| Cyclonic (4) | 3 to 4 days | 1000 to 2000 km | OF4 |
| Planetary (5) | 10 to 30 days | 5000 to 10 000 km | OF5 |

Bouchet (1963) believed net available energy or difference between net radiation and ground heat ($Q_n$) consumed by $Q_{ER}$ should be considered uniform throughout the system of interest to allow determination of how $Q_{E_{pan}}$ is affected by the influencing climate. Understanding the connection between $Q_{ER}$ and climatic interactions would garner the linkage between the cause and effect of $Q_{E_{pan}}$ with respect to $Q_{ER}$.

The beginning for determining which components of the surface energy budget (SEB) contributes to $Q_{ER}$, after Bouchet (1963), can be expressed as,

$$(1-\alpha)K^{\downarrow} + (1-\alpha')L^{\downarrow} - L^{\uparrow} + O_{Fx} = E - C = Q_{ER} \quad (1.1)$$

where $\alpha$ is the surface albedo, $K^{\downarrow}$ is the incoming shortwave radiation, $\alpha'$ is the reflected fraction of the incoming longwave radiation from the atmosphere, $L$ is the longwave

radiation with the arrows denoting incoming (↓) or outgoing (↑), $O_{Fx}$ is the oasis effect, $E$ is the energy involved in evaporation, $C$ is the energy released by condensation all in W $m^{-2}$.

$L^{\uparrow}$ can be defined as a function of surface temperature, $T_0$ expressed through the Stefan-Boltzmann law as,

$$L^{\uparrow} = \varepsilon\sigma {T_0}^4 \quad 1.2$$

where $\varepsilon$ is the emissivity of the surface, $T_0$ here is in K, and $\sigma$ is the Stefan-Boltzmann constant of $5.67 \times 10^{-8}$ W $m^{-2}$ $K^{-4}$. Like $L^{\uparrow}$, the entire term $(1 - \alpha')L^{\downarrow}$ can be expressed as Equation 1.2 but $T$ must be of the atmosphere ($T_a$) and converted to K. Research has been published that $\varepsilon$ of the atmosphere is variable and should be accounted to accurately calculate $L^{\downarrow}$ to the surface (Alados, Foyo-Moreno and Alados-Arboledas 2012). However, the methodology presented by Alados, Foyo-Moreno and Alados-Arboledas (2012) is site specific and beyond the scope of this study.

To determine the surface net radiation ($Q^*$) from Equation 1.1, the $O_{Fx}$ term is omitted and expressed as,

$$Q^* = \left(K^{\downarrow} - K^{\uparrow}\right) + \left(L^{\downarrow} - L^{\uparrow}\right) = K^* + L^* \quad 1.3$$

where $K^{\uparrow}$ is the outgoing shortwave radiation, $K^*$ is the net shortwave radiation and $L^*$ is the net longwave radiation. An evaluation of the comparative energy balances of pan and surroundings appears in Chapter 4.

Bouchet (1963) argued $Q_{EP}$ would only be limited by $Q_n$ during periods when moisture availability for $Q_{ER}$ was unrestricted due to the surface being thoroughly wet and hypothesized $Q_{ER}$ should be equivalent to $Q_{EP}$. This understanding by Bouchet (1963) was acknowledged as the following equality,

$$Q_{ER} = Q_{EP} = Q_{EP0} \quad 1.4$$

where $Q_{EP0}$ is the $Q_{EP}$ process when $Q_{ER}$ and $Q_{EP}$ are equal, otherwise known as wet equilibrium $ET$.

The complementary behaviour of $Q_{EP}$ with $Q_{ER}$ during periods of moisture restriction gives Bouchet's (1963) hypothesis its name. Bouchet (1963) claimed increases in $Q_{EP}$ due to increases in sensible heat resulting from restricted moisture availability will exactly balance decreases of $Q_{ER}$. The term $Q_{EP0}$ can be referred to as the reference $ET$ from which to measure change of $Q_{ER}$ ($\delta Q_{ER}$). It represents the evaporation from the landscape prior to the onset of moisture restrictions. It is important to distinguish between this reference evaporation when the surface was still wet and potential evaporation measured after the surface has dried since in the latter case enhancement of evaporation is already occurring. The CR can be expressed in its entirety as,

$$Q_{EP} - Q_{EP0} = -\delta Q_{ER} = Q_{EP0} - Q_{ER} \quad 1.5$$

from which it follows that,

$$Q_{ER} = 2Q_{EP0} - Q_{EP} \quad 1.6$$

signalling the complementarity as,

$$Q_{ER} + Q_{EP} = 2Q_{EP0} \quad 1.7$$

Bouchet's (1963) original hypothesis was published in French with no translation which slowed its appearance in the mainstream literature. In that seminal paper, Bouchet suggested a suitable reference for $ET$ over wet surfaces should be set equal to half of the net radiation. At the end of his paper, Bouchet (1963) determined that an index indicating aridity of a region can be expressed as,

$$A = Q_{ER}/Q_{EP} \quad 1.8$$

When $Q_{ER}$ and $Q_{EP}$ are equal, an index value of unity would indicate humid environments. Reduction of moisture availability has opposite effects on $Q_{ER}$ and $Q_{EP}$ and the ratio approaches zero. $A = 0$ would signify arid environments such as a desert, which experiences negligible to no observable evaporation but extremely large values of potential evaporation $Q_{EP}$. The utility of $A$ would allow easy identification of moisture regimes in varying environments and better understanding of the HC.

A final notable remark about Bouchet's (1963) paper was that he graphed the hypothetical interaction between $Q_{ER}$ and $Q_{EP}$. Here it has been reproduced as Figure 1.2. Figure 1.2 has been the subject of interest for over 50 years.

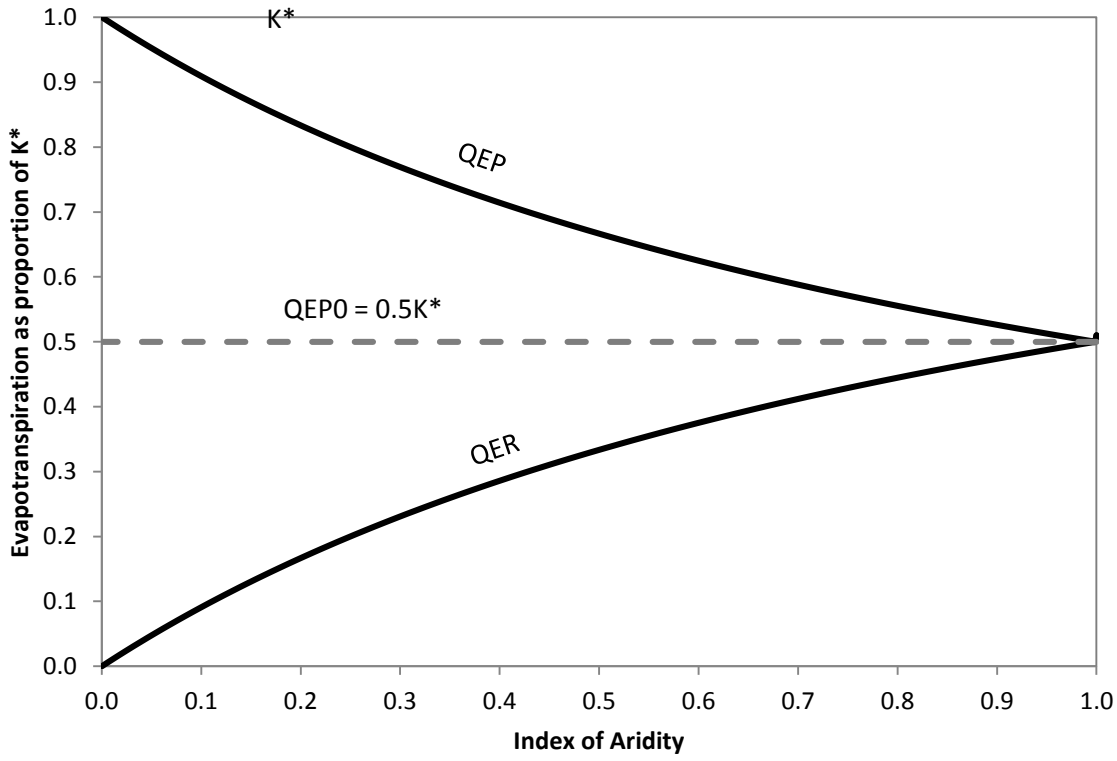


Figure 1.2. Diagram of hypothetical model of the complementary relationship.

### *1.1.3 F. I. Morton and the Advection Aridity approach by W. Brutsaert and H. Stricker*

Morton (1965) was the first to attempt developing a physically based relational model to account for the CR (Kovacs 1987). Morton's (1965) first order of business was to redefine $Q_{EP}$ as the evaporative loss of water from a small, unrestricted water source that will not affect the over passing air by water vapour loading. This new definition by Morton (1965) allowed calculation of $Q_{EP}$ to be based on climatological observations of the region, which can be influenced by $Q_{ER}$. Factually, Morton (1965) was making reference to $Q_{EP}$ experienced from a CAEP and needed to make this distinction very clear.

Morton (1965) asserted there are limitations to handling computations of $Q_{ER}$. This is due to the application of SEB and mass transfer approaches need for accurate $T_0$ measurements, which are very difficult to obtain with respect to $Q_{ER}$. Morton (1965) argued the limitation of accurate regional $T_0$ is overcome by models documented by Penman (1948) and Ferguson (1952). Penman (1948) and Ferguson (1952) combined mass transfer and SEB approaches, thereby eliminating the need for $T_0$ and calculating estimates of $Q_{ER}$ from the landscape. The combination of mass transfer and SEB approaches increased the effectiveness for developing a CR and estimates $Q_{ER}$.

Morton's (1965) investigation had two major objectives. His first objective was to use the concepts documented by Bouchet (1963) and Ferguson (1952) in a synthesized form for the calculation of $Q_{ER}$. The other objective was to test calculated $Q_{EP}$ with $Q_{E_{pan}}$ data and compare calculated $Q_{ER}$ with river basin $ET$, which were based on $P$ and runoff ($RO$) records. The results of Morton's (1965) investigation lead to two conclusions that differences in $Q_{ER}$ due to water availability changes may be detected from effects on $Q_{EP}$ and there is supporting evidence that use of the difference between $K^*$ and $Q_{EP}$ to estimate $Q_{ER}$ could be used as a working hypothesis for better understanding the CR.

Morton (1965) argued that Penman's (1948) combination approach (CA) has several disadvantages, namely the slope of the saturation vapour pressure temperature curve ($\Delta$) is unable to be evaluated correctly due to unknown $T_0$. This is why it was common practice to use average air temperature ($T_{\bar{a}}$) to determine $\Delta$ but this assumption

may lead to errors if significant differences between $T_a$ and $T_0$ are present. Morton (1965) asserted it is challenging to understand the physical significance of variations in climatological observations when artificial terms like Δ are used to solve for $Q_{ER}$.

Morton (1965) maintained that the solution to the Penman (1948) CA is complex and cumbersome and argued the issues could be dampened with the approach presented by Ferguson (1952). Morton (1965) thus contended the CA can be generalized and applicable to CAEP. Therefore, the CA simply should be applicable to water surfaces expressed as,

$$\frac{f(u)}{p}\left(e^*_{T_{0_{pan}}} - e_{T_d}\right) = kK^* + m_{M65}L^* - n_{M65}Q_H \qquad 1.9$$

where $k$ is the ratio of the $K^*$ area to the evaporating surface area, $m_{M65}$ is the ratio of radiant heat transfer area to the evaporating surface area, $n_{M65}$ is the ratio of the sensible heat flux, $Q_H$ area to the evaporating surface area, $p$ is the atmospheric pressure, $f(u)$ is the wind function, $e_{T_d}$ is the vapour pressure at the dew point temperature and $e^*_{T_{0_{pan}}}$ is the saturation vapour pressure of the CAEP surface. With Equation 1.9, Morton (1965) argued the radiant heat transfer is directed towards the sky from the evaporating surface and presented a radiant heat transfer model as,

$$(L\uparrow - L\downarrow) = f_{rh}(T_0 - T_a) = B = -L^* \qquad 1.10$$

where $f_{rh}$ is the radiant heat transfer coefficient.

Morton (1965) believed the radiant heat from non-evaporating surfaces will take on the energy from the surrounding environmental objects and were assumed to be at the daily $T_{\bar{a}}$. This new understanding allowed Morton (1965) to express the total radiant heat transfer as,

$$m_{M65}B = f_{rh}(T_0 - T_a) + (m_{M65} - 1)f_{rh}(T_0 - T_{\bar{a}}) \qquad 1.11$$

where $T_{\bar{a}}$ is the average daily air temperature.

Morton (1965) argued that during periods of moisture limitations from the surface, the vapour transfer function is not applicable but the SEB approach remains valid. He upheld that Bouchet's (1963) analysis of regional SEB will vary the amount of $Q_{ER}$ due to limitations of water availability reflected through $Q_{EP}$. This theoretical acceptance would then allow for computations of $Q_{ER}$ and $Q_{EP}$ through observed and estimated climatological interactions.

Morton (1965) chose to express the CR when $A = 1$ and hypothesized when terrestrial land cover moisture regimes transition as $A \to 0$, the SEB for each of the conditions within the same region, including the whole region and some moist surface like a CAEP, within the region will change according to,

$$Q_{ER} - Q_{ER_{Hu}} = (K^* - K^*_{Hu}) - \left(B_R - B_{R_{Hu}}\right) - (Q_{H_R} - Q_{H_{R_{Hu}}}) \quad 1.12$$

and,

$$Q_{EP} - Q_{EP_{Hu}} = (K^* - K^*_{Hu}) - \left(B_{pan} - B_{pan_{Hu}}\right) - (Q_{H_{pan}} - Q_{H_{R_{Hu}}}) \quad 1.13$$

where subscript $Hu$ refers to humid environmental conditions of $A = 1$, subscript $R$ refers to the region as a whole and subscript $pan$ refers to a CAEP. Morton (1965) asserted it is not essential for the analysis of a small moist area to be present because it would be too small to have any effect on the air passing above. Additionally, $Q_{ER_{Hu}} = Q_{ER_{max}}$ and $Q_{EP_{Hu}} = Q_{EP_{min}}$ based on the assumption of the inverse relationship of the CR.

Morton (1965) contended the air passing above a CAEP, that has not equilibrated with the environment, may transfer heat to the CAEP surface and be expressed as,

$$Q_{H_{pan}} - Q_{H_{pan_{Hu}}} = -\left(Q_{H_R} - Q_{H_{R_{Hu}}}\right) - (M - M_{Hu}) \quad 1.14$$

where $M$ is energy advected into the region by large scale air mass movements.

During periods when the regional surface and CAEP are freely evaporating at the same rate, Morton (1965) proposed a solution based on the combination of Equations 1.12, 1.13, and 1.14 to yield,

$$Q_{EP} + Q_{ER} = 2Q_{EP_{Hu}} + (K^* - K^*_{Hu}) + (M - M_{Hu}) + \left[K^* - B_R - B_{pan}\right] - \left[K^*_{Hu} - B_{R_{Hu}} - B_{pan_{Hu}}\right] \quad 1.15$$

Morton (1965) asserted $2Q_{EP_{Hu}}$ is independent of changing regional moisture conditions and the total effect of the other terms is small. The largest amount of $Q_{EP}$ occurs when the geographic area is completely arid and $Q_{ER} = 0$. This situation Morton (1965) expressed as,

$$Q_{EP_{Ar}} = 2Q_{EP_{Hu}} + (K^*_{Ar} - K^*_{Hu}) + (M_{Ar} - M_{Hu}) + \left[K^*_{Ar} - B_{R_{Ar}} - B_{pan_{Ar}}\right] - \left[K^*_{Hu} - B_{R_{Hu}} - B_{pan_{Hu}}\right] \quad 1.16$$

where the subscript $Ar$ refers to $A = 0$. During environmental conditions of aridity, the sensible heat transfer will be present from the air above to the pan surface below. Morton (1965) argued this could create a compensating effect and cause the radiant heat transfer to be from the CAEP to the atmosphere. Morton (1965) stressed it might be reasonable to assume the largest $Q_{E_{pan}}$ or $Q_{EP}$ can be equal to $K^*$ of the region expressed as,

$$Q_{EP_{Ar}} = K^*_{Ar} + M_{Ar} \quad 1.17$$

Morton (1965) calculated $Q_{EP}$ based on climatological observations and did not use $Q_{E_{pan}}$ data because he considered it a special type of $ET$. Due to this notion, Morton

(1965) compared values of $Q_{EP}$ based on climatological data with $Q_{E_{pan}}$ and excluded records that did not have $T_0$ or $u$ data.

Morton (1968) argued two physical considerations are necessary for the SEB of a CAEP because they do not resemble the surrounding landscape or natural $Q_{ER}$ processes. The CAEP wall and bottom interact with $K^{\downarrow}$ and this affects the vapour and heat transfer characteristics. This understanding allowed a general form of the CA to be applied to a CAEP but Morton (1968) argued a more general model may be used which allows application to all moist surfaces when representative weather observations are available. Morton (1968) hypothesized a simple SEB of the CAEP is given as,

$$K^*_{pan} = Q_{E_{pan}} + Q_{H_{pan}} + B_{pan} \quad 1.18$$

and contested $Q_{E_{pan}}$, $Q_{H_{pan}}$ and $B_{pan}$ to the surrounding space is dependent upon $T_0$ but highlighted $K^*_{pan}$ is the energy source the pan receives. He determined that $Q_{E_{pan}}$ could be modelled as,

$$Q_{E_{pan}} = f_{v_{pan}}(e_{T_{0_{pan}}} - e_{T_d}) \quad 1.19$$

so that $e_{T_{0_{pan}}} - e_{T_d}$ could be related to the vapour transfer function of the pan ($f_{v_{pan}}$). However, $f_{v_{pan}}$ was empirically derived as a function of the $u$.

Morton (1968) argued cloud cover and height will determine $B$ at $T_a$ and partially by $T_a$ and vapour pressure ($e$). This was due to the relationship between $B_{pan}$ and $T_0$ based on several newly developed relationships. $T_{0_{pan}}$ would then be influenced by climatic factors that dominate and thereby reflected by the SEB. Morton (1968) maintained the difficulty of obtaining $T_0$, and re-expressed Equation 1.19. With his previously held beliefs, Morton (1968) wanted to be able to model $Q_{H_{pan}}$ and $B_{pan}$ so that he could better understand what impacts the $Q_{E_{pan}}$ values.

Morton (1968) followed the Penman (1948) CA but generalised the formulation with the heat transfer function of the pan ($f_{h_{pan}}$). A variable ($b$) was given to account for changes in $f_{rh}$ to space with $T_0$. Morton (1968) argued that $n_{M68}$ should account for $f_h$ through the bottom and wall of the CAEP. With the proposed environmental relationships, Morton (1968) algebraically expressed $Q_{H_{pan}}$ and $B_{pan}$ can be modelled respectively as,

$$Q_{H_{pan}} = \frac{n_{M68}\gamma p}{\Delta_2 + f_{h_{pan}}}\left(K^*_{pan} - B - f_{v_{pan}}VPD\right) \quad 1.20$$

and,

$$B_{pan} = \frac{f_{h_{pan}} - n\gamma p}{\Delta_2 + f_{h_{pan}}}\left(K^*_{pan} - B - f_{v_{pan}}VPD\right) + B \quad 1.21$$

The following year, Morton (1969) maintained the connection between $Q_{ER}$ and $Q_{EP}$ may be found in the factors that govern changes in $T_a$ and $e_{T_d}$, which resulted from moisture supply differences of the region. He asserted the Bowen ratio ($\beta$) can provide significant understanding of $Q_n$ processes because water vapour and heat will have the same eddy diffusivities, at a minimum in the layers near the ground, especially over a CAEP that is very low to the ground.

Morton (1969) used a modified version of the CA than reported in his previous work for estimating $Q_{EP}$ as,

$$Q_{EP} = f_{v_R}e^*(1 - RH) + \frac{\Delta_{M69}}{\Delta_{M69} + h_R}\left[K^* - B - f_{v_R}e^*(1 - RH)\right] \quad 1.22$$

where $RH$ is the relative humidity and,

$$\Delta_{M69} = \frac{\delta e^*}{\delta T} \quad 1.23$$

and argued Equation 1.22 may be applied to a CAEP so that,

$$Q_{EP} - Q_{E_{pan}} = \frac{\Delta_{M69}}{\Delta_{M69} + h_R}\left(K^* - K^*{}_{pan}\right) + \frac{\Delta_{M69}}{\Delta_{M69} + h_R}\frac{h_E - h_R}{h_E}\left(K^* - B - Q_{E_{pan}}\right) + \left(1 - \frac{\Delta_{M69}}{\Delta_{M69}+h_R}\right)\left(f_{v_R} - f_{v_{pan}}\right)e^*(1 - RH) \quad 1.24$$

where,

$$h_E = \frac{b_{pan}}{f_{v_{pan}}} + p\gamma n_{pan} \quad 1.25$$

Equation 1.24 is useful to determine the surface processes that are able to impact the difference between $Q_{E_{pan}}$ and $Q_{EP}$ because of the isolated variables accounting for changes in $e$ and $T$ of the pan and the surrounding landscape.

Morton (1969) claimed if the CR is theoretically correct then $Q_{EP}$ should be equal to $K^*$ when $A = 0$ and should be equal to half $K^*$ when $A = 1$. This would also premise $0.5K^* = Q_{EP0}$ when $A = 1$ and $K^* = 2Q_{EP0}$ when $A = 0$, by convention of the CR. The implications of $Q_{EP} = K^*$ during periods of $A = 0$ and $Q_{EP} = 0.5K^*$ during conditions of $A = 1$ were examined with experimental CAEP data collected from near-arid environments in the southwestern United States and near humid inland regions of Ireland.

Morton (1969) presented advection observations in the lower atmosphere was evident of the Ireland coastal $Q_{EP}$ study due to values being higher than the humid model during the winter months. The term $M$ was theorized to transfer heat from the sea and cause enhanced $Q_{E_{pan}}$. The same physically based process was observed for CAEP that were as far as 20 km inland from the coast when the intervening area was a relatively smooth bog that contained few surface roughness ($z_0$) elements but were not apparent in CAEP that were four kilometres inland of the coast where the intervening zone was a rough surface, such as a hedgerow or small field. Morton (1969) argued that $u$ pattern or

atmospheric stability could not explain the difference of transitional zone influence and $z_0$ is the only possible explanation. Morton (1969) was sure of this because greater $z_0$ elements cause deceleration of eddies thereby forcing maritime air aloft and assisting in the formation of a bottom atmospheric layer being in equilibrium with surface conditions. In the case of the bog, $u$ does not change substantially and influences $Q_{E_{pan}}$.

Davenport and Hudson (1967) provided supporting evidence of $u$ and $z_0$ relationships with respect to transitional zones in Sudan, Gezira. As air transitioned from a smooth desert to a rough irrigated cotton field, $u$ decelerated by 25% and achieved $e$ equilibrium with the irrigated surface in less than 300 m. Morton (1969) supported the findings by Davenport and Hudson (1967) and argued the narrow transitional zone should be the only likely cause for the effects of deceleration and have to be reinforced by the effects of increased atmospheric stability due to $T$ and $e$ inversions.

Morton (1971) affirmed $Q_{ER}$ may be defined as $ET$ from water, soil and vegetated surfaces of an area so large that exchange of $Q_{ER}$ and $Q_H$ from the surface controls $ET$ of the lower atmosphere. Thus, the region must have an area where $M$ interacts within the lower layer of the atmosphere to reach equilibrium with the surrounding surface and the effects of net $M$ in the lower atmosphere may be ignored.

Morton (1971) believed that during periods of restricted moisture supply for $Q_{ER}$, the resultant changes in $Q_{ER}$ and $Q_H$ alter the condition of the lower atmosphere. The results are so small they are assumed to be negligible and these include changes in radiation, heat transfer coefficients and vapour transfer functions. The governing factors for the relationship between $Q_{ER}$ and $Q_{EP}$ were presumed to be the changes in $T_a$ and $e$ which are in equilibrium with the region and may occur for air as well as being significantly forced by convection.

Morton (1971) hypothesized if the eddy diffusivities of heat ($K_H$) and water vapour ($K_V$) are similar in the equilibrium layer of the lower atmosphere then changes in $Q_{ER}$ may be reflected with the heat and vapour transfer equations.

Morton (1971) reported the effects of change in $T_a$ and $e$ on $Q_{EP}$ are estimated from the vapour transfer and SEB solutions for the CAEP at specific geographic locations

within a region. This understanding allowed Morton (1971) to calculate $Q_{EP}$ to be proposed from the physical observations of the CAEP and allowed him to yield a solution that produced a relationship where $T_{0_{pan}}$ does not change in response to changes of water availability within the region.

Morton (1971) asserted the equilibrium heat content in the lower atmosphere will change due to increases of the $Q_H$ transfer. Hot air passing above the CAEP with unchanged $T_0$ would create an increase of the $Q_H$ transfer unit that is opposite in sign and most likely equal in size of the regional thermal expansion.

Morton (1971) proposed a notable hypothesis that if $T$ differences could be related to $Q^*$ then the following expression can be given as,

$$Q_{EP} + Q_{ER} = \frac{1}{M_{71}} Q^* \qquad 1.26$$

The term $M_{71}$ presented enhanced challenges because it is an unknown quantity but he had confidence in the CR theory, as displayed from Figure 1.2, and that it would allow the connection to determine available water content from any terrestrial location.

In 1975, Morton claimed the new techniques presented may provide a bypass mechanism so that reliable estimates of $Q_{ER}$ can be achieved. He acknowledged that experimental sites where environmental conditions of $A = 1$ and $A = 0$ are adjacent to one another is virtually non-existent and $Q_{E_{pan}}$ data provide a distorted reflection of $Q_{EP}$. Therefore, Morton (1975) evaluated the CR using two CAEP located in the southeast desert basin of California. Death Valley, CA is considered one of the most arid environments in North America and the $Q_{E_{pan}}$ data would be reflective of $A = 0$ environmental conditions. The second pan, approximately 350 km south of Death Valley, located in the Indio US Date Garden, CA represented a thoroughly irrigated oasis reflecting environmental conditions of $A = 1$.

With three years of $Q_{E_{pan}}$ data from the two sites, Morton (1975) performed linear regression modelling without having to account for severe geographical

differences. The first monthly grouping (January to June) of $Q_{E_{pan}}$ data generated a line of best fit as $Q_{E_{pan_{Hu}}} = 0.40 + 0.57Q_{E_{pan_{Ar}}}$, with a standard deviation of 0.5 mm $d^{-1}$ and correlation coefficient of 99%. The second monthly grouping (July to December) of $Q_{E_{pan}}$ data produced a line of best fit as $Q_{E_{pan_{Hu}}} = 0.36 + 0.52Q_{E_{pan_{Ar}}}$, with the same standard deviation and correlation coefficient as the first monthly grouping. Morton (1975) confidently concluded the regression models computed from $Q_{E_{pan}}$ data differs only slightly from the CR, which suggests a slope of 0.50.

Many of the model elements used by Morton (1975) to better understand the CR are empirically based and documented in the literature. Morton (1975) reported several variables had to be determined through calibration. The calibration used monthly climatological data from meteorological stations in Texas and Arizona. Morton (1975) calculated regression constants until the standard error reached its lowest value, which returned a correlation coefficient of 0.954.

The following year, Morton (1976) acknowledged that Lange et al. (1971) identified that periods of low $e$ could influence the stomata of plants to dilate or constrict and act as a mechanism of controlling $Q_{ER}$ and impacting how the CR responds. This is the first account of physiological controls being theorized to help better understand the CR and the limitations. Morton (1976) maintained the supposed paradoxical nature of $Q_{E_{pan}}$ and $Q_{ER}$ has made research on the CR complicated with respect to $Q_{ER}$. He argued the model developed in 1976 will provide accurate estimates of $Q_{ER}$ from routine climatological observations and may afford an opportunity for simplification that will permit greater understanding of $Q_{ER}$ processes. Morton (1976) contended the model is simple because no assumption is needed regarding the soil-vegetation system because estimates are solely based on $T_a$ and $e$ of the overpassing air with respect to the interactions of the evaporating surfaces.

The newly established theory by Morton (1976) to estimate $Q_{EP}$ accounted for $T$ changes. His new theoretical proposition was strictly from observations of climatological processes and was documented by Kohler and Parmele (1967) first and modified from the

Penman (1948) formulation by the replacement of the psychrometric constant ($\gamma$) for $\lambda_{76}$. Morton (1976) argued the substitution of $\gamma$ for $\lambda_{76}$ will account for effects of $T_0$ changes through $L^*$. The expected results caused $Q_H$ to increase with decreases of $Q_{ER}$ because of restricted moisture availability.

Morton (1976) proposed the Priestley and Taylor (1972) value ($\alpha_{PT72}$) presented a logical basis and alternative solution of the amount of additional energy required to promote $ET$ from saturated surfaces. This allowed him to test his new model with the $\alpha_{PT72}$, which was not the normally quoted value from their seminal paper.

Morton (1976) argued the same rationale as 1975 when $Q_{ER}$ estimates may exceed $Q_{EP}$. Similar to Morton (1975), the regression analysis by Morton (1976) was an improved model that yielded a correlation coefficient 0.957, which was 0.003 greater than Morton (1975).

Morton (1978) performed similar regression analysis procedures and developed a model that was computed continuously until the lowest standard error of estimate was achieved. His tests were based on long term WB drainage calculations that came from gauged streams to determine $Q_{ER}$ estimates. He made gains through the correlation coefficient being 0.002 greater than the model reported in 1976, yielding a value of 0.959.

A different approach for understanding the CR was presented in 1979 by Brutsaert and Stricker. Brutsaert and Stricker (1979) recollect Slayter and McIlroy (1961) theorized that $e$ will resemble the saturation level of a large, uniform, saturated surface that has established well-adjusted atmospheric conditions. Brutsaert and Stricker (1979) used the equilibrium $ET$, given as,

$$Q_{EQ} = \frac{\Delta}{\Delta+\gamma}(Q^* - Q_G) \qquad 1.27$$

was recognized as the lower limit of $Q_{ER}$ from thoroughly saturated surfaces. They hypothesized the atmospheric boundary layer is never uniform because it is continually responding to changes of large-scale weather patterns that experience condensation and

turbulence. This means that equilibrium conditions over wet surfaces are rarely present. Brutsaert and Stricker (1979) acknowledged $Q_{EQ}$ allowed Priestley and Taylor (1972) to perform their analysis on experimental data, which yielded the empirical relationship of $Q_{EP}$ during negligible advection as,

$$Q_{EP} = \alpha_{PT72} Q_{EQ} \quad 1.28$$

The model proposed by Brutsaert and Stricker (1979) was based on the synthesis of the first part of the CR and integrated with theory presented by Slatyer and McIlroy (1961) on regional advection effects who argued the aerodynamic term of the CA can reflect large scale advection effects. Brutsaert and Stricker (1979) asserted the $\alpha_{PT72}$ model represents $Q_{EP}$ during periods of minimal advection and assumed it would occur when $A = 1$. Thus, Brutsaert and Stricker (1979) modelled $Q_{ER}$ by using the CR wherein $Q_{EP}$ was determined based on the CA. $Q_{EP0}$ was calculated by the expression of $Q_{EP}$ under environmental conditions of minor advection. This allowed Brutsaert and Stricker (1979) to construct their advection aridity (AA) model by integrating the Penman (1948) CA, with inclusion of the ground heat flux ($Q_G$), and the $\alpha_{PT72}$ model into Bouchet's (1963) CR, which was improvement from previously held beliefs.

Overall, Brutsaert and Stricker (1979) were able to obtain better results for values of 3-day averages than daily values from Bowen ratio energy balance (BREB) measurements. The model with $\alpha_{PT72}$ = 1.28 displayed less data scatter than the model with $\alpha_{PT72}$ = 1.26 most probably because the model is not highly sensitive to exact $\alpha_{PT72}$ values or the empirical wind function.

After Brutsaert and Stricker's (1979) AA model, Morton (1983) published his CR areal $ET$ model (CRAE). It has long been recognized that stomatal resistance ($r_s$) may be controlled by vapour pressure deficit ($VPD$) between the stomatal cavity and $T_a$ (Morton 1983). His model was different from previously published versions as it considers $p$ as a multiplicative factor with $\gamma$. This is the first time Morton (1983) documented the CA, as it accounts $Q_{EP}$ estimate increase during periods when $VPD$ increase, reflecting increase

atmospheric demand and acceptability of more water from the surface. One result of a larger $VPD$ is due to increased $T_a$ without increased of $e$. Morton (1983) believed this is the first response expected when $Q_H$ increase and $Q_{ER}$ decrease, due to suppressed availability of water.

This is the first documentation by Morton (1983) giving estimations of $Q_{ER}$ with inclusion of the aerodynamic resistance ($r_a$) and canopy resistance ($r_c$). Morton (1983) argued including $r_a$ and $r_c$ allows $Q_{ER}$ of a small area to be estimated as,

$$Q_{ER} = Q_{EP}(\Delta + \gamma p)/\left[\Delta + \gamma p\left(1 + \frac{r_a}{r_c}\right)\right] \quad 1.29$$

and,

$$r_a = {\rho_a c_p}/{\gamma p f_{v_R}} \quad 1.30$$

where $c_p$ is the specific heat of air at constant pressure. Aerodynamic resistance is related to $f_{v_R}$ which plays a critical role in the determination of how quickly the atmosphere can transport $H_2O$ away from where it originated.

Morton (1983) was frustrated the CR depends on too many assumptions to be deemed rational. Morton (1983) argued his model of the lower atmosphere and the improved CR by Morton (1971) can be joined together. He applied this understanding by introducing the $Q_{EP}$ equilibrium temperature ($T_{eq}$) to be used for estimates of $Q_{EP}$. $T_{eq}$ is the observed value when the SEB equation and the vapour transfer function of a moist surface are equal.

### *1.1.4 Kovacs*

Kovacs (1987) presented his understanding of the CR and acknowledged Morton (1975, 1976, and 1978) was able to develop understanding of the CR with better detailed physics and more data availability with suggestions based on publications from several

scholars (Christiansen 1966; Solomon 1966, 1967; Fortin and Seguin 1975; and Seguin 1975). Kovacs (1987) modified the CRAE model by making it better and simpler.

Kovacs (1987) study was novel in the sense that it isolated the factors influencing $ET$. His proposal was an interesting organizational scheme that grouped the energy and atmospheric terms of the CA into single terms. This allowed Kovacs (1987) to assess the energetic influence at the surface consumed by $Q_{ER}$ and $Q_H$.

Kovacs (1987) argued the CR is based on $Q_{EP}$ being dependent on $T$ and $e$ gradients, where $Q_{EP}$ is greater with higher $T$ and is suppressed with lower values of $e$. He indicated both these atmospheric interactions are influenced by $Q_{ER}$ because lower values of $Q_{ER}$ will result in increased $T_a$ and $VPD$ due strictly to the availability of water allowed to enter the atmosphere.

Kovacs (1987) agreed when $A = 1$ water is freely available for $Q_{ER}$ and $Q_{EP} \rightarrow Q_{EP_{min}}$ and is only being controlled by $Q_{EQ}$. He suggested during periods of unrestricted moisture supply the CR may be expressed as,

$$Q_{EP0} = Q_{E_{Rad}} = Q_{ER_{max}} = Q_{EP_{min}} \tag{1.31}$$

Kovacs (1987) supported Bouchet (1963) and Morton (1983) who both acknowledged Equation 1.31 represents an adequate humid boundary condition and stressed when $Q_{EP_{max}}$ occurs, $Q_{EP0}$ is double, which is reflective of the CR hypothesis. Kovacs (1987) supposed the situation that when $Q_{ER} \rightarrow 0$,

$$Q_{ER} + Q_{EP} \rightarrow Q_{EP_{max}} = Q_{ER_{min}} = 2Q_{E_{Rad}} = 2Q_{EQ} = 2Q_{EP0} \tag{1.32}$$

A very interesting study identified by Kovacs (1987) was the work of Mukammal and Neumann (1977) who analyzed $\alpha_{PT72}$ values based on $u$ and $\theta_V$ of a field outfitted with a CAEP. Their study published CAEP $\alpha_{PT72}$ values that were higher than 1.5 when the vegetation approached close to the wilting point and as low as 1.1 when $\theta_V$ reached field capacity.

Analysis of the theory presented by Kovacs (1987) prompted advice from F. I. Morton. A first assumption was with respect to a variable being constant regardless of moisture availability at the surface. Slatyer and McIlroy (1961) proposed the use of the wet-blub depression ($D_z$) in a modified CA of the ventilation term in a $Q_{EP}$ model. Kovacs (1987) argued it should be applied with dependence of the variable on $T$. Second, if the CAEP is representative of $Q_{EP}$, Kovacs (1987) executed multiple regression analysis to determine whether $Q_{E_{pan}}$ exhibits a more causative nature to $VPD$ or $D_z$. The results indicated negligible differences but Kovacs (1987) preferred use of $VPD$ due to slightly superior relations than $D_z$.

Kovacs (1987) posed the situation of the $Q_{EP}$ ventilation term is zero when $A = 1$. He argued Priestley and Taylor (1972) calculated an average $\alpha_{PT72}$ of 1.26 for $Q_{ER}$ from freely available water sources, which was confirmed by experimental research at Tsukuba University by Nakagawa (1984) but of a grass covered surface during periods when the leaves were saturated due to dew formation. Thereby, Kovacs (1987) hypothesized when $A = 1$, $Q_{EP}$ can be referenced to a $Q_{E_{Vent_{min}}}$ value that is 14 – 26% of $Q_{E_{Rad}}$.

### *1.1.5 Nash*

Two years after Kovacs (1987), Nash (1989) got involved in the debate regarding the CR. Nash (1989) agreed that a predefined set of external influences control $Q_{ER}$ but the existence of a validated connection of the CR ensures there to be feedback mechanisms. He argued that if $Q_{ER}$ was strictly expressed on the external influences, the effect of differences of a single factor would provide ease of assessment. But within a feedback framework, Nash (1989) asserted change in an independent $Q_{ER}$ variable would affect the calculation and effect on $Q_{ER}$ would be difficult to evaluate.

Nash (1989) stated that Morton (1983) maintained $Q_{EP}$ as an inverse function to $Q_{ER}$, albeit a steady state environment exists, and agreed the CR is limited by the moisture regimes of $A = 1$ and $A = 0$. Those moisture regimes were used to provide logic of how the relationship physically interacted. Nash (1989) referred to Figure 1.2 and noted wet or dry $Q_{EP}$ values are equal to proportions of $Q^*$. However, Nash (1989)

does explain the slope of $Q_{EP}$ and $Q_{ER}$ across $A$ will be equal in magnitude but opposite in sign. Nash (1989) suggests warning, in agreement with Morton (1983), that $2Q_{EP0}$ may be approximately equivalent to the energetic input but the relationship remains to be thoroughly and accurately analyzed.

### *1.1.6 Granger*

Granger (1989a) reported an approach to evaluate the CR and believed the CR is a universally applicable theory due to its responsive nature to water availability. Granger (1989a) argued that Granger (1989b) used a hierarchical approach to define several $Q_{EP}$ parameters and documented one of the $Q_{EP}$ models cannot be evaluated independently due to the numerous variables and limited theory to describe the environment.

Granger (1989a) contended the proposed $Q_{EP}$ inequalities have a complementary-like behaviour where the differences between each of the respective values determine drying environments whereas no differences may be attributed to $ET$ of saturated surfaces. He believed $Q_{EP0}$ does not arise directly from the CA and thus Bouchet (1963) assumed symmetrical complementarity, thereby contesting the CR is not symmetrical but behaves complementary.

### *1.1.7 Szilagyi*

Szilagyi (2001a) presented his first publication of the CR and stated his study follows Morton (1983) and Morton et al. (1985). Szilagyi (2001b) stated that Hobbins et al. (1999) argued the model presented by Morton et al. (1985) is an improvement of a previously published model by Morton (1983), which performed better at estimating $Q_{ER}$ than the model presented by Brutsaert and Stricker (1979). He contended the changes in $Q_{ER}$ is a negative relationship to changes in $Q_{EP}$ when $Q^*$ is constant, provided on a monthly basis.

He hypothesized to prove the CR exists by indicating if the $T$ difference related to the $VPD$ comes into unity during constant monthly periods of $Q^*$ then the CR is validated. Szilagyi (2001a) cautioned this does not mean the CR is only valid during periods of constant $Q^*$. He acknowledged a method validating the CR under any

environmental conditions was given by Parlange and Katul (1992) through a model based on the AA model and by Kim and Entekhabi (1997) who performed modelled simulations. His goal was to show the CR could be demonstrated based on fewer presumptions than presented by Morton (1965, 1983).

Szilagyi et al. (2001) proposed a new development for estimating $Q_{ER}$ based on the CR and stated that the assumptions presented by Brutsaert and Parlange (1998) support the argument that $Q_{EPO}$ is not variable between the two different periods they used. Szilagyi et al. (2001) concluded the CR reported in their study predicted increase of $Q_{ER}$ using $Q_{E_{pan}}$ data may be overestimated because $Q^*$ values used were constant. This caused inconsistent analysis because in reality $Q^*$ changes seasonally and daily. They correlated $ET$ WB estimates with CR $Q_{ER}$ model results and corroborated their evidence. The conclusion they reached was a near constant average long term $VPD$ indicates constant average $Q^*$. Area weighted means $ET$ WB observed of 3% increase resulted in 6% CR $Q_{ER}$ modelled results, which was twice as large for a 50 year analysis.

In Szilagyi's 2007 study, he modified the AA model with respect to $Q_{E_{pan}}$ data. It served as an operational $Q_{ER}$ estimate method whereby $Q_{EP}$ can be replaced by $\varrho Q_{E_{pan}}$ in which $\varrho$ is a pan coefficient, assumed to be at unity. The asymmetric nature from the inequality is directly linked to the definition of apparent $Q_{EP}$ and not restricted only to CAEP measurements. Szilagyi (2007) assumed the following relationship between $Q_H$ and $Q_{ER}$ with constant $Q^*$ in order to present a working hypothesis for the CR as an inverse.

Szilagyi (2007) argued the CR is symmetric and independent of $T_0$ when energy transfer is not present from the region to pan. This may occur when $Q_{E_{pan}}$ is equilibrated with the surrounding environment and that $Q_{E_{pan}}$ and $Q_{H_{pan}}$ are inverse of each other.

Szilagyi (2007) concluded that the asymmetrical characteristic of the CR is observed in nature when the time rate of change between $Q_{ER}$ and $Q_{E_{pan}}$ is considered. His hypothesis predicts asymmetry based on the SEB of a dry environment because the surface processes are easier to model and argued $Q_{E_{pan}}$ consumes more local $Q_n$ than

when assumptions are made about a constant $Q^*$. This introduced a limitation in his study. In the end of Szilagyi's (2007) study, he used the model and applied it in an operational $ET$ model in finite differences between actual environmental conditions and when $A = 1$.

### *1.1.8 Szilagyi and Jozsa*

Szilagyi and Jozsa (2008) presented the CR and stated change of $Q_H$ ($\delta Q_H$) will have a corresponding impact on $Q_{EP}$. They argued during periods of moisture loss two interactions occur simultaneously in the form of increased $Q_H$ and $VPD$, which both impact $Q_{EP}$ and is needed for the CR to be present. Szilagyi and Jozsa (2008) identified that $\delta Q_H = -\delta Q_{ER}$ and will be valid over terrestrial environments but not over water surfaces due to restricted water supply on land and added heat transferred from land over water.

Over open water surfaces, increased water $T_0$ could foster enhanced evaporation during conditions of constant $Q_n$. $Q_H$ would experience modification. Szilagyi and Jozsa (2008) believed $\delta Q_H$ will be consumed by the corresponding increase in open water evaporation. Szilagyi and Jozsa (2008) suggested water $T_0$ will not change significantly to the exchange of $Q_H$ over water surfaces due to evaporative cooling, granted the warmer air above is not saturated. They argued Morton (1983) and Szilagyi (2001b and 2007) affirmed this conclusion as well. Szilagyi and Jozsa (2008) maintained the fundamental linkage of the CR would be that constant water $T$ could allow for better physical principles to understand the CR. Their $Q_{EP}$ study relied upon the AA model and then altered it with validation from long-term mean annual $Q_{ER}$ estimates from the CRAE model and compared them to one another. Two $Q_{EP}$ methods were used and reported on monthly and annual WB. They argued the method of Kahler and Brutsaert (2006) reported by Szilagyi (2007) altered the AA symmetric nature so $Q_{E_{pan}}$ data could be used. That model of the AA would follow the notion that $Q_{E_{pan}}$ is small enough that water $T_0$ would resemble dry land $T_0$ in arid conditions. Szilagyi and Jozsa (2008) suggested that with this understanding $\beta$ of the CAEP with the heat diffusivity across the

boundary layer. They believed this physical air layer may be big in size if a large difference between $T_{0_{pan}}$ and $T_a$ exists.

The AA model computes estimations of $Q_{EP0}$ at $T_a$ and not $T_{eq}$. Szilagyi and Jozsa (2008) argued $T_{eq}$ can be determined very easily. By expressing $\beta$ of open water and representing a $Q_{EP}$ source,

$$\beta_{SJ08} = \frac{Q_H}{Q_{EP}} = \frac{Q_{EP0} - Q_{EP}}{Q_{EP}} = \gamma \frac{T_0 - T_a}{e^*_{T_0} - e^*_{T_a}} = \gamma \frac{T_{eq} - T_a}{e^*_{T_{eq}} - e^*_{T_a}} \quad 1.33$$

where the unknown $T_{eq}$ can be determined iteratively due to all the other terms being known (Szilagyi and Jozsa, 2008). With this $T_{eq}$ value, it was applied to the CR in order to calculate $Q_{EP0}$ at the given $T_{eq}$ expressed as,

$$Q_{ER} = 2Q_{EP0_{T_{eq}}} - Q_{EP} \quad 1.34$$

Szilagyi and Jozsa (2008) argued their modified AA model used the correct $Q_{EP}$ values. They also affirmed that $\Delta$ is calculated at $T_a$ but in reality the correct $T$ value to be used in the model should be at the wet environment surface temperature ($T_{0_{Q_{EP0}}}$). They then attempted to evaluate how the modified AA model using $Q_{E_{pan}}$ values compared with Morton's (1983) model of long-term average $Q_{ER}$ estimates. Overall, Szilagyi and Jozsa (2008) achieved highly correlated results with long-term average $Q_{ER}$ estimates, whilst obtaining better coefficient of determination and claiming to correct the over- and underestimated values in arid and humid regions. The model was able to achieve long-term average $Q_{ER}$ estimates which were closer to the results obtained from the model proposed by Morton (1983).

The following year, Szilagyi and Jozsa (2009) provided the latest technique for estimating $Q_{ER}$ through the CR, based on their coupled 2-D turbulent heat and vapour transport theory. They ensured the general solutions will be used under the premise that

$Q^*$ remains constant as $A \rightarrow 0$. Again, this is not the ideal environment and not representative of reality. Their ambition was to connect change in terrestrial moisture regimes to change in $T_0$ of a drying landscape using sound environmental science. They were confident in use of their atmospheric transport equations by considering two specific environments.

Szilagyi and Jozsa (2009) proposed another working assumption that at the surface $Q_n$ remain constant spatially and temporally as the saturated surface becomes restricted of moisture. The newly proposed theory allowed $Q_{ER}$ and $Q_H$ change at the same rate over a saturated surface but was complementary in sign. They compared the monthly $Q_{ER}$ values with the AA model based on the CR and found the AA model only contains a single free variable, which is $\alpha_{PT72}$ to be at 1.29 for their study. It is slightly higher than the average quoted value of 1.26. Szilagyi and Jozsa (2009) confirmed that execution of the AA approach was sought after over the CRAE model because of the incorporation of $u$ and this prompted their overall attitude to adopt the AA model for $Q_{ER}$ estimations and used to verify $Q_{EP0}$.

### *1.1.9 Hobbins et al.*

Hobbins et al. (1999) was first to provide a comparative analysis of the AA and CRAE models on a national scale of the conterminous US with WB estimates. Their most valuable results with respect to the wind relationship was observed for the growing season from May to September. The consequence of their analysis was that potential $ET$ values would be greater because of the enhancement of the drying power of the air. They cautioned that the climate of the environment affects the models where the CRAE model underestimates in slightly humid environments and overestimates in arid moisture conditions whilst the AA model underestimates $ET$ values in all environmental moisture conditions except drought moisture regimes.

Hobbins et al. (2001a) attempted to better understand the CR on large scale spatial extent by following up on the research performed in 1999. More error analysis was sought out with respect to the models presented by Morton (1983) and Brutsaert and Stricker (1979) and better understanding the CR. The modelled estimates of $Q_{EP0}$ and

$Q_{EP}$ of the the CRAE model exceeded the AA model. Spatial differences also resulted with modelled $Q_{ER}$ values and showed that negative latitudinal gradients in the eastern half of the conterminous US and positive elevation gradients of the western half. Their analyses of the western half anomalies were attributed to precipitation where the spatial coverage and magnitude of precipitation deficits could be used to indicate that $Q_{ER}$ modelled values were higher than expected. Additionally, the positive error values of both modelled approaches were thought to result from effects of agricultural irrigation and violate the assumption of least impact to the evaluation.

Hobbins et al. (2001b) chose to model two different modified approaches of the AA model to determine what changes to the physically based model would better allow for understanding of the CR. As the AA model is dependent on a wind function, Hobbins et al. (2001b) investigated how the model changes impact the estimated values from the spatial modelled results. Their statistical analysis did result in improved estimates derived from the enhanced AA models and that closure errors experienced by the AA modelled values may be attributed to poor calibrated wind function.

The final notable paper by Hobbins et al. (2004) lends support that the CR is complementary and not a paradox based on observations of CAEP data, as was hypothesised by several researchers (Brutsaert and Parlange 1998; Brutsaert and Stricker 1979; and Morton, 1983). Therefore, Hobbins et al. (2004) examined the trends in CAEP data and regional $ET$ of the conterminous US by estimating $ET$ based on residual WB analyses. Their analysis yielded that with decreasing $Q^*$, $Q_{ER}$ increased with decrease of CAEP data over a 42 year time span.

### *1.1.10 Other Notable Contributions to the Complementary Relationship Theory*

Other notable contributions to the CR have been published by LeDrew (1979), Parlange and Katul (1992), Ramirez et al. (2005), Pettijohn and Salvucci (2006), Lhomme and Guilioni (2010) and Huntington et al. (2011). The contributions from these authors will be given brief acknowledgement of their work in this subsection, as the analysis published by their research has followed much of the pervious theory given above by Morton (1983) and Brutsaert and Stricker (1979). Only slight modifications,

minor enhancements or utility of the CR has been presented by these papers but they do warrant attention.

LeDrew (1979) followed the same principles as Bouchet (1963) and Morton (1968, 1969, 1970, and 1975) and performed diagnostic analysis of models to better understand the CR. He noted that two observations of Morton's and Bouchet's models were not included that consider synoptic scale advection and net radiation changes with respect to moisture availability. With the statistical analysis, LeDrew (1979) was able to make conclusions with respect to the models. Testing the applicability of the CR, LeDrew (1979) selected summer micrometeological data from 1974 collected at Woodbridge, Ontario. Overall, LeDrew (1979) used nine days of data that satisfied the conditions of the experiment but the results of the CR lead to much error for individual days and was unable to consider a hypothesis that would reflect a relationship from the field experimentation.

Parlange and Katul (1992) studied the AA model by Brutsaert and Stricker (1979) and use a function to describe the advection of dry air that does not require calibration. They presented great understanding of the CR and AA model and proposed specific conditions on the respective models when the atmosphere and surface conditions became important and need account. Parlange and Katul (1992) report nine days of research that proved their work to be credible and correlated high results with lysimeter data. The limitation of their research was due to the fact that their land surface of interest was bare ground where plants or other important surface processes can impact the CR. Although the CR does not strictly give importance to the latent heat flux, the physical structure of the surface would impact response of a CAEP.

Ramirez et al. (2005) support the CR with WB data collected from regional areas in the US and concluded that their study was the first to offer direct large-scale observational evidence of the CR with regional $ET$. They also showed that the CR is evident within individual basins. They acknowledged that there is no theoretical proof of the CR except for the heuristic arguments given by Morton (1983) or the assumptions presented by Szilagyi (2001a). Ramirez et al. (2005) identify models that follow the CR

theory that have been successful at predicting $Q_{ER}$ have been given by Brutsaert and Stricker (1979), Hobbins et al. (2001), Kim and Entekhabi (1998), and Morton (1983). They warranted that much work has been invested to better understand the CR but the true relationship is still uncorroborated.

Pettijohn and Salvucci (2006) report their research used the understanding presented by Parlange and Katul's (1992) study that used a framework to investigate the role of canopy conductance, which was not represented in the AA model version by Parlange and Katul (1992). Pettijohn and Salvucci (2006) contended that the studies present by Hobbins et al. (2001b) and Ramirez et al. (2005) hold merit but they rely on the Penman (1948) wind function, which does not advance the CR from traditional heuristic methods. Pettijohn and Salvucci (2006) identified two improvements to the Parlange and Katul (1992) model, which yielded better estimates of $Q_{ER}$, simplicity of the CR and insight to previously erroneous CR modelling. Overall, their results suggested that the CR theory should not neglect the ability of plants to control $ET$ fluxes that regulate the symmetry between $Q_{ER}$ and $Q_{EP}$.

Lhomme and Guilioni (2010) approached the CR issue with use of a framework that focussed on the diurnal development of the convective boundary layer by determining the linking mechanisms between $Q_{ER}$ and $Q_{EP}$. They state that the study re-examines the theoretical results of two previously published articles by Lhomme (1997a and 1997b). Lhomme and Guilioni (2010) claim that their analysis showed the CR is only valid during completely humid environmental conditions and that their modelled, local $Q_{EP}$ exceeds their modelled $Q_{EP0}$ due to two underlying issues that were identified as large scale and medium scale advection interactions. Their approach is not ideal and they acknowledge the work cannot fit with the long term and statistical analyses made by Morton (1983). Thus, their work on the CR is out of scope to be applicable on larger timescales.

The latest published development of better understanding the CR comes from Huntington et al. (2011) that used 10 years of meteorological data collected from five eddy correlation stations to test Bouchet's (1963) hypothesis and demonstrate the

symmetrical nature of the relationship between $Q_{ER}$ and $Q_{EP}$ in an arid shrubland that did not consider wet environment surface temperature. They cautioned that evaluating $Q_{EP0}$ with $T_a$ or $T_{eq}$ only becomes problematic in arid environment. Other remarks made by Huntington et al. (2011) relate to $\theta_V$ change and the CR. Huntington et al. (2011) concluded that the analysis and attempt to relate soil moisture with the CR is not useful because measurements at one depth are unable to provide acceptable conditions of $\theta_V$ as well as the inability to determine regional $ET$ responses with respect to moisture limited regions. Huntington et al. (2011) were able to demonstrate the CR in their study region and they claim their method is robust for predicting rapid changes in $Q_{ER}$ at monthly and annual temporal scales. However, their model is limited with respect to study region and time of use and relied upon the Priestley-Taylor (1972) model to determine the location of $Q_{EP0}$ of the CR.

## 1.2 Introductory Summary

There has been much investment in research and theory development to better understand the HC and the CR. From Bouchet's (1963) initial paper to the many contributors of the CR, much debate is currently present with respect to appropriate model parameters. Additionally, there is confusion regarding the interaction between $Q_{ER}$ and $Q_{EP}$ or $Q_{E_{pan}}$and how these surface processes respond to large scale atmospheric phenomenon. Furthermore, models such as the Penman-Monteith combination model introduce uncertainty because terms such as the canopy resistance have to be determined based on local measurements of the environment. Thus, trying to better understand $Q_{EP0}$ and its limitations has been pursued as an alternative to estimating $Q_{ER}$ without having to parameterize variables that are difficult to obtain.

Although, many of the responses to reasons why environments experience increases and decreases of $Q_{ER}$ have been agreed upon scientifically, the models presented have not been able to efficiently produce a universally operational model. For example, Szilagyi tried to show that better understanding the CR may be linked to how the $Q_H$ responds to changes of $Q_{ER}$. He also did this with modelled values in a

hypothetical environment. Alternatively, Morton was able to use short and long term datasets that were collected from local and regional study regions to gain new insight of the influences impacting $Q_{ER}$ from the landscape and the response of the CR.

Many of the studies published to determine the physical relationships of the CR have allowed hydrometerology to gain new scientific knowledge. However, $Q_{EP0}$ is still an unknown variable with respect to the CR model with the best given estimate of the Priestley and Taylor (1972) model. Brutsaert and Stricker (1979) and Szilagyi and Jozsa (2008 and 2009) have both used the Priestley and Taylor (1972) model to better understand the CR and the true relationship of $Q_{ER}$ and $Q_{EP}$ with $Q_{EP0}$ but that has not become a reality to date. This thesis will address several aspects of the CR model treated in the literature review and in particular try to provide a better understanding of the CR with an extension to theory in efforts to determine the linkage of the CR and the reference evaporation, $Q_{EP0}$.

# Chapter 2 Materials and Methods

## 2.1 Materials

### *2.1.1 Study Site*

The research site for better understanding the CR and development of $ET$ estimates for a CAEP was located in a field at the Kortright Centre for Conservation (KC), Woodbridge, Ontario. KC is located at 9550 Pine Valley Road, between Major Mackenzie Drive and Rutherford Road. It is managed and operated by the Toronto and Region Conservation Authority (TRCA). The experimental herbaceous covered area was approximately four hectares in extent. The coordinate node of the instruments used for the study was located at 43°50’7” N latitude and 79°35’34” W longitude. The study site topographically can be characterised as undulating and gently sloping downwards from northwest to southeast, ranging in elevation from 200 m to 215 m above sea level. The study field itself is bounded by other fields and vegetated surfaces. From a watershed scale, KC is located within the Humber River watershed.

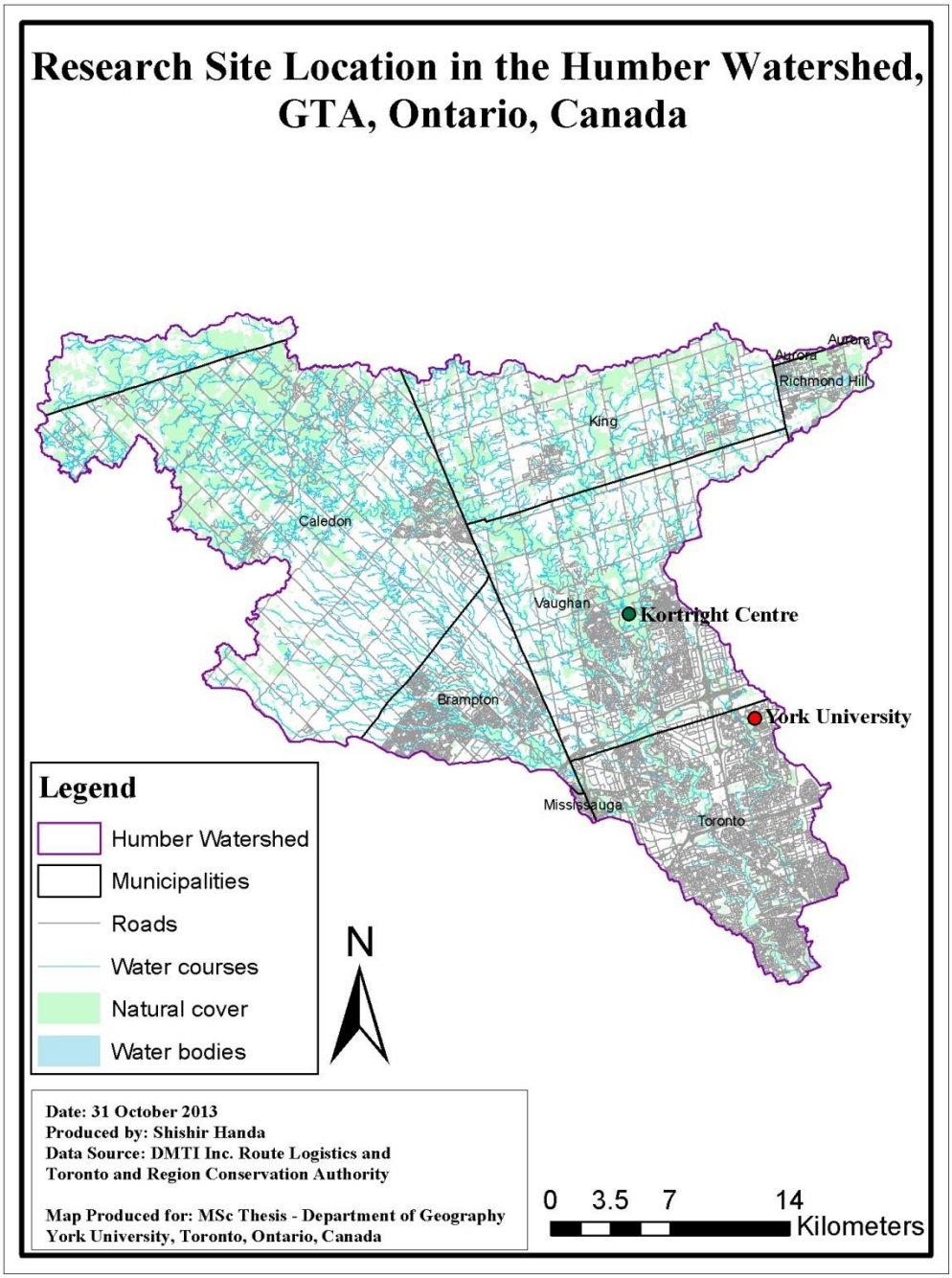


Figure 2.1. Map of the Humber River Watershed and the location of the Kortright Centre for Conservation experimental site.

The plant community at the experimental site can be characterised as a mix of herbaceous and woody plant species. The study site is a fallow field, which was previously planted with Timothy grass (*Phleum pratense*) approximately 10 years ago. The conservation centre is now constituted as a controlled natural access system and is gradually being recolonized by naturalised or native plant species such as Queen Anne's lace (*Daucus carota*), wild oat grass (*Avena fatua* L), purple vetch (*Vicia americana*), cow vetch (*Vicia cracca*), Canada thistle (*Cirsium arvense*), swamp thistle (*Cirsium muticum*), black-eyed Susan (*Rudbeckia hirta*), red clover (*Trifolium pratense*), New England asters (*Aster novae-angliae*), Canadian goldenrod (*Solidago canadensis*) and tall goldenrod (*Solidago altissim*). The soil substrate has the ability to infiltrate rainfall where plant roots can access $\theta_V$ during the growing season for photosynthesis. Soil analysis was not performed and a detailed description of the soil substrate cannot be documented.

### *2.1.2 Class A Evaporation Pan*

A standard NWS CAEP was installed adjacent to a multi-tiered Bowen ratio energy balance (BREB) system and TRCA meteorological station as a means to determine the relationship between pan evaporation ($Q_{E_{pan}}$), potential evaporation ($Q_{EP}$) and real or actual evaporation ($Q_{ER}$). The CAEP began data collection in 2010 and could only be used during the ice-free months to minimize damage to the individual components. The NWS CAEP has a diameter of 120.6 cm and depth of 25.4 cm and was not mounted on top of wooden slat supports thereby maintaining contact with the ground surface below. The CAEP (255-200 Evaporation Pan) was purchased from NovaLynx, USA by the TRCA. Change in water level was measured using an analog output evaporation gauge from NovaLynx (255-100 Evaporation Gauge).

The evaporation gauge sensor could measure change in water level from 0.0 – 25.4 cm and was housed within a stilling well. The stilling well was connected with a 1.27 cm National Pipe Thread valve opening on the CAEP with a 1.27 cm stainless steel pipe that was approximately 75 cm in length, with fittings. Two thermistor temperature probes measured the temperature of the pan water and ground below. Automatic filling of water was accomplished with a float valve and timer connected to a water reservoir. The

float valve timer was programmed to refill the CAEP every 48 hours. This would ensure that CAEP water level was consistently filled to maintain adequate water levels. Data collection of ground and water $T$ and water level was semi-automated with an Onset Hobo U12 4-Channel External Data Logger (U12-008). CAEP data collection was performed on a weekly basis.

Figure 2.2. In the foreground, the Class A evaporation pan with the stilling well, water reservoir, float valve and timer, solar panels and tipping bucket rain gauge can be seen. In the mid-ground, the Bowen Ratio Energy Balance system and top of the 6 tier wind profile system can be seen.

The CAEP SEB was calculated by measuring $Q^*$ at the surface of the CAEP water, $Q_G$ beneath the pan, pan water depth, and pan water temperature. A Middleton CN1 (serial #1471) net pyrradiometer to measure $Q^*_{pan}$ was suspended approximately 13 cm in the centre, above the rim of the pan. The height of 13 cm was determined by

selecting to have a view factor accounting for 95% of the CAEP surface with the given formula,

$$VF = \frac{r^2}{r^2+h^2} \quad 2.1$$

where $VF$ is the view factor, $r$ is the radius of the CAEP of 60.3 cm and $h$ is the height above the surface the CN1 1471 sensor was positioned and evaluated to be 13.8 cm. The CN1 1471 was positioned above the CAEP in the south facing direction to minimize any additional shadows cast by the equipment installation. Figure 2.3a and 2.3b displays the instrumentation of the CN1 1471 net pyrradiometer above the CAEP.

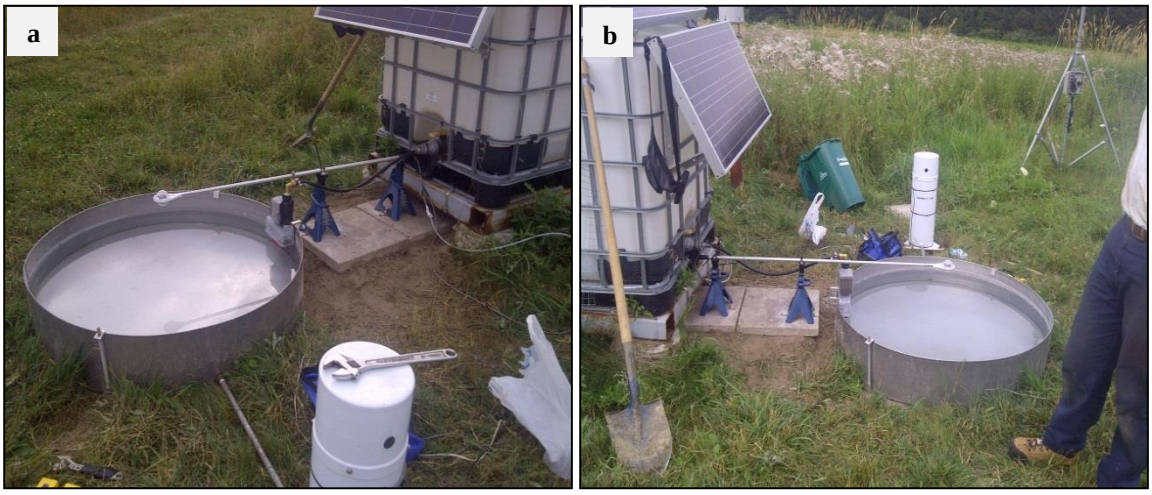

Figure 2.3. (a) displays the installation of the CN1 1471 net pyrradiometer above the Class A evaporation pan, supported by car axel stands affixed to patio stones. The view is from the west side of the Class A evaporation pan. (b) the view of the same installation of the CN1 1471 above the Class A evaporation but from the east side of Class A evaporation pan.

Four Middleton soil heat flux plate(s) (SHFP) to measure pan ground heat flux ($Q_{G_{pan}}$) were positioned beneath the CAEP in the cardinal directions. Each SHFP was positioned approximately 20 cm from the edge towards the centre and in direct contact with the bottom of the CAEP. The SHFP were used to detect whether any $Q_{G_{pan}}$ measurements varied spatially. The digital compass used to determine the cardinal

direction to position the Middleton SHFP beneath the CAEP was an integrated application using the magnetometer of the Motorola® Atrix mobile phone as seen in Figure 2.4a.

Middleton SHFP serial number G298 was used to calibrate the other uncorrected Middleton SHFP serial numbers F383, F169, and F669 while underneath the CAEP, collecting $Q_{G_{pan}}$. This would allow the SHFP to experience similar diurnal cycles of $Q_{G_{pan}}$. After the $Q_{G_{pan}}$ corrections were appropriately analyzed and executed, the same calibration coefficients were used to correct $Q_G$ data that was collected of the field during the 15 day sampling period, which were placed in close proximity to the Bowen ratio energy balance (BREB) system SHFP.

The Middleton CN3 SHFP physical dimension measured approximately 6 mm in thickness. An 8 mm layer of mortar sand was spread beneath the pan to eliminate gaps that would be present if the SHFP were placed beneath the CAEP without any gap filling, as can be seen in Figure 2.4b. The sand also provided direct thermal contact with the base of the CAEP and the ground. Data collection of the CAEP SEB instruments were semi-automated with a Campbell Scientific CR10x data logger, powered with the 12V batteries connected to the photovoltaic solar panels housed in the weather resistant utility box.

Figure 2.4. (a) displays the cardinal direction calibration of the spatial arrangement of the four Middleton soil heat flux plates used to measure ground heat flux of the Class A evaporation pan. (b) is an image of grading the mortar sand to finalize the level of the sand so the Class A evaporation pan may be positioned level with the ground and directly in contact with the soil heat flux plates.

An additional flux of the CAEP SEB had to be considered. The CAEP is an elevated medium and not a flat surface. $Q^*{}_{pan}$ consumed by heating and cooling of the CAEP had to be considered in the SEB as,

$$Q^*{}_{pan} = Q_{E\,pan} + Q_{H\,pan} + Q_{G\,pan} + Q_W \qquad 2.2$$

where $Q_W$ is the amount of energy consumed by the water during cooling and heating phases.

Typically, the SEB of a lake is given by Equation 2.2 (Bello and Smith 1990). Therefore, the energy budget of a lake can be applied similarly to a CAEP. Following Bello and Smith (1990), $Q_W$ was evaluated as,

$$Q_W = c_w(\Delta T/\Delta t)\Delta z \qquad 2.3$$

in which $c_w$ is the heat capacity of water, $\Delta T$ is the change in temperature from initial to final change in depth, $\Delta z$ and $\Delta t$ is the time step of the recorded measurement in seconds.

### *2.1.3 Calibration of Class A Evaporation Pan Surface Energy Budget Instruments*

The CN1 1471 was calibrated and reported by Middleton Solar on 30 April 2010 with no need of any additional corrections. The calibration uncertainty provided by Middleton Solar of CN1 1471 was determined to be ±3%. Middleton Solar's procedure of calibration was performed indoors at normal incidence by comparison to a reference net pyrradiometer, with a tungsten lamp as the source of shortwave radiation and black body emitter at 373 K as the longwave radiation source.

The values recorded of the CAEP with the CN1 1471 were accepted as representative $Q^*{}_{pan}$ data. Only SHFP CN3 G298 was recently calibrated on 19 April 2011 by Middleton Solar and was subsequently used to adjust measurement errors of the uncorrected CN3 SHFP.

Two periods of negative $Q_{G_{pan}}$ data was used for the calibration calculations. The first continuous dataset was from 31 July 2011 at 2315 to 1 August 2011 at 0815. The second continuous dataset used for SHFP calibration was from 2 August 2011 at 2215 to 3 August 2011 at 1015. A total of 86, 15 minute intervals were used for the SHFP calibration. Table 2.1 and Figure 2.5 display the averaged least squares linear regression equations used to calibrate the uncorrected $Q_{G_{pan}}$ values.

Table 2.1. Calibration coefficients used for Middleton soil heat flux plates under the Class A evaporation pan at the Kortright Centre for Conservation with respective unique identifier and cardinal position.

| Middleton soil heat flux plate | Cardinal position | Calibration equation |
|---|---|---|
| F383 | North | y = 0.92046x + 1.85243 |
| F669 | East | y = 1.25907x – 5.37693 |
| G298 | West | y = x |
| F196 | South | y = 0.60042x + 3.65956 |

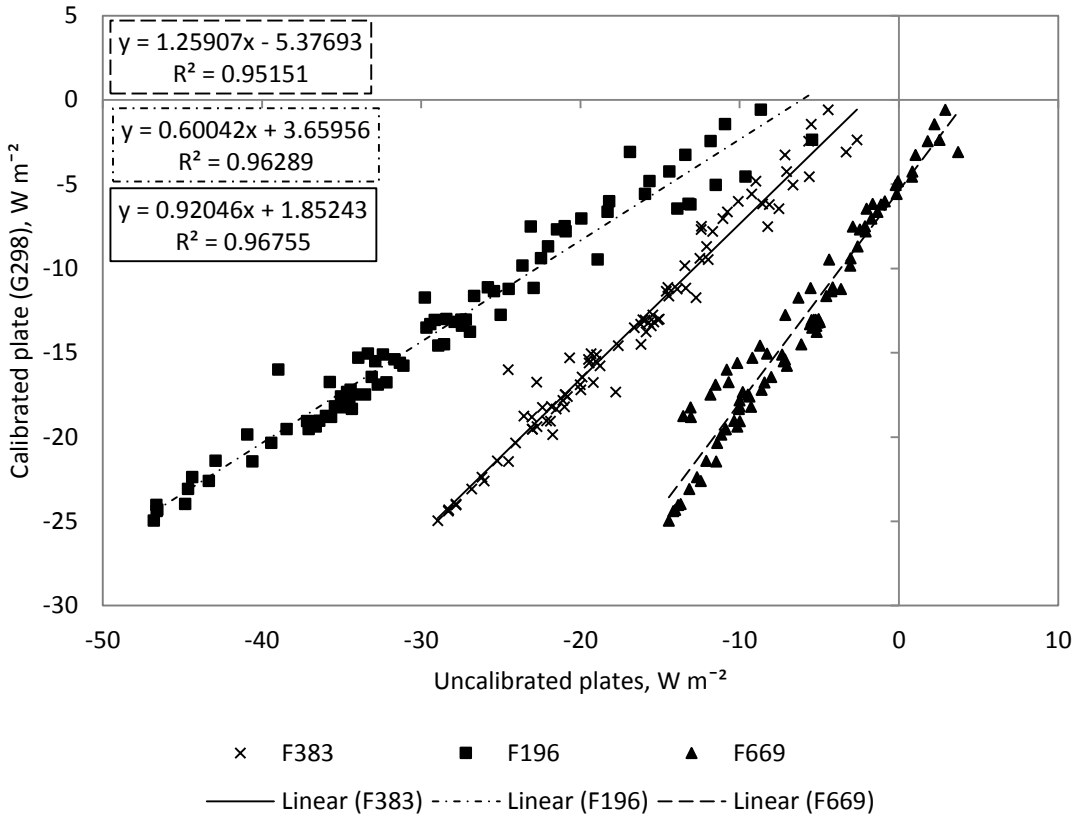


Figure 2.5. Linear regression correlations of calibrated to uncorrected Middleton CN3 soil heat flux plates used to correct ground heat flux beneath the Class A evaporation pan.

### *2.1.4 Six Level Wind Profile System*

A six level anemometer mast system was deployed on 8 June 2010 at the experimental site to construct wind speed profiles of the field. Six Davis Instruments 7911 anemometers and 7914 wind vanes were erected on a 3.81 cm diameter galvanized steel mast at heights of 0.75, 1.00, 1.50, 2.25, 3.00 and 4.00 m above the ground surface, with guy wires to help minimize sway from wind gusts. Figure 2.6 displays the anemometer mast deployed in the field on 8 June 2010. A Campbell Scientific CR1000 data logger was used to semi-automate $u$ data collection, drawing power from the same power supply as the pan SEB system. Wind speed measurements were sampled at 5 second intervals and averaged to produce 15 minute averages.

Wind profile measurements enabled aerodynamic characterization of the field site and better understanding of the fluid mechanical properties of the plant-atmosphere

interface. The wind speed profile system was ultimately used to calculate the aerodynamic resistance of the field given as,

$$r_a = \frac{\left[ln\left(\frac{z-d}{z_0}\right) - \Psi_v\right]\left[ln\left(\frac{z-d}{z_0}\right) - \Psi_m\right]}{\kappa^2 u} \quad 2.4$$

where $\kappa$ is the von Kármán constant of 0.41 and $\Psi_v$ and $\Psi_m$ are the height integrated stability corrections for water vapour and momentum, respectively (Monteith and Unsworth 1990).

Monteith and Unsworth (1990) say the mean wind speed will increase logarithmically with height above the zero-plane displacement height. The standard wind profile function takes on the differentiation form as,

$$\frac{\delta u}{\delta z} = \frac{u^*}{k(z-d)} \quad 2.5$$

where $u^*$ accounts for the mechanical velocity changes of the air above a surface. The friction velocity can be expressed as,

$$u^* = k\frac{\delta u}{\delta[ln(z-d)]} \quad 2.6$$

because the wind profile function is given as,

$$u = \left(\frac{u^*}{k}\right)\ln\left\{\frac{z-d}{z_0}\right\} \quad 2.7$$

Monteith and Unsworth (1990) confirm the two best parameters to account for stability of the atmosphere are the Richardson number ($R_i$) and the Monin-Obukhov length ($L$). $R_i$ is calculated from the gradients of $T$ and $u$ whereas $L$ is determined through fluxes of heat and momentum. $R_i$ is given as,

$$R_i = -\frac{g\delta\theta_v\delta z}{\overline{\theta_v}\delta u^2} \quad 2.8$$

and

$$L = \frac{\hat{z}}{Ri} \text{ when } R_i < -0 \quad 2.9$$
$$L = \hat{z}\left(\frac{1}{Ri} - 5\right) \text{ when } R_i > 0$$

where

$$\hat{z} = e^{\left[\frac{(\ln z_1 + \ln z_2)}{2}\right]} \quad 2.10$$

which is identified as the geometric mean height.

The virtual potential temperature ($\theta_v$) was calculated as,

$$\theta_v = \frac{\theta}{1-\frac{e}{p}(0.378)} \quad 2.11$$

Monteith and Unsworth (1990) give that during unstable atmospheric conditions,

$$\phi_M{}^2 = \phi_H = \phi_V = [1 - 16\zeta]^{-0.5} \quad 2.12$$

and that during stable and slightly unstable atmospheric conditions,

$$\phi_M = \phi_H = \phi_V = [1 + 5\zeta] \quad 2.13$$

where

$$(z - d)/L = \zeta \quad 2.14$$

The dimensionless stability correction factors for momentum, heat and water vapour, $\phi_M$, $\phi_H$, and $\phi_V$ respectively were used in the calculation of $\Psi_V$ and $\Psi_M$ as,

$$\Psi_V = 2\ln\left(\frac{1+Y_\phi}{2}\right) \quad 2.15$$

and,

$$\Psi_M = 2\ln\left(\frac{1+X_\phi}{2}\right) + \ln\left(\frac{1+X_\phi{}^2}{2}\right) - 2\tan^{-1}X_\phi + \frac{\pi}{2} \quad 2.16$$

where,

$$Y_\phi = \frac{1}{\phi_V} \quad 2.17$$

and,

$$X_\phi = \frac{1}{\phi_M} \quad 2.18$$

Figure 2.6. This image displays the six level, anemometer mast with Davis anemometers and wind vanes, which were used to construct wind profiles of the experimental field site. Three stainless steel guy wires are anchored to the ground and attached to the mast to prevent mast sway from wind gusts. The mast was grounded with a copper grounding wire to divert lighting strikes into the ground and away from the electrical systems.

### *2.1.5 Calibration of Davis Anemometers*

Six new Davis 7911 anemometers were calibrated prior to deployment at the KC study site at York University. The anemometers were setup on a horizontal, galvanized steel tube with a diameter of 3.18 cm at York University, in a field at the south western portion of Keele campus for calibration.

The Davis 7911 anemometers were calibrated with a Vaisala acoustic anemometer (model #WMT700) to ensure accurate calibration coefficients were implemented prior to deployment to the KC field site. Linear regression analysis was performed and the results of the calibrations are reported in Table 2.2. Data for anemometer calibration was collected for approximately 5 and a half hour on 25 May 2010.

Table 2.2. Calibration coefficients used for anemometer mast at Kortright Centre for Conservation with respective unique identifier and height above surface.

| Davis Anemometer | height above surface (m) | Calibration equation |
|---|---|---|
| D1 | 0.75 | y = 0.9319x + 0.5227 |
| D2 | 1.00 | y = 0.9341x + 0.5409 |
| D3 | 1.50 | y = 0.9136x + 0.6330 |
| D4 | 2.25 | y = 0.9186x + 0.6618 |
| D5 | 3.00 | y = 0.9413x + 0.5207 |
| D6 | 4.00 | y = 0.9688x + 0.4406 |

### *2.1.6 Bowen Ratio Energy Balance System*

BREB systems use the vertical gradients of potential temperature ($\theta$) and vapour pressure ($e$) and scale the gradient measurements to local measurements of $Q_n$ to calculate $Q_{ER}$ or its mass equivalent ($ET$). Mathematically this is expressed as,

$$Q_{ER} = \frac{Q^* - Q_G}{1+\beta} = \frac{Q_n}{1+\gamma\frac{\Delta\theta}{\Delta e}} \qquad 2.19$$

$Q^*$ was measured with a Middleton CN1 net pyrradiometer aspirated with dry air supplied by an aquarium pump through a desiccant chamber. $Q_G$ was measured directly with a SHFP (Campbell Scientific Inc., HFT3), buried 2 cm below the soil surface. $T_a$

profile was measured using shielded copper-constantan thermocouples (Omega: special limits of error type T). There are four measurement levels on the BREB system which are 0.25, 0.75, 1.50 and 3.00 m and at those same heights $e$ was calculated using the LICOR Biosciences LI-840 infrared gas analyzer (IRGA). It measured $H_2O$ and $CO_2$ concentrations simultaneously. Figure 2.7 displays the BREB fully deployed at the experimental field site.

Figure 2.7. This image displays the Bowen Ratio Energy Balance system, deployed at the Kortright Centre for Conservation experimental research site used to calculate actual evapotranspiration. In the background the multilevel wind profile system can be seen.

Although Equation 2.19 to calculate $Q_{ER}$ only requires $\theta$ and $e$ to be measured at a minimum of two levels in the atmosphere to determine gradients the multi-level system provided a check of internal consistency of flux estimates. The multi-level system also allowed for flux estimates at different spatial scales, if desired (Davies 1972). The highest point of the BREB system allows $Q_{ER}$ to be measured of an area of 300 m radius, with

the assumption of 1:100 height to fetch ratio (Heilman et al. 1989). Ambient air was sequentially drawn through stainless steel mesh insect filters then down from each level through 6.35 mm diameter Bev-A-Line® tubing to minimize gas absorption and diffusion. An aquarium air pump and series of 3 way 12V DC solenoid valves sequentially purged ambient air at a rate of 0.35 $dm^3$ $min^{-1}$ from each level before gas concentrations were sampled. The ambient air was purged for one minute and then sampled for three minutes on each 15 minute cycle. Hourly averages were computed from four 15 minute replicate cycles from each measurement height. Due to the same IRGA unit being used to sample $e$ at all heights, systematic errors were eliminated in the calculation of the $e$ gradients required for Equation 2.19. This allowed calculations of $Q_{ER}$ to maintain high accuracy of $e$ gradients.

An additional component in the design of the BREB system was the incorporation of 16V AC heating tapes (<1.0 W @-30C) attached to each of the flow lines to maintain tubing wall temperatures above the dew point temperature ($T_d$) and eliminating periods of condensation. All inlet lines and heating tapes were encapsulated within 5.08 cm polyvinyl chloride tubing and insulted from environmental $T$ effects with closed-cell polyurethane foam pipe insulation. Inlet air was filtered through a 1 $\mu$m filter before entering the pump and IRGA to extend component life and reduce the need for recalibration. Solenoid valve switching was accomplished with a Campbell Scientific SDM16 relay control module. Data was logged every five seconds on a Campbell Scientific CR1000 data logger to collect 15 minute averaged values. Data was normally retrieved manually on a weekly basis.

The BREB system was initially deployed in August 2008 and several iterations of the photovoltaic solar panel and battery systems have been employed since that time. The solar panels were able to generate a maximum of 240W to charge the two 6V DC marine grade batteries wired in series.

### *2.1.7 Calibration of Bowen Ratio Energy Budget System Components*

The BREB CN1 net pyrradiometer was calibrated with the calibrated CN1 1471 to adjust for sensor drift due to sensor degradation. CN1 1471 was placed approximately

25 cm adjacent to the BREB CN1 from 13 July 2011 at 1815 to 27 July 2011 at 1100. Figure 2.8 displays the physical setup of the CN1 sensor comparison experiment from 13 July to 27 July.

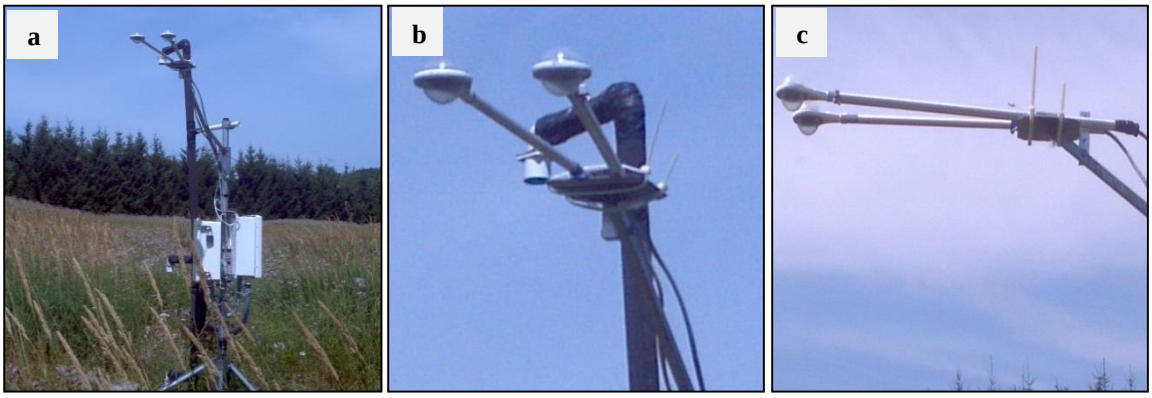


Figure 2.8. (a), (b) and (c) display the setup of the CN1 net pyrradiometer comparison. CN1 1471 was the most recently calibrated net pyrradiometer and is the unit on the right in figure (a) and (b). This comparative study was performed to determine any difference between the two net pyrradiometers units.

The comparative $Q^*$ data collection from adjacent BREB and pan CN1 instruments over grass was perform for 15 days but only three periods of approximately two days total of data was collected due to erratic data logger function. A total of 540, 15 minute interval data values were used for calibration coefficient correction of ${Q^*}_{BREB}$. The 3 interval used for CN1 calibration were from 13 July 2011 at 1815 to 15 July 2011 at 1315, 17 July 2011 at 0730 to 19 July 2011 at 0900 and 25 July 2011 at 0930 to 27 July 2011 at 1100. After determination of the BREB CN1 calibration drift, CN1 1471 was used to measure ${Q^*}_{pan}$. Figure 2.9 displays the least squares regression correlation of ${Q^*}_{CN1\ 1471} = 1.0218{Q^*}_{BREB} - 4.0755$ with a very high coefficient of determination of 0.999. Regression analysis determined the model to be statistically significant (p-value = $6.89 \times 10^{-22}$).

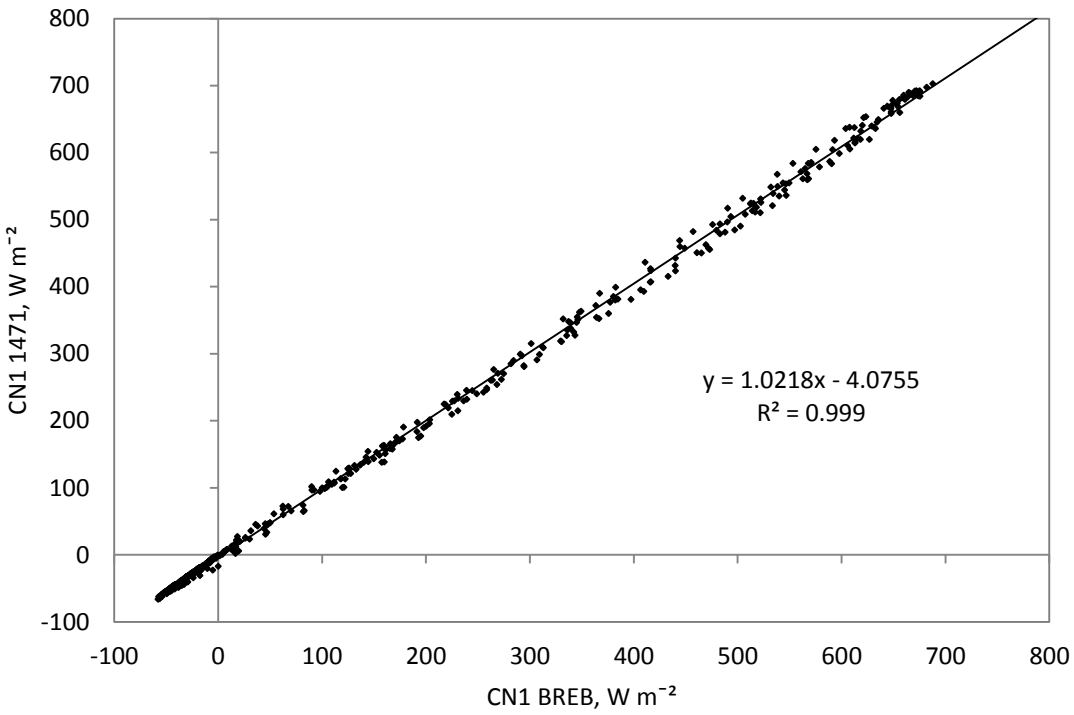


Figure 2.9. Least squares regression results of the CN1 1471 with the CN1 BREB.

The four Middleton CN3 SHFP were spatially distributed in the field in close proximity to the BREB SHFP. Figure 2.10 displays the physical installation of the SHFP and Figure 2.11 displays the correlation with a quadratic trend line fit to the data of $Q_{G_{\overline{field}}} = 0.08146{Q_{G_{BREB}}}^2 + 5.38328Q_{G_{BREB}} + 12.21254$ with a coefficient of determination of 0.90. After removal of the Middleton SHFP from the field, they were spatially arranged under the CAEP in the cardinal directions to determine any spatial variability of $Q_{G_{pan}}$, visualized in Figures 2.4a and 2.4b.

This procedure was performed for all CN3 SHFP. The only variable that would considerably affect $Q_G$ values of the field would be their spatial position at the experimental site. This experiment was executed so that representative average $Q_G$ values of the field could be collected and analyzed. Spatially distributing the CN3 SHFP in the same vicinity as the BREB SHFP would allow for better understanding of the complexity of $Q_G$ variability of the field.

The recorded $Q_G$ values of the field were collected during the same comparative analysis period as the CN1 1471 and the CN1 BREB. The CN1 1471 and CN3 SHFP were semi-automated with a CR10x Campbell Scientific data logger. After the two week sampling period, which ended on 27 July 2011 at 1100, the CN1 1471 and the 4 CN3 SHFP were installed above and below the CAEP, respectively.

Of the four CN3 SHFP only G298 had been recently calibrated. Due to erratic logger error, only $Q_G$ values from 25 July – 27 July were used for the purpose of calibrating the $Q_{G_{BREB}}$ because given the time lapse from the installation on 13 July 2011 would have allowed for the disturbed soil to equilibrate with the surrounding environment and reflect considerable $Q_G$ field values.

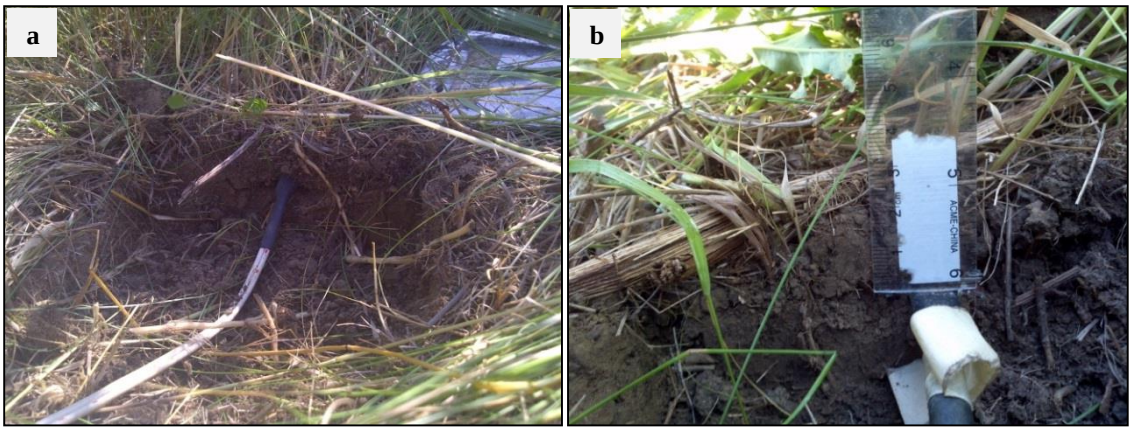


Figure 2.10. (a) displays the block of soil removed from the experimental site with the Middleton soil heat flux plate installed horizontally. The block of soil was repositioned in the opening from where it was remove to allow the soil environment to equilibrate. 2.11b displays a Middleton soil heat flux plate positioned horizontally in the field soil substrate with a ruler displaying the depth below the organic layer of the soil. 2.11a and 2.11b are examples of the process that was performed to record ground heat flux values of the field.

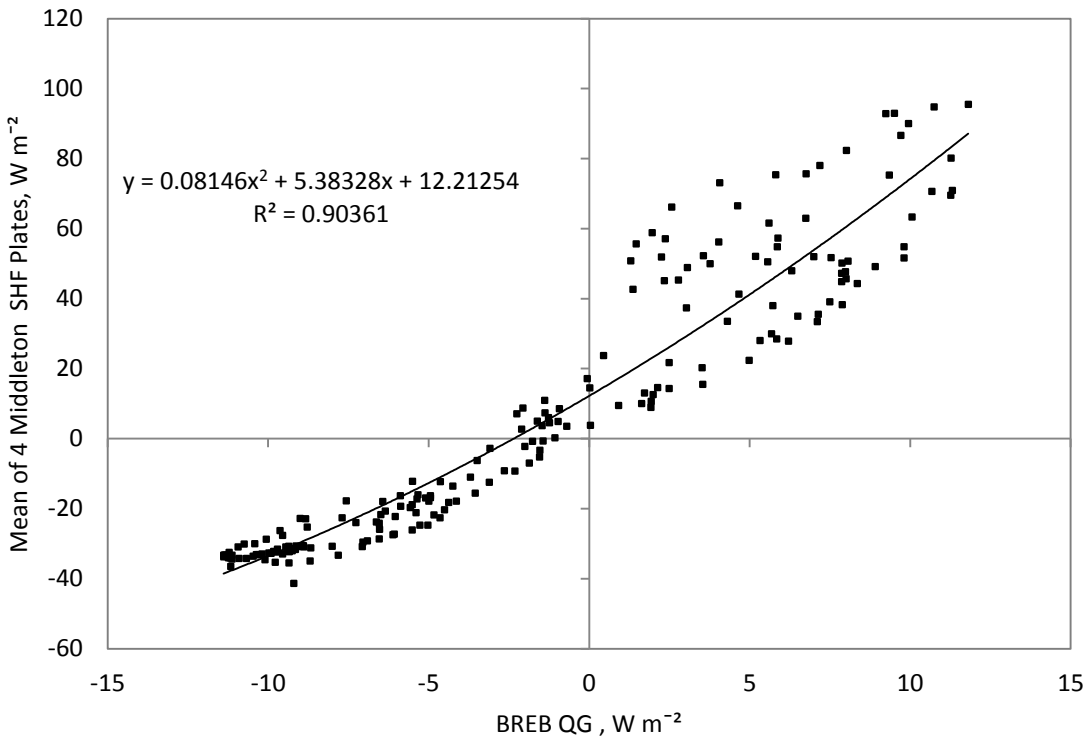


Figure 2.11. Results of the mean of the Middleton soil heat flux plates plotted against the Bowen Ratio Energy Balance soil heat flux plate. A quadratic trend line could be fit through the data and yielded $Q_{G\overline{field}} = 0.08146{Q_{G}}_{BREB}^{\ 2} + 5.38328{Q_{G}}_{BREB} + 12.21254$ with a 90.4% coefficient of determination.

### *2.1.8 Toronto and Region Conservation Authority Meteorological Station*

To enable calculations of $Q_{ER}$ and $Q_{EP}$ the TRCA meteorological station, as displayed in Figures 2.12a and 2.12b, augmented the BREB, wind profile and CAEP systems deployed at the research site. Precipitation ($P$) was measured with a Hydrological Service Ltd. TB3 tipping bucket rain gauge (0.2 mm tip$^{-1}$), displayed in Figure 2.12b. Atmospheric pressure ($p$) was measured with an Onset Barometric Pressure Sensor S-BPA-CM10. Incoming shortwave radiation was measured with an Onset S-LIA-M003 silicon pyranometer. All TRCA meteorological weather station sensors were semi-automated with Onset's HOBO weather station data logger (H21-001) housed in a weather resistant enclosure.

### *2.1.9 Calibration of Toronto and Region Conservation Authority Meteorological Station instruments*

The TRCA meteorological station instruments were previously calibrated from their respective distributors and did not need any additional corrections.

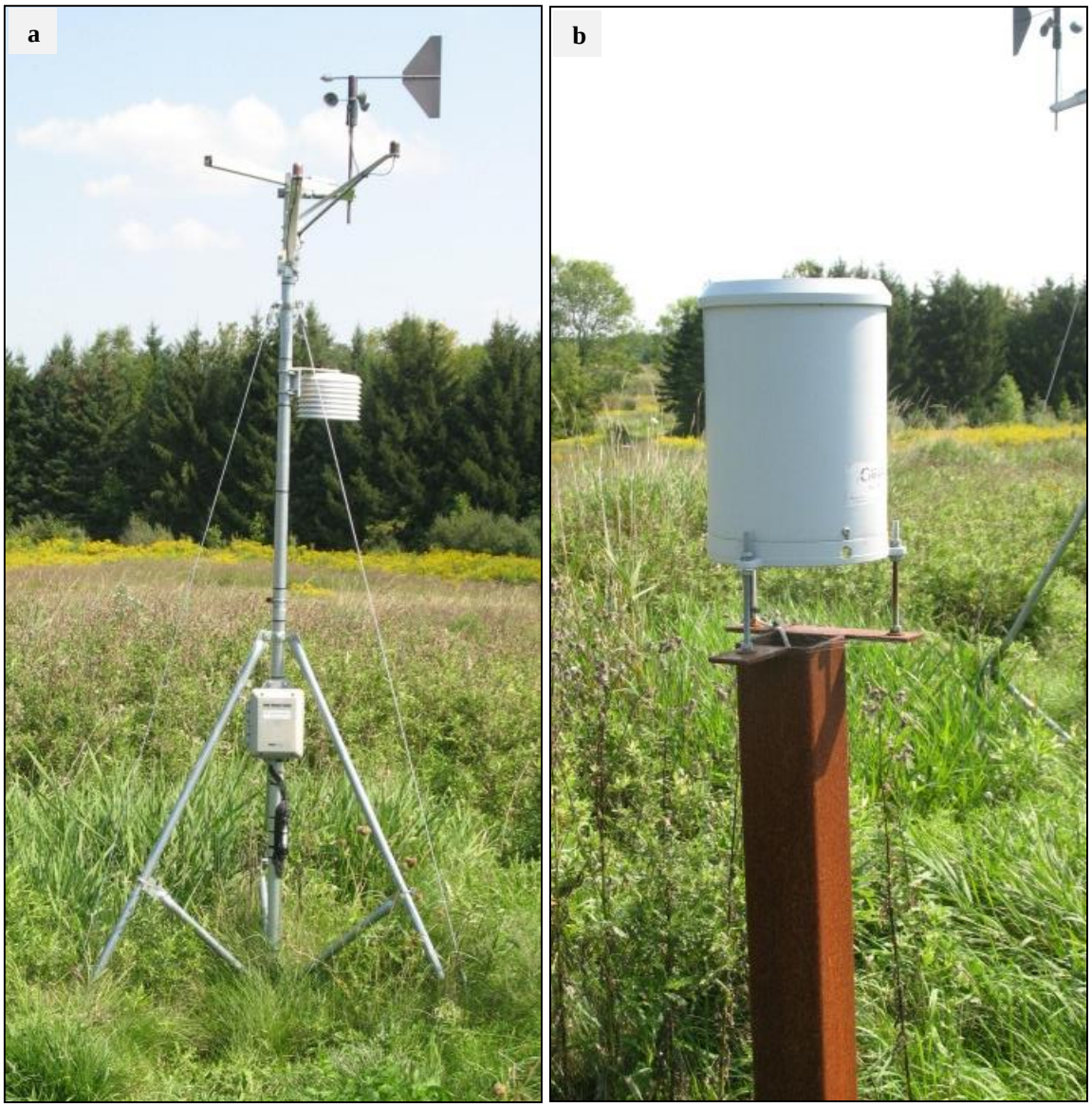


Figure 2.12. (a) is an image of the Toronto and Region Conservation Authority meteorological station, which was used to enable water and energy budgets of the experimental site at the Kortright Centre for Conservation. (b) is the tipping bucket rain gauge used with the meteorological station to measure precipitation.

## 2.2 Theoretical Basis of Analysis

Analysis for this study during the measurement periods of 2010 and 2011 was based on theory compatible with the instruments at the KC field site. The four systems used in this study to better understand evapotranspiration and the CR were previously in place since 2010. Only the addition of the CN1 1471 and CN3 SHFP apparatus were newly instrumented in 2011 at the experimental field site.

The analysis relied on the commonly acknowledged SEB (Oke 1987; Bonan 2008) expressed as,

$$Q^* = Q_{ER} + Q_H + Q_G \quad 2.20$$

Measured decreases in CAEP water level ($ET_{pan}$, mm $s^{-1}$) can be converted into the latent heat energy equivalent of water vapour transitioning into the atmosphere as,

$$Q_{E_{pan}} = L_v ET_{pan} \quad 2.21$$

The BREB system measures $Q_{ER}$ by scaling $Q_n$ according to the relative strengths of the vertical $\theta$ and $e$ gradients given by Equation 2.19. $\beta$ is the Bowen ratio given as,

$$\beta = \frac{Q_H}{Q_{ER}} \quad 2.22$$

For this research $\beta$ was calculated as,

$$\beta = \gamma \frac{\Delta\theta}{\Delta e} \quad 2.23$$

The Penman-Monteith CA for the $Q_{ER}$ partitions total $ET$ into three factors responsible for dynamic flux, which are energy availability, atmospheric demand and moisture availability as,

$$Q_{ER} = \frac{\Delta(Q^* - Q_G) + \rho c_p {}^{VPD_z}/_{r_a}}{\Delta + \gamma\left(1 + \frac{r_c}{r_a}\right)} \quad 2.24$$

where $VPD_z$ is the $VPD$ of the air at height $z$. Similarly, $Q_{ER}$ may be partitioned into the three factors responsible for dynamic flux, given after Slayter and McIlroy (1961) as,

$$Q_{ER} = \frac{\Delta}{\Delta+\gamma} Q_n + \frac{\rho c_p}{r_a}(D_z - D_0) \quad 2.25$$

in which $D$ is the wet-bulb depression at the surface (0) and at some height above the surface ($z$). $D$ is determined as the difference of $T$ at varying heights between dry-bulb ($T$) and wet-bulb ($T'$) temperatures.

Equation 2.24 is rearranged to solve for $r_c$ as,

$$r_c = (1 + \beta) r_i + \left(\beta\left(\frac{\Delta}{\gamma}\right) - 1\right) r_a \quad 2.26$$

where $r_i$ is the isothermal or climatological resistance (DeBruin and Holtslag 1982) given as,

$$r_i = \frac{\rho c_p}{\gamma} \frac{VPD_z}{Q_n} \quad 2.27$$

Data collected from the BREB system was augmented with the six level $u$ profile system to provide hourly estimates of $r_a$ from Equation 2.4. Estimates of $r_a$ can be used to provide hourly estimates of surface resistance (or moisture supply) from equation 2.26.

The CR and parameterizing the reference point for potential evaporation when water actually is freely available ($Q_{EP0}$) of Bouchet's (1963) hypothesis is important. It is hypothesized the sensitivity of $VPD$ in the atmosphere to surface drying will vary with season and air mass type and be influenced by $r_i$, which expresses the relative importance of the local energy supply and $VPD$, driving $Q_{ER}$. Hence, the atmospheric demand change

depends on the ratio of $D$ to $r_a$. For example, if $T$ and $VPD$ increases as will $D$ and if $u$ increases, $r_a$ decreases. Aside from $Q_{ER}$ being controlled by $Q_n$ and $VPD$ are the reduced amounts of $Q_{ER}$ resulting from the restriction of moisture available to enter the atmosphere from the surface. Moisture availability will be represented by $D_0$, which increases as volumetric soil moisture ($\theta_V$) depletes. During rainfall or dewfall, the surface is considered saturated and $D_0$ should diminish to zero. This indicates the air next to the ground is unrestricted of water and saturated and allows the expression of the latent heat flux in a simplified form expressed as,

$$Q_{EP} = \frac{\Delta}{\Delta+\gamma} Q_n + \frac{\rho c_p}{r_a} D_z \qquad 2.28$$

The flow of water vapour in the fully adjusted boundary layer upwards from any plane will be equal to $Q_{ER}$ from the surface. Equation 2.28 creates reduced values of $Q_{EP}$ away from the surface as height increases, thereby limiting the usefulness of determining surface dryness with $Q_{EP}$ measurements. There is some chance that errors associated with the observations of $Q_{EP}$ will shed new perspective of how $D_z$ is related to $D_0$ or if there is a relationship between $\delta D_z$ to $D_0$.

The flux computed from Equation 2.28 will always be greater than the flux computed from Equation 2.25 due to the absence of any moisture limitations at the surface. $Q_{EP}$ is controlled by and will vary with $Q_n$, $r_a$, and $VPD$ diurnally, seasonally and spatially and represents the greatest possible $ET$ that may be experienced from the surface of interest because moisture is unrestricted to enter the atmosphere from the surface. Equation 2.28 may also be applied to open water surfaces like CAEP that are consistently filled with water, fulfilling the requirement of unrestricted moisture availability.

Described by Equation 2.28, $Q_{EP}$ applies to surfaces that experience unrestricted moisture availability or from a CAEP. Since equation 2.28 is quite similar to Equation 2.25, opportunity may exist to measure $Q_{EP}$ using a CAEP and convert those observed values into $Q_{ER}$ of the surrounding landscape.

The net result of $Q_{ER}$ is not clearly straightforward from the increased observations of $D_0$ or $D_z$ overlaying the same surface. Equation 2.25 indicates no net change in $Q_{ER}$ will be experienced if $D_0$ and $D_z$ both increase or decrease by the same quantity. If $D_0$ increases greater than $D_z$ overlaying the same surface then $Q_{ER}$ must decrease. However, if the opposite is present and $D_z$ overlaying the same surface increases greater than $D_0$, then $Q_{ER}$ should increase.

The complementary behaviour of $Q_{E_{pan}}$ or $Q_{EP}$ with respect to $Q_{ER}$ happens when moisture supply is restricted from the surrounding landscape due to increased $\theta_V$ deficit or $r_c$, due to plants conserving water and maintaining turgor pressure by reduced stomatal opening periods. In the scenario when $\theta_V$ becomes limited $Q_{ER}$ is suppressed and $Q_{EP}$ or $Q_{E_{pan}}$ should advance. Bouchet (1963) hypothesized the greater quantity of $Q_{EP}$ due to restricted moisture supply from the surrounding landscape will be balanced by the reduced amount of $Q_{ER}$.

There is presently no routine method of estimating $D_0$ to determine the true dryness of the region but measurements of $r_c$ do allow for determination of moisture availability for the surface or canopy. Another confounding issue is that $D_z$ measured at present is greater than what would have been observed if the surface was truly saturated because of the enhanced ability of the atmosphere to accept and hold water vapour due to global climate warming. Recalling Morton (1969, 1971, 1975, 1976, and 1983) and Brutsaert and Stricker's (1979) attempted investigation of the environmental controls of $Q_{EP0}$ and issues restricting clearly defining the CR has been long withstanding. Brutsaert and Stricker (1979) approached the issue of parameterizing $Q_{EP0}$ by assuming that over a wet surface the atmospheric demand term was a constant proportion of the energy availability term of the Penman-Monteith CA. The constant was set to an average 0.27, which is in close range to the more commonly quoted $\alpha_{PT72}$ value of 0.26 expressed as,

$$Q_{EP0} = 1.27\frac{\Delta}{\Delta+\gamma}Q_n \qquad 2.29$$

This would be analogous to establishing the second part of the first term of Equation 2.28 equal to 0.27 and allowing for the solution of $D_z$ as if the surface was completely saturated with moisture as,

$$D_{z_{Q_{EP0}}} = 0.27 \frac{r_a}{\rho c_p} \frac{\Delta}{\Delta + \gamma} Q_n \qquad 2.30$$

Brutsaert and Stricker (1979) provide substantial evidence that the assumption of Equations 2.29 and 2.30 are valid for three-day estimates of $Q_{ER}$. However, their study was performed during a drought summer in the Netherlands and resulted in undesirable conditions, yielding unrealistic estimates of $Q_{ER}$ during $A = 1$. As an example, if Equations 2.28 and 2.29 are substituted into Equation 1.6 we obtain,

$$Q_{ER} = 2 \left[1.27 \frac{\Delta}{\Delta + \gamma} Q_n\right] - \left[\frac{\Delta}{\Delta + \gamma} Q_n + \frac{\rho c_p}{r_a} D_z\right] = 1.54 \frac{\Delta}{\Delta + \gamma} Q_n - \frac{\rho c_p}{r_a} D_z \qquad 2.31$$

During environmental conditions when $D_0 = D_z$ and $A = 1$, a coefficient given by 1.54 suggests an overestimated $Q_{ER}$ value of 54% in comparison to the expected value given by the Penman-Monteith CA from equation 2.25 of $A = 1$. At present, a more physically-based theoretical understanding of $Q_{ER}$ has not been suggested to uncover the appropriate response factors of $Q_{EP0}$.

The averaged $\alpha_{PT72}$ of 26% originated empirically from the review publication by Priestley and Taylor (1972) indicating, on average, over saturated surfaces the atmospheric demand term in Equation 2.28 is approximately 26% of the energy availability term. The partitioning of the atmospheric terms from the energetic terms was observed from multiple field experiments. The conceptualization of the linkage between the energy supply role to the atmospheric demand role driving $Q_{ER}$ had been variously attributed to large scale advection or alternately cloud formation. Evidence supporting the former is based on the argument the experimental evidence collected from saturated surfaces were downwind from surfaces that exhibit unsaturated moisture conditions. The

expectation was air masses originating from areas of $\theta_V$ deficit would create non-saturated atmospheric conditions in the advected air mass within the surface boundary layer when passing over the moist surfaces. The latter observation was supported by evidence based on water vapour sinks, represented by cloud condensation. Residual air dryness commonly observed in the atmosphere and over oceans results from continuous removal of water vapour through processes of cloud formation at the oceanic and global scales.

Priestley and Taylor (1972) indicated common observations of non-saturated atmospheric conditions are commonplace over many landscapes, both terrestrial and aquatic. As the ground surface dries the additional humidity deficit created by the reduced local $Q_{ER}$ process will facilitate greater $Q_{E_{pan}}$ resulting in a complementary manner where $D_z = D_{z_A} + D_{z_L}$, in which $D_{z_A}$ is observed as the advective proportion of the humidity deficit and $D_{z_L}$ is observed as the local proportion of the humidity deficit. $Q_{ER}$ can be expressed as,

$$Q_{ER} = Q_{EQ} + \frac{\rho c_p}{r_a}(D_{z_A} + D_{z_L} - D_0) \qquad 2.32$$

There are environments that experience $Q_{EQ}$ and through examination of Equation 2.25 those environments are found when conditions of $D_0 = D_z$ are met. Special cases when $D_0 = D_z = 0$, $Q_{ER}$ is driven strictly by the energy supply term. In this case, no amount of atmospheric turbulence will influence $Q_{ER}$ when the surface and the overlaying air are similarly saturated because eddies transporting water vapour upwards are replaced by eddies of the same amount of water vapour resulting in no net change of vapour exchange. Therefore, the atmospheric demand is neither enhanced nor suppressed at the surface under these conditions. However, if cool moist air is advected over the surface under such conditions then the $VPD$ should decrease with height ($D_0 > D_z$) and convection will ultimately suppress $Q_{ER}$ lower than $Q_{EQ}$ yielding sub-equilibrium evaporation ($Q_{EQ_{sub}}$). Conversely, if warmer dry air is advected over the surface then the $VPD$ should increase with height ($D_0 < D_z$) and convection will enhance $Q_{ER}$ greater than

$Q_{EQ}$. This observation will be termed as supra-equilibrium $ET$ ($Q_{EQ_{sup}}$) because it is greater than or above $Q_{EQ}$. Of special note, when $D_z$ or $r_a$ increases with height then $D_{z_A}/D_z$ will increase with height due to $D_{z_L}/D_z$ decreasing with height and thereby allowing mechanisms of the atmospheric interactions to be parsed out with respect to their impact on the surface.

$Q_{ER}$ is constant with height within the fully adjusted boundary layer (Oke 1987). Since $Q_{EQ}$ is constant with height the second term in Equation 2.32 should also be constant as well. Aerodynamic resistance increases with height from the surface and sum of the terms in the brackets remains constant with height with respect to the total flux. To the extent that changes with height in $r_a$ are measured or modelled accurately, change with height in the sum of the bracketed terms of Equation 2.32 can be estimated. Important to note, without an *a priori* knowledge of $D_0$ multiple solutions for $D_z$ as a function of $r_a$ can be calculated. Although, in micrometeorological experimental settings where $Q_{ER}$, $r_a$, and $D_z$ are observed, a unique solution for $D_0$ is achievable by re-arranging the terms in Equation 2.32.

A comparison of how surface drying influences estimates of $Q_{EP}$ using Equation 2.28 allow for better understanding of factors controlling $Q_{ER}$. After Priestley and Taylor (1972), defining the ratio of $Q_{ER}$, Equation 2.25, to $Q_{EQ}$ given by $\alpha_{PT72} = Q_{ER}/Q_{EQ}$ and to a similar ratio of $Q_{EP}$, from Equation 2.28, to $Q_{EQ}$ given by $\alpha_{PT72*} = Q_{EP}/Q_{EQ}$ will allow for better understanding of the processes driving the $Q_{ER}$ hydrological process. Therefore, the proportional error from using Equation 2.28 to estimate $Q_{ER}$ during periods of moisture restriction can be determined with comparison of the newly proposed ratios expressed as,

$$\frac{\alpha_{PT72*}}{\alpha_{PT72}} = 1 + \left(\frac{\gamma}{\gamma+\Delta}\right)\frac{r_c}{r_a} \qquad 2.33$$

Interestingly, $\frac{\alpha_{PT72*}}{\alpha_{PT72}} \rightarrow 1.0$ with increase in height because $r_a$ increases with distance from the surface. This indicates the common misapplication of Equation 2.28

with respect to estimation of $Q_{EP}$. For example, Brutsaert and Stricker (1979) use Equation 2.28 to estimate $Q_{EP}$ as if it represents enhanced $Q_{EP}$. This "measured" $Q_{EP}$ reduces as sensor height increases indicating an inverse relationship. As $\frac{\alpha_{PT72*}}{\alpha_{PT72}}$ varies with height, it becomes incorrect to presume $Q_{EP}$ as constant with height.

Equation 2.33 reveals that Equation 2.28 allows no error in computed values of $Q_{ER}$ when $r_c = 0$ or when $D_0 = 0$ and $A = 1$. This also indicates that departure of $Q_{EP}$ from $Q_{ER}$ becomes greater as $r_c$ increases. Equation 2.32 displays the magnitude of error is inversely proportional to $r_a$. If moisture availability becomes limited then errors are introduced by lack of attention to the role of the moisture supply. Accordingly, the role of moisture availability will be restricted as wind speed decreases or be enhanced as wind speed increases.

## 2.3 Extension of Theory

The change of $T_a$ as a function of *surface drying* can be expressed through a series of equations as,

$$\delta T_0 - \delta T_a = (Q_{EP0} - Q_{ER})\frac{r_a}{\rho c_p} \quad 2.34$$

where $\delta T_a = D_z = T_a - T_a'$. The wet-bulb temperature at some height in the atmosphere is denoted as $T_a'$.Thus, it can be presumed larger values of $\delta T_a$ will be resultant of hotter air temperature causing increased sensible heating due to decrease in moisture availability. $\delta T_0 = D_0$ and represents the analogous increase in $T_0$ associated with surface drying. Similarly,

$$\delta T_0 = (Q_{EP*} - Q_{ER})\frac{r_a}{\rho c_p} \quad 2.35$$

$$\delta T_a = (Q_{EP*} - Q_{EP0})\frac{r_a}{\rho c_p} \quad 2.36$$

$$D_z = \left(Q_{EP*} - Q_{EQ}\right)\frac{r_a}{\rho c_p} \quad 2.37$$

According to the CR, the expression for reduction of $Q_{ER}$ below $Q_{EP0}$, given by Equation 2.34, is only equivalent to the enhancement of $Q_{EP*}$ greater than $Q_{EPO}$, given by Equation 2.36, when $T_0$ warming is exactly double of measured $T_a$ warming, which corresponds to $\delta T_0 = 2\delta T_a$. An exception of this unique condition is observed when $Q_{EP*}$ does not satisfy $Q_{EP}$, required to meet adequate conditions of the CR. Within the fully adjusted boundary layer, both $Q_{EP0}$ and $Q_{ER}$ are constant with height and $\delta T_0 - \delta T_a$ must increase directly proportional to $r_a$. All changes accompanying $r_a$ must be accommodated by $\delta T_a$ because $\delta T_0 = D_0$ will be invariant with height. With this understanding, a definition of a critical resistance, $r'$ will correspond to a height in the atmosphere above the surface where warming due to surface drying diminishes to zero such that,

$$r' = \frac{\rho c_p D_0}{Q_{EP0} - Q_{ER}} \qquad 2.38$$

Equation 2.38 suggests that as surface drying increases, the height in the atmosphere experiencing corresponding gains of $T$ due to moisture reduction will also proportionally increase as a result of surface drying. During periods of small residuals of $Q_{ER}$ generated by consequences of surface drying, observations at greater heights in the atmosphere must be sought after to register a negligible $T$ change between $A = 1$ and $A = 0$ environmental conditions. For example, $T$ of 288.15 K with $Q_{EPO} - Q_{ER} = 1\ W\ m^{-2}$, $r' = 1200\ D_0$.

Combining Equation 2.34 and 2.38 provides insightful characteristics of $r'$, which follows as,

$$\frac{\delta T_a}{\delta T_0} = 1 - \frac{r_a}{r'} \qquad 2.39$$

and describes the relative warming in the atmosphere to that of the surface warming as a function of height as a function of $r'$ and $r_a$.

A solution for $Q_{EPO}$ can be sought after from Equation 2.38 expressed as,

$$Q_{EP0} - Q_{ER} + Q_{ER} = \frac{\rho c_p}{r'} D_0 + Q_{EQ} + \frac{\rho c_p}{r'} (D_z{}' - D_0) \Rightarrow Q_{EP0} = Q_{EQ} + \frac{\rho c_p}{r'} D_z{}' \quad 2.40$$

from which it follows,

$$Q_{EP0} - Q_{EQ} = \frac{\rho c_p}{r'} D_z{}' \Rightarrow D_z{}' = \left(Q_{EP0} - Q_{EQ}\right) \frac{r'}{\rho c_p} \quad 2.41$$

where $D_z{}'$ is $D_z$ at $r'$. By definition, $D_z{}'$ remains unchanged due to surface drying because $\delta T_a$ is zero at $r'$.

Likewise from Equation 2.37,

$$Q_{EP*}{}' - Q_{EQ} = \frac{\rho c_p}{r'} D_z{}' \Rightarrow D_z{}' = \left(Q_{EP*}{}' - Q_{EQ}\right) \frac{r'}{\rho c_p} \quad 2.42$$

Through combination of Equations 2.41 and 2.42, $Q_{EP*}{}' = Q_{EP0}$ at the observed $r'$.

$Q_{EP*}$ will always be larger than $Q_{ER}$ and can thus be easily estimated at a single height of $T$, provided $Q_n$ and $u$ are observed. The solution to Equations 2.31 and 2.28 yields,

$$\frac{\alpha_{PT72*}}{\alpha_{PT72}} = \frac{Q_{EP*}}{Q_{ER}} = 1 + \frac{\gamma}{\Delta + \gamma} \frac{r_c}{r_a} \Rightarrow Q_{EP*} = Q_{ER} \left(1 + \frac{\gamma}{\Delta + \gamma} \frac{r_c}{r_a}\right) = Q_{EQ} + \frac{\rho c_p}{r_a} D_z \quad 2.43$$

$Q_{EP*}$ is unique because measurements can be obtained from a single height in the atmosphere through a single measurement of $D_z$ at the same height. The rate of change from $Q_{EP*}$ as $r_a$ increases with height is only predictable provided $r_c$ is known. However, if one instance of $Q_{EP*}$ is measured then it is assumed to be constant with height and a solution for $D_z{}'$ of varying values of $r_a$ can be obtained, which preserves flux constancy

with height. The theoretical $T$ profile will always intersect with an actual $T$ profile with the corresponding $r_a$ at the measurement height.

For this study, $T_a{}'$was not measured due to resource limitation and theoretical $T_a{}'$were used to calculate $D_z$. The iterative process given by Abbott and Tabony (1985) was used to determine $T_a{}'$. Use of aspirated psychrometers would have bypassed need to model wet-bulb temperature values.

# Chapter 3 Study 1: Comparison of Water and Energy Budgets of a Field and Rooftop in the Humber River Watershed from April to November in 2010 and 2011

## 3.1 Introduction

The urban environment is increasingly becoming more complex from a hydrological perspective due to changes in land use, temperature and weather patterns (Grimmond et al. 1986). Since the industrial revolution, increase of atmospheric temperature of 2 to 4 $^{o}$C is putting greater pressure on access to ecosystem services (Elkin et al. 2013) and water resources (Fung et al. 2011). Although the cause of global temperature increase is due to greater $CO_2$ loading, the increased amount of $CO_2$ may be attributed to factors such as mass migration and increased populations (Evans 2013), which are directly related to increased consumption of many essential environmental resources. However, the relative impact of the individual anthropogenic activities accelerating global climate change is largely unknown on water resources and ecosystem services.

Better understanding the water balance (WB) and surface energy budgets (SEB) of urban areas, in light of recent global climate trends, will play a critical determining feature for future land use planning and decision making (Correa et al. 2012; Dasgupta et al. 2013). The resilience of urban environments to disturbances will be pushed to their limits due to perceived future extreme climate events like enhanced wind velocity and more frequent flooding events (Wang et al. 2012). With the threat of irreversible ecosystem changes, this study was commissioned to compare the WB and SEB of two contrasting land cover types within the Greater Toronto Area (GTA), Ontario, Canada during the ice-free period (April to November) of 2010 and 2011.

Actual evapotranspiration, the mass equivalent of the latent heat flux, was measured using two custom designed multi-tiered Bowen ratio energy budget (BREB) systems. Supplementary evaporation values were calculated using a weighing lysimeter that was constructed by the Toronto and Region Conservation Authority (TRCA) and deployed at the Toronto, Ontario, Canada research site.

The measurement of the latent heat flux in this study uses the BREB technique to quantify $Q_{ER}$, the real or actual latent heat flux as,

$$Q_{ER} = \frac{(Q^* - Q_G)}{(1+\beta)} \quad 3.1$$

where $Q^*$is the net radiation, $Q_G$ is the ground heat flux, and $\beta$ is the Bowen ratio. The latent heat flux measurements are obtained within the fully adjusted boundary layer of the individual research sites (Oke 1987).

It is important for water managers and decision makers to know the amount of actual evapotranspiration from any land cover type because it is the component of the WB that allows linkage to the SEB (Grimmond and Oke 1991; Grimmond and Oke 1999). It has been suggested that evapotranspiration is a surface process that may have been neglected in urban environments because of its perceived small magnitude (Grimmond and Oke 1999). Trout and Ross (2006) contend better understanding and accurate quantification of evapotranspiration from the landscape is critical for hydrological model development and land management.

Grimmond and Oke (1991 and 1999) give a thorough account of the SEB and WB due to the complexity of land cover types they investigated. In the present study, the SEB and WB models were simplified with respect to the instrumentation and research sites so that comparison of the surface-atmosphere interface could be completed during the 2010 and 2011 study periods of the two research sites.

The WB components of the research sites was given as,

$$\Delta S = P - ET - RO \quad 3.2$$

where $P$, the input of water to the system, is precipitation. No water was piped in and irrigation at the research sites was omitted from the WB model. $ET$ and $RO$, evapotranspiration and runoff, respectively are the outputs and $\Delta S$ is the rate of change in storage of the system, all in measurements of mm. Typically, $\Delta S$ is zero over annual time periods and Equation 3.2 can reduce to,

$$P = ET + RO \quad (3.3)$$

$ET$ values were incorporated into Equation 3.4 of each study site by the following relationship,

$$\lambda ET = Q_{ER} \quad (3.4)$$

where $\lambda$ is the latent heat of vaporization in units of J $kg^{-1}$.

The SEB is given as,

$$Q^* = Q_{ER} + Q_H + Q_G \quad (3.5)$$

where $Q_H$ is the sensible heat flux (energy used to heat the atmosphere closest to the surface) in W $m^{-2}$. With Equation 3.4 the linkage between the WB and SEB model becomes clear with respect to the importance of $ET$ in hydrological studies (Grimmond and Oke 1986). Similar to the simplification of Equation 3.3, Equation 3.5 represents a modest SEB model which does not account for anthropogenic heat released by combustion and net heat storage change as documented by Grimmond and Oke (1986) or net heat advection as reported by Grimmond and Oke (1991).

## 3.2 Methods and Materials

### *3.2.1 Study Site*

This study was performed in the Humber River Watershed, within the jurisdiction of the TRCA of the Greater Toronto Area, Ontario, Canada. Map 3.1 shows the Humber River Watershed, the research sites and York University.

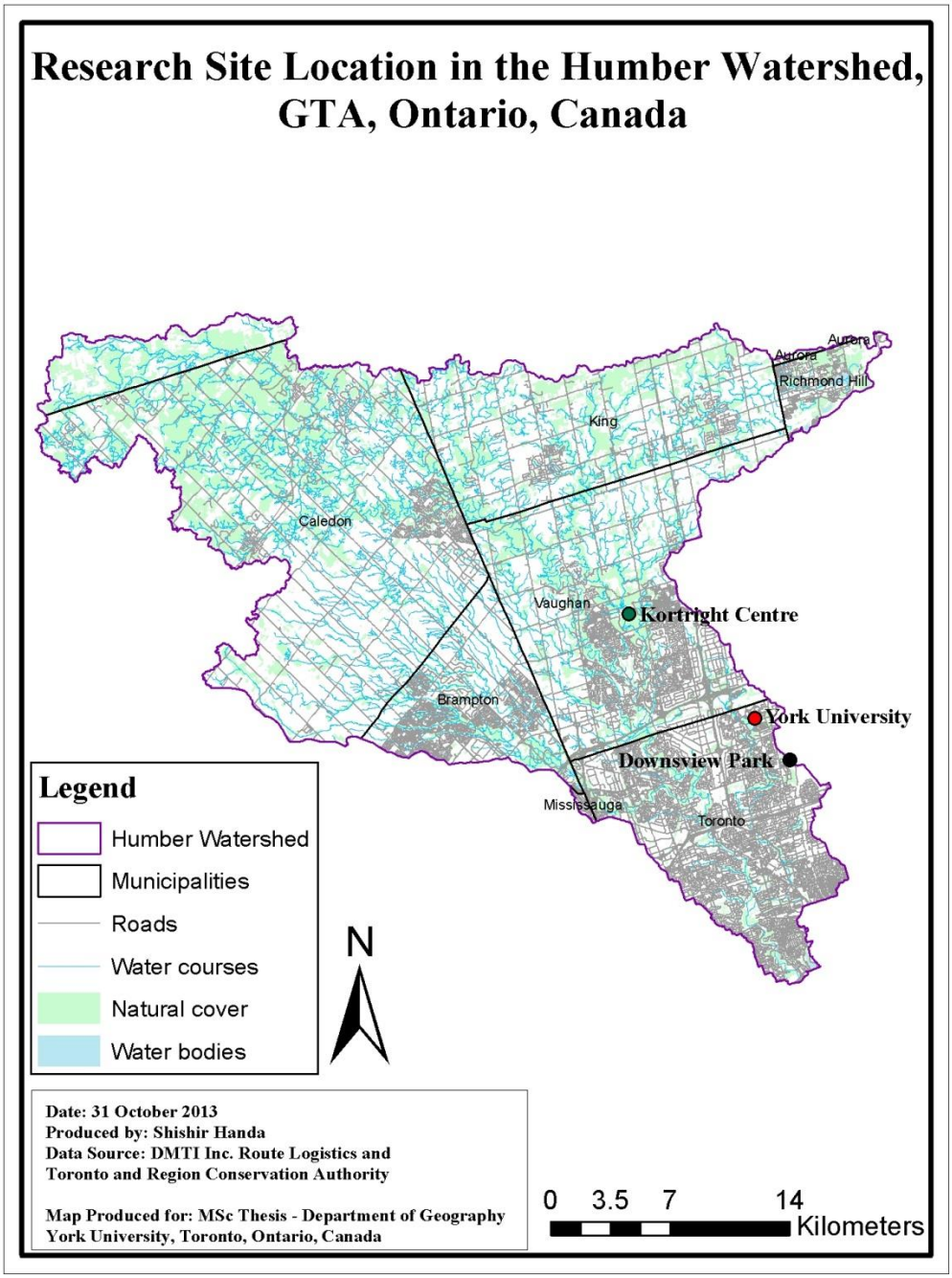


Map 3.1. The map shows the Humber River Watershed and the study sites, in addition to their relative location to York University.

#### *3.2.1.1 Kortright Centre for Conservation*

The research site used as representation of a rural land cover type was located in a field at the northern portion of the Kortright Centre for Conservation (KC), Woodbridge, Ontario, Canada. KC is located at 9550 Pine Valley Road, between Major Mackenzie Drive and Rutherford Road. It is managed and operated by the TRCA. Thus, KC was the control site and its uniqueness, with respect to the land development, represented low urban development.

The herbaceous field of the KC research site is approximately 44 700 $m^2$. Topography of the KC research site is mildly undulating, sloping gently downwards from the northwest to southeast. The coordinate node of the instruments used for modelling the WB and SEB at KC were located at 43°50’7” N latitude and 79°35’34” W longitude. The KC study site ranges in elevation from 200 m to 215 m above sea level. From a watershed scale, KC is located within the Humber River Watershed.

The instrumentation deployment site was chosen with ample fetch to the north, south and east. There is restricted fetch to the west owing to a row of trees mostly comprising of pine. The KC site is unique owing to its status as a controlled-access, naturalizing system. The plant community at the KC experimental site can be characterised as a mix of herbaceous and woody plant species that is gradually being recolonized by southern Ontario native and naturalised plants such Queen Anne’s lace (*Daucus carota*), wild oat grass (*Avena fatua* L), purple vetch (*Vicia americana*), cow vetch (*Vicia cracca*), Canada thistle (*Cirsium arvense*), swamp thistle (*Cirsium muticum*), black-eyed Susan (*Rudbeckia hirta*), red clover (*Trifolium pratense*), New England asters (*Aster novae-angliae*), birdsfoot trefoil (*Lotus corniculatus*), common milkweed (*Asclepias syriaca*), Canadian goldenrod (*Solidago canadensis*) and tall goldenrod (*Solidago altissima*). The KC study site was a fallow field, which was previously planted with Timothy grass (*Phleum pratense*) approximately 10 years prior. The soil matrix has the ability to absorb excess rainfall and plant roots can access soil moisture during the growing season for transpiration, thereby making KC an oasis surrounded by intensive suburban development.

#### *3.2.1.2 Downsview Park*

The Downsview Park (DP) research site, representing an urban, built land cover type, was located near the intersection of Keele Street and Sheppard Avenue in Toronto, Ontario, Canada. The building used at the DP research site can be located at 40 Carl Hall Road. The exact geographic coordinates of the field site can be found at 43° 44.58' 00" N latitude and 79° 28.45' 00" W longitude.

The linear distance separating KC and DP research sites is approximately 20 km. The DP site is a flat rooftop of an extensive triple storey building. The building was originally constructed as a military storage facility for the Canadian Forces Base Downsview, approximately 40 years ago. The area of the DP rooftop is 140 000 m², measuring 200 by 700 m. The DP site represents an impervious surface cover, with no soil to act as a water retention medium. Similarly, the rooftop does not have plants to promote water loss to the atmosphere through transpiration. Both of these characteristics of the roof limit this land surface cover type's capacity to retain excess rainfall for evaporation. The impervious rooftop is covered with a waterproof tar membrane, overlain by 5.715 cm Styrofoam insulation, a semi-permeable fabric layer and then approximately a 5 cm deep layer of course stream bed aggregate. Water collecting on the lower membrane is routed to the stormwater sewer system through roof drains spaced approximately 50 m apart.

### ***3.2.2 Methods***

#### *3.2.2.1 Bowen Ratio Energy Budget Method*

The Bowen Ratio Energy Budget (BREB) approach has its foundations of calculating $Q_{ER}$ in the SEB given by Equation 3.1 (Todd et al. 2000). In this study $Q_{ER}$ was chosen as the flux to be calculated for closure of the SEB at the research sites because of the technical limitations of calculating $Q_H$ with the meteorological instruments and the methodological feasibility presented by Denmead and McIlroy (1970).

The Bowen ratio (1926) is defined as,

$$\beta = \frac{Q_H}{Q_{ER}} \qquad 3.6$$

but was determined using the following relationship,

$$\beta = \gamma \frac{\Delta\theta}{\Delta e} \quad 3.7$$

where $\Delta\theta$ is the potential temperature gradient measured in ℃, $\Delta e$ is the vapour pressure gradient measured in kPa and $\gamma$ is the psychrometric constant, kPa ℃$^{-1}$ computed as,

$$\gamma = \frac{C_p p}{0.622\lambda} \quad 3.8$$

where 0.622 is the ratio of the molecular weight of water, $M_w$ = 18.015 g mol$^{-1}$ to the molecular weight of air, $M_A$ = 28.963 g mol$^{-1}$, and $p$ is the atmospheric pressure measured in kPa (Monteith and Unsworth 1990).

The potential temperature takes into account the dry adiabatic lapse rate of 0.0098 ℃ m$^{-1}$ (Oke 1987) and calculated as,

$$\theta = T_a + 0.0098z \quad 3.9$$

where $T_a$ is the air temperature in $^{o}$C at the reference height.

*3.2.2.2 Lysimeter Method*

For this study, a weighing lysimeter was calibrated in 2010 and used as a supplementary means of evaluating $ET$ from the urban surface type. In November 2011, the lysimeter was able to register its maximum amount of rain held by the roofing material of 10.06 mm. The model presented by Lockwood (1985) was used to calculate drainage ($D$) given as,

$$D = D_s \exp[b_{D_s}(C_{D_s} - S)] \text{ when } C_{D_s} \geq S \text{ and } D = 0 \text{ when } C_{D_s} < S \quad 3.10$$

where $D_s$ is the drainage rate when the canopy storage is at capacity, $C_{D_s}$ is the actual storage of the roofing material, $S$ is the maximum storage capacity and $b_{D_s}$ is an empirical drainage coefficient. Rutter et al. (1971 and 1975) identified the components of the WB that would impact the rainfall interception and when specific surface processes would occur depending on the relationship between $C_{D_s}$ and $S$. The maximum storage capacity of the roof aggregate was found to be 2.1 mm after drainage ceased. The sensitivity of the lysimeter measurements were achievable because of the load capacity of the weighing device allowing changes to be detected to a hundredth of a mm.

### *3.2.3 Equipment*

#### *3.2.3.1 Kortright Centre for Conservation Bowen Ratio Energy Balance System*

BREB systems measure vertical gradients of $T_a$ and vapour pressure ($e$) and scale the gradient measurements to local measurements of net available energy to calculate $Q_{ER}$ (Denmead and McIlroy 1970; Davies 1972). $Q^*$ was measured with a Middleton CN1 net pyrradiometer, 2.75 m above the ground surface and aspirated with dry air supplied by an aquarium pump through a desiccant chamber to limit the amount of moisture condensing on the inside of the polyethylene dome. $Q_G$ was measured directly with a soil heat flux plate (Campbell Scientific Inc., HFT3), buried 2 cm below the soil surface. $T_a$ profiles were measured using shielded copper-constantan thermocouples (Omega: special limits of error type T) that were installed to design specifications of the BREB system. Four measurement levels on the KC BREB system at 0.25, 0.75, 1.50 and 3.00 m above the ground enable gradient measurements. At the same heights $T_a$ was measured, $e$ was calculated by measuring water vapour concentrations with LICOR Biosciences' LI-840 closed-path infrared gas analyzer (IRGA). Figure 3.1 displays the BREB flux station fully deployed at the KC experimental field site.

Figure 3.1. This image displays the Bowen Ratio Energy Budget system, deployed at the Kortright Centre for Conservation experimental research site used to calculate actual evapotranspiration.

Equation 3.1 only requires $\theta$ and $e$ to be measured at a minimum from two levels in the atmosphere to determine gradients but a multi-level system allows redundancy for internal consistency of flux estimates. The multi-level BREB system also provides flux estimates at different spatial scales, if desired (Davies 1972). The highest measurement level of the KC BREB system allowed $Q_{ER}$ to be calculated from an area of 300 m radius, with the assumption of 1:100 height to fetch ratio (Heilman et al. 1989). Ambient air was

sequentially drawn through stainless steel mesh insect filters then down from each of the gradient profile levels through 6.35 mm diameter Bev-A-Line® tubing to minimize gas absorption and diffusion. An aquarium air pump and series of 3 way solenoid valves sequentially purged ambient air at a rate of 0.35 $dm^3$ $min^{-1}$ from each level before gas concentrations were sampled. The ambient air was purged for one minute and then sampled for three minutes on each 15 minute cycle. Hourly averages were computed from four, 15 minute replicate cycles from each measurement height.

Due to use of the same IRGA unit, samples of $e$ at all heights were systematically void of errors because equation 3.13 relies on concentration differences between height measurements. This allowed calculations of $Q_{ER}$ to maintain high accuracy of $e$ gradients. Additionally, the IRGA accuracy was not affected by cross sensitivity to gases, sub-freezing temperatures or hysteresis due to the use of one IRGA unit operating during the ice-free period.

A critical component in the design of the BREB system was the incorporation of self-temperature-regulating 16V AC heating tape (<1.0 W @-30C) attached to each of the flow lines to maintain tubing wall temperatures above dew point temperatures, thereby eliminating periods of condensation. All inlet lines and heating tapes were encapsulated within 5.08 cm polyvinyl chloride tubing and insulted from environmental temperature effects with black, closed-cell polyurethane foam pipe insulation. Inlet air was filtered through a 1 $\mu$m filter before entering the pump, which also provided extended component life to the IRGA and limited the need for recalibration. Solenoid valve switching was accomplished with a Campbell Scientific SDM16 relay control module. Data was logged every five seconds on a Campbell Scientific CR1000 data logger to collect 15 minute averaged values. Data was normally retrieved manually on a weekly basis.

The KC BREB system was initially deployed in August 2008 and several iterations of the photovoltaic solar panel and battery systems have being pursued. During the study period, the solar panels were able to generate 240W to charge the 12V DC marine grade batteries.

#### *3.2.3.2 Toronto and Region Conservation Authority Meteorological Station*

TRCA meteorological station data was used to enable calculations of WB and SEB values. Precipitation records were measured with a Hydrological Service Ltd. TB3 tipping bucket rain gauge (0.2 mm $tip^{-1}$). Atmospheric pressure was measured with an Onset Barometric Pressure Sensor S-BPA-CM10, which provided average atmospheric pressure measurements at the logging interval between the range of 66 and 107 kPa. The TRCA meteorological weather station sensors were semi-automated with Onset's HOBO weather station data logger housed in a weather resistant enclosure.

#### *3.2.3.3 Downsview Park Bowen Ratio Energy Balance System*

The DP BREB system is very similar to the KC BREB system. DP BREB was configured with three levels measuring at 0.25, 0.50 and 1.00 m. $Q^*$ was calculated using the Kipp and Zonen CNR2 net radiometer installed 1.55 m above the roof gravel surface, which measures net solar radiation ($K^*$) and net longwave radiation ($L^*$) independently. Combing the $K^*$ and $L^*$ gives $Q^*$. The DP BREB does not have a meteorological station in close proximity and $p$ and $P$ measurements were integrated into the flux station using a R. M. Young 61025V Barometric pressure transducer and a Davis tipping bucket rain gauge 7852, respectively.

At DP, ambient air was flushed for 30 seconds and then sampled for two minutes at each level for two complete cycles every 15 minutes. Hourly averages were then computed from four 15 minute replicate cycles from each measurement level. DP BREB executes its operations using the Campbell Scientific CR3000 data logger, which is powered by the building through a 110 V AC outlet. Figure 3.2 displays the DP BREB in its full form, deployed on the rooftop.

Figure 3.2. This image displays the Bowen Ratio Energy Balance system, deployed on top of rooftop at Downsview Park research site, used to calculate actual evapotranspiration.

#### *3.2.3.4 Downsview Park Lysimeter*

During the field campaign of 2010, a weighing lysimeter was deployed on the rooftop at the DP research site, immediately adjacent to the DP BREB system. The

custom designed weighing lysimeter consisting of a 30 × 30 cm metal lath basket and Omegadyne model LCCD-50 load cell was constructed in the TRCA workshop. The basket was suspended ~5 mm above the roofing fabric and filled in-situ with the roof gravel removed from the installation site. Measurements of basket weight (± 0.01 mm) were recorded every five seconds for one minute averages at the end of each 15 minute measurement period to determine weight change over each 15 minute measurement interval. The same Campbell Scientific CR3000 data logger used to execute the DP BREB operations was used to record measurements of weight change from the lysimeter. Figure 3.3 shows the custom fabricated lysimeter deployed on the rooftop, adjacent to the DP BREB.

Weighing lysimeter model data was used to supplement DP BREB $ET$ calculations due to solenoid valve closure failure resulting in contamination of IRGA samples. $Q_{ER}$ values at DP were supplemented with $ET$ values from the lysimeter and converted with Equation 3.5 for the months of June – October in 2010 and May – October in 2011.

Figure 3.3. This image displays the weighing lysimeter, deployed on top of the rooftop at the Downsview Park research site adjacent to the Bowen ratio energy balance system, used to model drainage and evaporation from the roofing material.

## 3.3 Results

### *3.3.1 Water Balance*

During both study periods at KC and DP, total *P* values were very similar but monthly values displayed that much spatial variability exists with respect to rain events between the two experimental sites. Distance between the research sites has a significant role with regards to monthly and, subsequently, changes in daily WB components. The receipt of water at KC and DP varied monthly and daily due to geographic separation. Both research sites received comparable and similarly ranging values of total *P* in 2010 and 2011. Strikingly, as seen from comparison of Figures 3.4a and 3.4c, KC and DP in 2010 received the largest input of water in June, close to 200 mm for the month and the least receipt of *P* was experienced in April of 2010 at both research sites. In 2011, KC received the most amount of rain in June (~123 mm) whereas DP had the largest monthly receipt of rain in May (~128 mm). At both research sites in 2011, July experienced the least input of water to the individual research sites, close to 40 mm, making July 2011 exhibit drought-like environmental conditions due to restriction of *P*. As graphically displayed in Figures 3.4b and 3.4d, following the months after July 2011, both KC and DP rebounded with respect to moisture due to sufficient rain events.

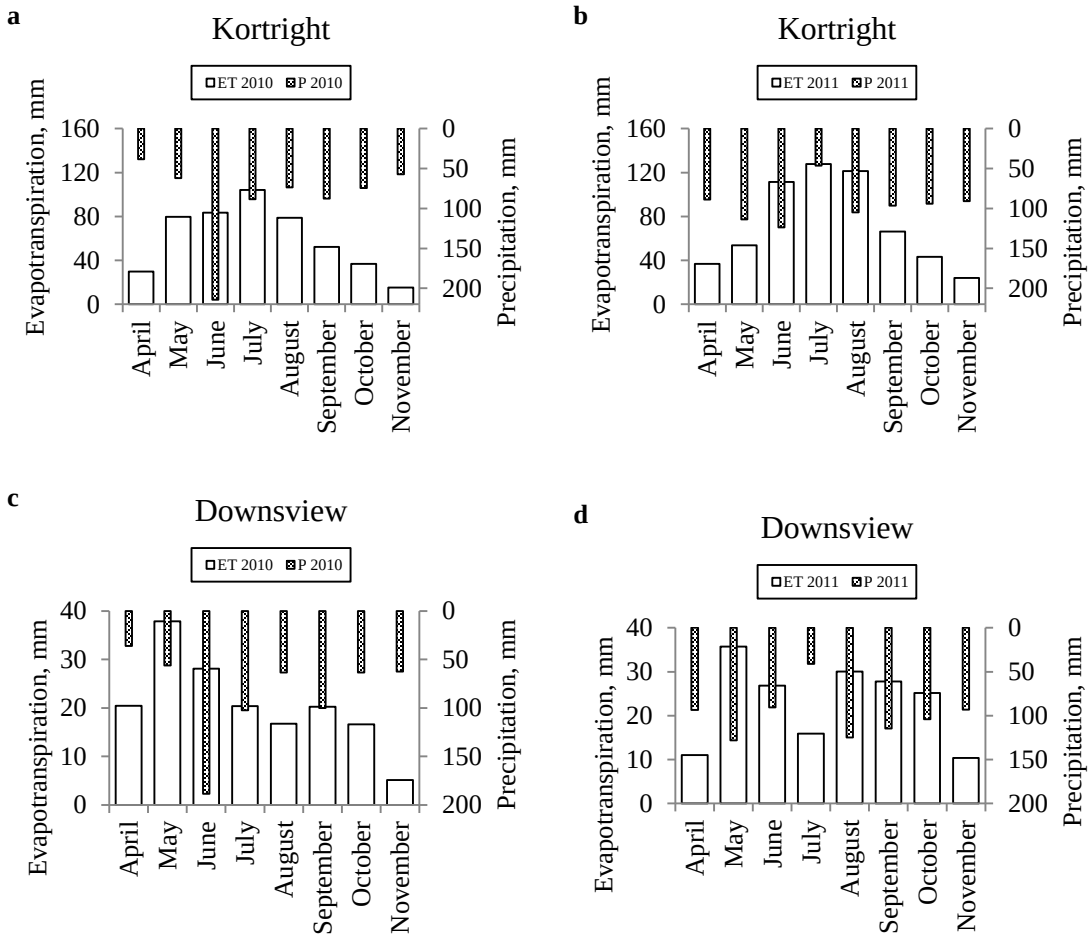


Figure 3.4. Monthly totals of precipitation and evapotranspiration at the field of the Kortright Centre for Conservation from April to November of (a) 2010 and (b) 2011 and from the rooftop of Downsview Park from April to November of (c) 2010 and (d) 2011.

Tables 3.1 and 3.2 display a column with the numerical values of *P* for KC and Tables 3.3 and 3.4 display a column with the numerical *P* values for DP. At both research sites, the 2011 study period received greater input of water than 2010 thereby making the 2011 sampling period wetter than 2010. Comparison of the *P* totals for the study period of 2010 between the contrasting study sites, given by Table 3.1 and 3.3 indicate a difference of approximately 23 mm of rain between KC and DP whereas the absolute difference between tables 3.2 and 3.4 of the *P* totals for the 2011 measurement period between KC and DP was approximately 31 mm. *P* of the two sites were distinctly different monthly and over the individual study periods. DP received >30 mm more rain

than KC in 2011 compared to <20 mm less rain in 2010, suggesting weather pattern variability exists with respect to storm systems on a yearly basis.

Table 3.1. Summary of monthly and study period water balance and energy budget values at the Kortright Centre for Conservation in 2010.

| Kortright 2010 | Temp (°C) | ET (mm) | P (mm) | ET/P | (P-ET)/P | ET ($mm\ d^{-1}$) | Q* ($MJ\ m^{-2}\ d^{-1}$) | QG ($MJ\ m^{-2}\ d^{-1}$) | QH ($MJ\ m^{-2}\ d^{-1}$) | QER ($MJ\ m^{-2}\ d^{-1}$) | Bowen Ratio |
|---|---|---|---|---|---|---|---|---|---|---|---|
| **April** | 10.21 | 29.8 | 38.4 | 0.78 | 0.22 | 0.99 | 10.561 | 4.653 | 3.425 | 2.482 | 1.38 |
| **May** | 15.19 | 79.5 | 62.0 | 1.28 | -0.28 | 2.57 | 13.130 | 4.211 | 2.569 | 6.350 | 0.40 |
| **June** | 18.30 | 83.5 | 214.4 | 0.39 | 0.61 | 1.45 | 13.230 | 3.644 | 2.656 | 6.930 | 0.38 |
| **July** | 22.16 | 104.1 | 88.4 | 1.18 | -0.18 | 3.36 | 15.164 | 3.720 | 3.463 | 7.981 | 0.43 |
| **August** | 20.73 | 78.7 | 73.4 | 1.07 | -0.07 | 2.54 | 12.115 | 2.619 | 3.251 | 6.245 | 0.52 |
| **September** | 15.11 | 52.2 | 87.6 | 0.60 | 0.40 | 1.74 | 7.269 | 0.788 | 2.230 | 4.251 | 0.52 |
| **October** | 8.61 | 36.8 | 74.4 | 0.49 | 0.51 | 1.19 | 4.389 | -0.466 | 1.952 | 2.902 | 0.67 |
| **November** | 2.81 | 15.1 | 57.0 | 0.27 | 0.73 | 0.50 | 2.202 | -0.768 | 1.781 | 1.189 | 1.50 |
| **Overall** | **14.14** | **479.7** | **695.6** | **0.69** | **0.31** | **1.79** | **9.757** | **2.300** | **2.666** | **4.791** | **0.56** |

*underlined values indicate total values; all other values are averages.

Table 3.2. Summary of monthly and study period water balance and energy budget values at the Kortright Centre for Conservation in 2011.

| Kortright 2011 | Temp (°C) | ET (mm) | P (mm) | ET/P | (P-ET)/P | ET (mm d$^{-1}$) | Q* (MJ m$^{-2}$ d$^{-1}$) | QG (MJ m$^{-2}$ d$^{-1}$) | QH (MJ m$^{-2}$ d$^{-1}$) | QER (MJ m$^{-2}$ d$^{-1}$) | Bowen Ratio |
|---|---|---|---|---|---|---|---|---|---|---|---|
| **April** | 6.22 | 36.7 | 88.6 | 0.41 | 0.59 | 1.22 | 7.577 | 1.903 | 2.632 | 3.042 | 0.87 |
| **May** | 13.92 | 53.8 | 113.8 | 0.47 | 0.53 | 1.74 | 9.478 | 3.040 | 2.192 | 4.246 | 0.52 |
| **June** | 18.33 | 111.3 | 123.6 | 0.90 | 0.10 | 3.71 | 13.525 | 2.545 | 1.881 | 9.099 | 0.21 |
| **July** | 22.89 | 127.8 | 46.4 | 2.76 | -1.76 | 4.12 | 15.230 | 2.234 | 2.941 | 10.055 | 0.29 |
| **August** | 19.76 | 121.4 | 104.8 | 1.16 | -0.16 | 3.92 | 12.373 | 1.122 | 1.743 | 9.508 | 0.18 |
| **September** | 15.99 | 66.2 | 96.4 | 0.69 | 0.31 | 2.21 | 8.505 | 0.780 | 2.409 | 5.316 | 0.45 |
| **October** | 9.00 | 43.3 | 94.0 | 0.46 | 0.54 | 1.40 | 4.595 | -0.642 | 1.746 | 3.491 | 0.50 |
| **November** | 5.28 | 24.1 | 90.6 | 0.27 | 0.73 | 0.80 | 2.432 | -0.382 | 0.880 | 1.934 | 0.46 |
| **Overall** | **13.92** | **584.7** | **758.2** | **0.77** | **0.23** | **2.39** | **9.214** | **1.325** | **2.053** | **5.836** | **0.35** |

*underlined values indicate total values; all other values are averages.

Table 3.3. Summary of monthly and study period water balance and energy budget values at the Downsview park rooftop in 2010.

| Downsview 2010 | Temp (°C) | ET (mm) | P (mm) | ET/P | (P-ET)/P | ET (mm d$^{-1}$) | Q* (MJ m$^{-2}$ d$^{-1}$) | QG (MJ m$^{-2}$ d$^{-1}$) | QH (MJ m$^{-2}$ d$^{-1}$) | QER (MJ m$^{-2}$ d$^{-1}$) | Bowen Ratio |
|---|---|---|---|---|---|---|---|---|---|---|---|
| **April** | 8.59 | 20.5 | 36.1 | 0.57 | 0.43 | 0.68 | 9.421 | -0.346 | 8.075 | 1.692 | 4.77 |
| **May** | 14.22 | 38.0 | 56.0 | 0.68 | 0.32 | 1.23 | 11.605 | -0.064 | 8.655 | 3.014 | 2.87 |
| **June** | 17.49 | 28.1 | 188.4 | 0.15 | 0.85 | 0.94 | 12.179 | 0.089 | 9.790 | 2.300 | 4.26 |
| **July** | 21.77 | 16.8 | 102.3 | 0.16 | 0.84 | 0.54 | 12.345 | 0.064 | 10.956 | 1.325 | 8.27 |
| **August** | 20.36 | 16.8 | 63.4 | 0.26 | 0.74 | 0.54 | 9.858 | -0.005 | 8.537 | 1.326 | 6.44 |
| **September** | 14.87 | 20.3 | 100.1 | 0.20 | 0.80 | 0.68 | 6.185 | -0.217 | 4.740 | 1.662 | 2.85 |
| **October** | 8.85 | 16.7 | 63.5 | 0.26 | 0.74 | 0.54 | 3.464 | -0.379 | 2.512 | 1.331 | 1.89 |
| **November** | 3.83 | 5.1 | 62.3 | 0.08 | 0.92 | 0.17 | 1.387 | -0.632 | 1.593 | 0.427 | 3.73 |
| **Overall** | **13.75** | **162.4** | **672.2** | **0.24** | **0.76** | **0.67** | **8.306** | **-0.186** | **6.857** | **1.635** | **4.20** |

*underlined values indicate total values; all other values are averages.

Table 3.4. Summary of monthly and study period water balance and energy budget values at the Downsview park rooftop in 2011.

| Downsview 2011 | Temp (°C) | ET (mm) | P (mm) | ET/P | (P-ET)/P | ET (mm d$^{-1}$) | Q* (MJ m$^{-2}$ d$^{-1}$) | QG (MJ m$^{-2}$ d$^{-1}$) | QH (MJ m$^{-2}$ d$^{-1}$) | QER (MJ m$^{-2}$ d$^{-1}$) | Bowen Ratio |
|---|---|---|---|---|---|---|---|---|---|---|---|
| **April** | 7.33 | 11.0 | 93.5 | 0.12 | 0.88 | 0.37 | 7.459 | -0.323 | 6.875 | 0.906 | 7.59 |
| **May** | 15.05 | 35.7 | 128.0 | 0.28 | 0.72 | 1.15 | 9.561 | -0.084 | 6.806 | 2.839 | 2.40 |
| **June** | 20.48 | 26.9 | 90.7 | 0.30 | 0.70 | 0.90 | 12.552 | 0.105 | 10.252 | 2.195 | 4.67 |
| **July** | 25.73 | 15.9 | 41.1 | 0.39 | 0.61 | 0.51 | 12.517 | 0.081 | 11.181 | 1.254 | 8.92 |
| **August** | 22.68 | 30.0 | 124.7 | 0.24 | 0.76 | 0.97 | 9.992 | -0.049 | 7.670 | 2.370 | 3.24 |
| **September** | 18.11 | 27.8 | 114.5 | 0.24 | 0.76 | 0.93 | 7.071 | -0.208 | 5.003 | 2.275 | 2.20 |
| **October** | 11.06 | 25.1 | 104.0 | 0.24 | 0.76 | 0.81 | 3.247 | -0.451 | 1.691 | 2.007 | 0.84 |
| **November** | 7.00 | 10.4 | 93.0 | 0.11 | 0.89 | 0.35 | 1.267 | -0.504 | 0.910 | 0.862 | 1.06 |
| **Overall** | **15.93** | **182.9** | **789.5** | **0.23** | **0.77** | **0.75** | **7.958** | **-0.179** | **6.299** | **1.838** | **3.43** |

*underlined values indicate total values; all other values are averages.

Evapotranspiration at KC and DP were markedly different during both study periods. From a general perspective, $ET$ differed by ~315 mm in 2010 between KC and DP and ~400 mm in 2011 indicating, from a WB framework, the KC research site experienced greater evaporative loss of water than DP. From the $RO$ perspective, DP exhibited ~294 mm more water drawn into $RO$ in 2010 than KC whereas in 2011 the difference between $RO$ values between DP and KC was ~433 mm. This clearly represents from a WB framework that built-up surface cover types, like the rooftop at DP, have a greater ability of directing the input of water into $RO$.

Figures 3.5a and 3.5c display the monthly and overall $ET$ as a proportion of $P$ at KC and DP for the 2010 and 2011 study periods, respectively. At DP, the $ET$ ratio is very well controlled and most ratio values do not exceed the 40% limit, except for two cases in 2010 of April and May where $ET$ ratio were 57% and 68%, respectively. Minima values of the $ET$ ratio at both KC and DP during both study periods occur in the month of November. This is due to restricted $P$ events, lower $T_a$ and change of yearly seasonal weather conditions. At KC, the vegetation would have stopped photosynthesizing; omitting transpiration from the WB and making the vegetated field site respond similarly to a built impervious structure like the DP rooftop, granted the soil water capacity was approaching or at field capacity. At KC 69% and 77% of $P$ went into $ET$ whereas 24% and 23% of $P$ was consumed by evaporation at DP during the 2010 and 2011 ice-free period, respectively. This clearly signals that KC exhibits greater potential to promote evaporative water loss than DP during the ice-free period in the Greater Toronto Area. Built-up areas increase the amount of $RO$ and reduce $ET$, leading to greater maximum surface water flows and lower minimum flows due to the transformation of pervious structures to impervious surface covers.

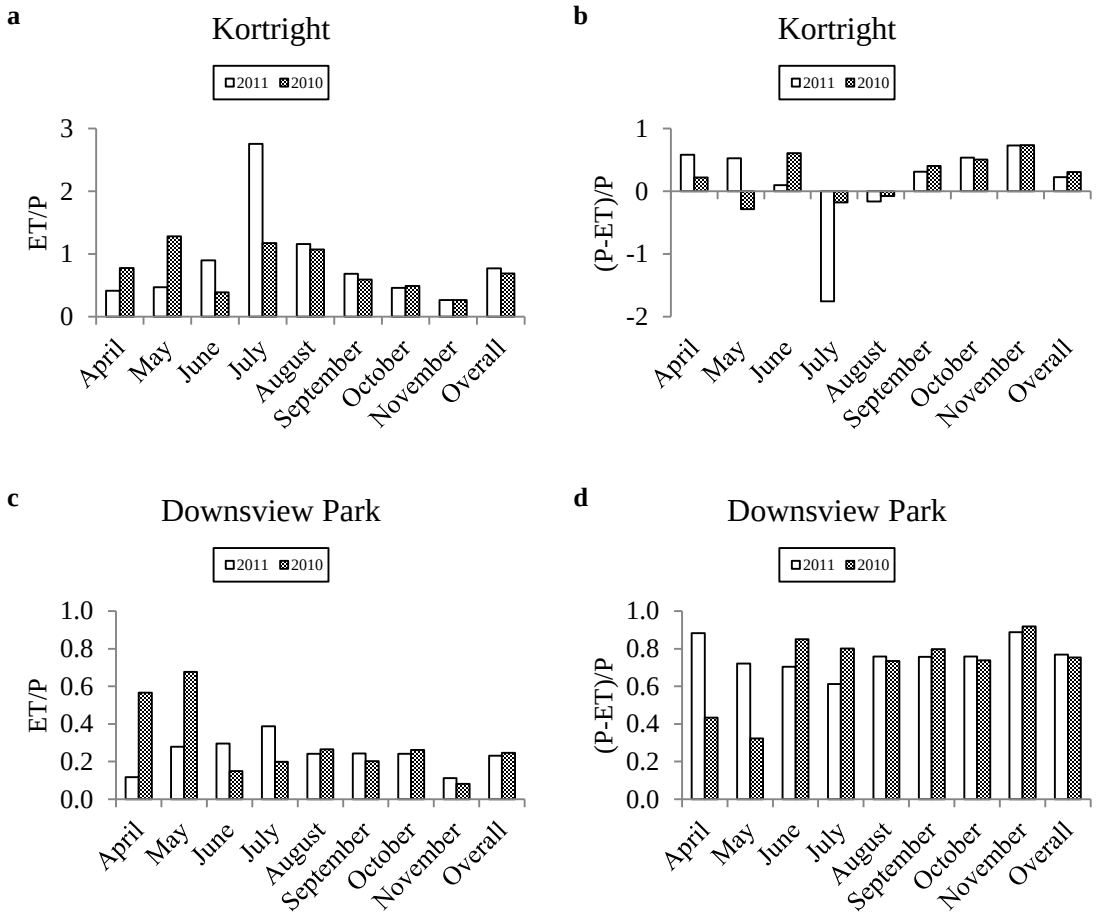


Figure 3.5. (a) Monthly ratio of evapotranspiration with respect to precipitation and (b) monthly ratio difference between precipitation and evapotranspiration with respect to precipitation at the field of the Kortright Centre for Conservation from April to November of 2010 and 2011. (c) Monthly ratio of evapotranspiration with respect to precipitation and (d) monthly ratio difference between precipitation and evapotranspiration with respect to precipitation at the rooftop of Downsview Park from April to November of 2010 and 2011.

Similar to the $ET$ ratio given by Figures 3.5a and 3.5c, $RO$ ratios were calculated as the difference between $P$ and $ET$ as a proportion of $P$. The bar graphs of the KC and DP $RO$ ratios, respectively, for 2010 and 2011 are displayed in Figures 3.5b and 3.5d. As stated above with respect to the $ET$ ratio, the DP $RO$ ratio was very similarly responding from month to month and year to year, where majority of the values ranged from 60% to 90%. However, two noticeable cases that fell below this range occurred in 2010 of April

and May, which experienced $RO$ ratio values of 43% and 32%, respectively. One of the central factors contributing to the high $RO$ ratios and low $ET$ ratios on the rooftop was the low water retention of the roofing material and absence of a soil medium. Receipt of water from rainfall was directly channelled into the drain and stormwater sewer system as soon as storage capacity limits were reached. Once the $P$ carrying capacity of the roof medium is achieved, excess rainfall begins to drain into the roof drainage system and interceptive capture of the roofing material is beyond the storage capacity limit. This characteristic of the DP site is representative of urban built form, particularly large industrial buildings that use comparable roofing design.

As a general observation, the $ET$ ratio and $RO$ ratio were more variable at KC than DP, regardless of month or study year. Figure 3.5b illustrates the variable nature of the KC research site and difficultly recognizing clear patterns of the WB. It is indicative that $ET$ was greater at KC than at DP during the two study periods, as given by comparison of Tables 1, 2, 3 and 4 and Figures 3.4a, 3.4b, 3.4c, 3.4d, 3.5a, 3.5c, 3.6a and 3.6c. Figure 3.5b visually depicts the monthly and overall study period $RO$ ratios at KC. Both July and August, during the 2010 and 2011 research campaigns, experienced negative $RO$ ratio values, signifying $ET$ was greater than $P$ and soil water reservoirs were strongly drawn upon. The soil water reservoir in July 2011 was much more strongly relied upon than any of the other negative $RO$ ratios, at -176%, signalling great water stress at KC. After August, 2010 and 2011, $RO$ ratios stabilized and maintained positive values and did not exceed 73%. The magnitude of the $RO$ ratio to the $ET$ ratio at KC was 0.45 and 0.30 in 2010 and 2011, respectively, whereas in the same years at DP the magnitudes of ratios were 3.17 and 3.35. The magnitudes of the ratios between the contrasting sites represent the impact difference in land-use contributes to the partitioning of water input to the output components of the WB model.

### *3.3.2 Lysimeter*

Lysimeter drainage coefficients were determined based on nocturnal time intervals after rainfall ceased when weight changes would reflect drainage rates alone.

Lockwood (1985) suggests that drainage calculation empiricism only impacts $ET$ calculations by affecting the amount of time needed to dry the surface after rain events. The drainage coefficient, $D_s$ was found to be 0.0004 mm min$^{-1}$ for the aggregate material on the rooftop. Lockwood (1985) reported the elements of the evaporation-interception model of forests focussing on the drainage components and supported the findings by Rutter et al. (1971) of the Corsician pine (*Pinus nigra*) stand research. As expected, the coefficients determined for the rooftop differ from the forest studies.

### *3.3.3 Surface Energy Budget*

Full closure of the SEB is achievable, provided $Q^*$ and $Q_G$ are measured accurately and $Q_{ER}$ is accurately quantified, thereby reducing errors that may be present in flux measurements (Cleugh and Oke 1986). The energy consumed by photosynthesis in the SEB was neglected because of its miniscule impact on surface energy processes (Davies and McCaughey 1968). This then allows for an understanding of the partitioning of net available energy using indices like the Bowen ratio, $\beta$.The Bowen ratio is highly descriptive where values that are $< 1$ indicate the dominant SEB process consuming $Q_n$ is $Q_{ER}$. When $\beta = 1$, $Q_H$ and $Q_{ER}$ are equally consuming $Q_n$ and neither SEB process is dominant. When $\beta > 1$, $Q_H$ is the dominant SEB process, indicating restricted available surface water is being used to increase surface temperature and promote the sensible heat flux as the dominant energy pathway.

The values of $Q_{ER}$ exhibit inaccuracy when $\beta \rightarrow -1$ during periods close to sunrise and sunset due to $T_a$ and $e$ inversions (Fritschen 1965). This happens because either $Q_H$ or $Q_{ER}$ is equivalent in magnitude but one of the fluxes is inverted with respect to the direction of the energetic flow. Due to the limitation of the BREB system with respect to environmental thermodynamic changes, error limitation algorithms were applied based on documented results of Bowen ratio error analysis (Fuchs and Tanner 1970; Sinclair et al. 1975; Ohmura 1982).

Steduto and Hsiao (1998) identified the limit of $Q_{ER}$ when the aerodynamic conductance goes to zero is known as $Q_{EQ}$. $Q_{ER}$ becomes infinitely small and not

representative of true water vapour fluxes. Dependence of the evaporation process is then controlled by the energetic term of the PM model. During specific time periods and based on the Bowen ratio error analysis theory used to substitute incorrect BREB $Q_{ER}$ values, $Q_{EQ} = \frac{\Delta}{\Delta+\gamma}(Q^* - Q_G)$ was calculated as a surrogate for inconsistencies only at KC.

During the study, to compute $Q_{ER}$ values, eddy transfer coefficients were assumed equal for water vapour and heat (Sinclair et al. 1975). Davies and McCaughey (1968) assert that transfer coefficients will be highly variable depending on wind velocity and atmospheric stability. Thus, the BREB method benefits from the proven similarities of the transfer coefficients which cancel out in the Bowen ratio but remain problematic in the individual relationships for $Q_{ER}$ and $Q_H$ calculations (Davies and McCaughey 1968; Sinclair et al. 1975).

Figures 3.6b and 3.6d visually display the $\beta$ monthly and ice-free season values for 2010 and 2011 at KC and DP, respectively. Bowen ratio values differed markedly between the research sites. Bowen ratio values were also variable on monthly and overall study period basis at the individual sites from year to year. DP experienced overall, ice-free seasonal $\beta$ values between 3.0 and 4.5 in 2011 and 2010, respectively whereas KC ranged from 0.3 to 0.6 in the same years. At DP, July exhibit the greatest $\beta$ values as can be seen from Tables 3.3 and 3.4, where the 2011 value was the largest, thereby signifying $Q_H$ was the dominant consumer of $Q_n$ during July. The only occurrence when $\beta$ is below unity at DP is October of 2011 at 0.84, whereby $Q_H$ was out competed by $Q_{ER}$ as the dominant consumer of $Q_n$ for the month. The $\beta$ value at DP for November 2011 was only marginally above unity, 1.06, signalling $Q_H$ for the month was only slightly more dominant than $Q_{ER}$.

For majority of the study period at KC, during both 2010 and 2011, $\beta$ was less than unity, indicating the dominant SEB process consuming $Q_n$was $Q_{ER}$. Due to this observation of $\beta$ values at KC being regularly less than unity, $ET$ was the dominant WB output from the field. This result is in agreement with Cleugh and Oke (1986) who observed less than one $\beta$ values and dominance of $ET$, thereby out competing other hydrological processes at their rural site. At KC in 2010, April and November were the

only months that exhibit $\beta$ values greater than one, signalling that availability of water for $ET$ was restricted and $Q_{ER}$ was dampened whilst $Q_H$ was enhanced. The lowest $\beta$ values at KC in 2010 and 2011 were experienced in June of 0.38 and August of 0.18, respectively.

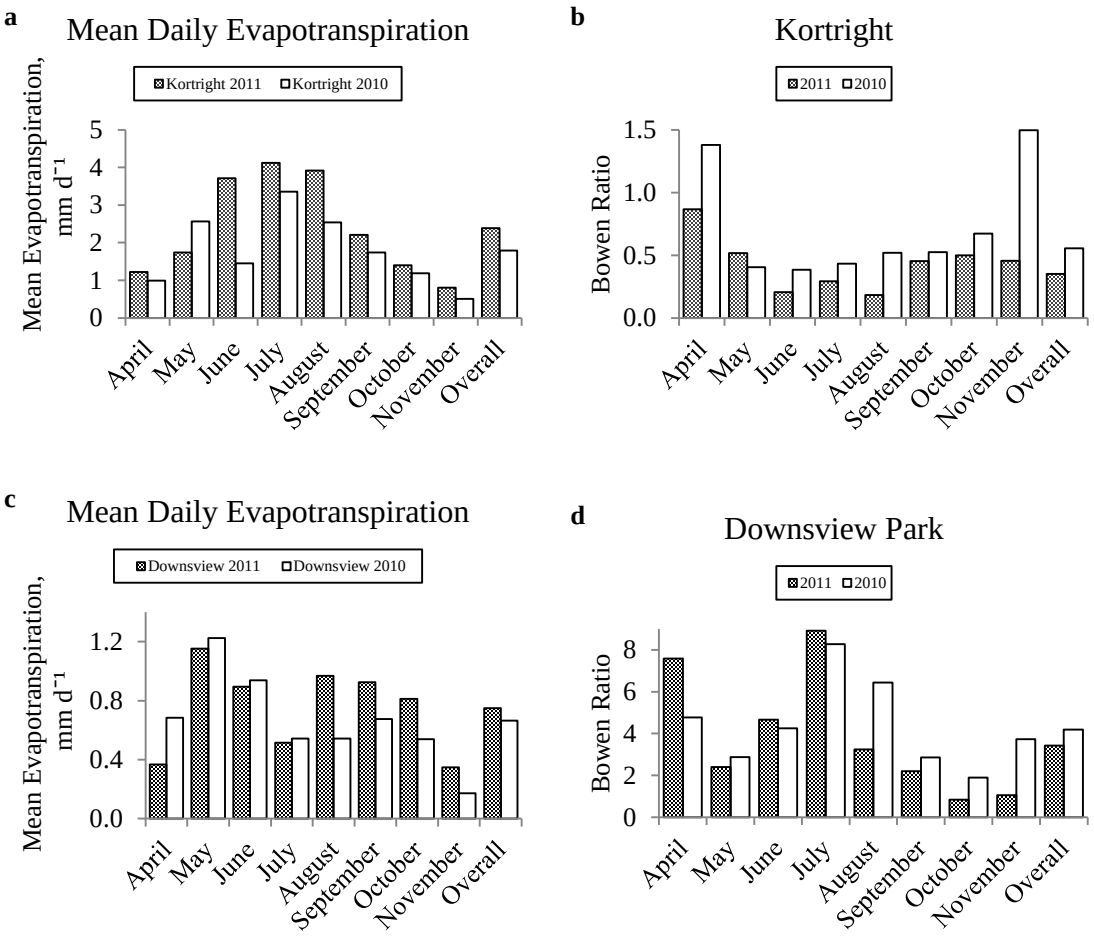


Figure 3.6. (a) Average daily evapotranspiration and (b) average monthly and study period Bowen Ratio at the field of the Kortright Centre for Conservation from April to November of 2010 and 2011. (c) Average daily evapotranspiration and (d) average monthly and study period Bowen Ratio at the rooftop of Downsview Park from April to November of 2010 and 2011.

## 3.4 Discussion

Hossen et al. (2012) state it is important to identify the different pathways the SEB is partitioned to better understand regional climates. Similarly, Correa et al. (2012),

Pearlmutter et al. (2005, 2009) all remark the SEB assessment is fundamental for understanding how the urban environment and urban design partition energy into the various energetic pathways. Figures 3.7a and 3.7b display the study period average daily fluxes of the SEB processes at KC for 2010 and 2011, respectively. July $Q^*$ yielded the greatest measured values at KC for 2010 and 2011 of 15.164 and 15.230 MJ $m^{-2}$ $d^{-1}$, respectively. Tables 3.1 and 3.2 and Figures 3.7a and 3.7b display $Q^*$ at KC for 2010 and 2011 were lowest in November. This is due to shift in geometry of the sun-Earth relationship and change of seasons transitioning from fall and approaching winter (Oke 1987). $Q_G$ at KC during both study periods was positive except for October and November. September at KC for the 2010 and 2011 study period years exhibit the lowest positive $Q_G$ values because of the transition to negative values in the following months.

Figures 3.7c and 3.7d display the daily average fluxes of the SEB processes at DP for 2010 and 2011, respectively. At DP in 2010, $Q^*$ peaked at 12.345 MJ $m^{-2}$ $d^{-1}$, which was only 0.166 MJ $m^{-2}$ $d^{-1}$ less than June as the second greatest receipt of $Q^*$ during the study period. In 2011, $Q^*$ peaks reversed roles between June and July at DP. June received the largest quantity of $Q^*$ with 12.552 MJ $m^{-2}$ $d^{-1}$, only being marginally larger than the second highest receipt of $Q^*$ during the 2011 study period at DP of 0.035 MJ $m^{-2}$ $d^{-1}$. Greatest receipt of $Q^*$ at DP interchanged between July and June during the 2010 and 2011 study periods, respectively. Similar to KC, DP experienced reduction of $Q^*$ from approximately August and onwards. Ground heat flux at DP does not exhibit the same pattern as KC. Only June and July of 2010 and 2011 exhibit positive $Q_G$ values indicating the flux was directed towards the building. Hypothetically, majority of the negative $Q_G$ values could be due to the internal temperature of the building being greater than the roof surface.

Net available energy at both KC and DP sharply decline after August during both study periods. The cause of $Q_n$ increasingly being restricted after August at both research sites can be attributed to the lower receipt of $Q^*$. Negative $Q_G$ values contribute to enhancing the amount of $Q_n$ to promote $Q_H$ or $Q_{ER}$ and thus the greatest influence of reduced $Q_n$ is due strictly to the reduced amount of $Q^*$.

The latent heat flux dominated the SEB at KC in both years whereas $Q_H$ dominated at DP over the same timeframe. As stated above, DP is a very well controlled surface cover type and can easily be predicted with respect to WB interactions and SEB components. The sensible heat flux ranged from approximately 11.0 to 1.0 MJ $m^{-2}$ $d^{-1}$ at DP, whereas $Q_{ER}$ ranged from approximately 3.0 to 0.5 MJ $m^{-2}$ $d^{-1}$ during both ice-free study periods. This shows that $Q_n$ on top of the rooftop was consumed largely by $Q_H$. The sensible heat flux was greater during 2011 than 2010 at DP and this may be indicative of the higher average $T_a$ values measured from the temperature profile, as shown in table 4. At KC, $Q_{ER}$ was the dominant consumer of $Q_n$ but the range of $Q_{ER}$ was larger in 2011 than 2010. The latent heat flux ranged from approximately 10.0 to 1.1 MJ $m^{-2}$ $d^{-1}$ at KC, whereas $Q_H$ ranged from approximately 3.5 to 0.8 MJ $m^{-2}$ $d^{-1}$ during both ice-free study periods. Terrestrial water fluxes are dominated by transpiration and this was verified by Jasechko et al. (2013) who used isotopes to show that transpiration is the dominant control mechanism for the loss of water to the atmosphere.

There are only two instances at KC during the 2010 study period when $Q_H$ is greater than $Q_{ER}$. April and November of 2010 at KC experienced $Q_{ER}$ lower than $Q_H$, as displayed in Figure 3.7a. Net radiation in April of 2010 at KC is very large compared to the 2011 values of the same month. This is due to the increased number of cloudy days in 2011 compared to the many days of fewer cloud periods in April of 2010 at KC. The April $Q_G$ is similarly higher by 2.750 MJ $m^{-2}$ $d^{-1}$ in 2010 than 2011 in addition to only slightly more $Q_n$ of approximately 0.234 MJ $m^{-2}$ $d^{-1}$, to be partitioned into the SEB processes, of the same years. From 2010 to 2011 at KC, $Q_H$ and $Q_{ER}$ exhibit role reversals as $Q_H$ dominates in 2010 for April and November but not for the 2011 study period. Net radiation and $Q_G$ for November in both study period years were very similar. The difference between $Q_n$ for November 2010 and 2011 was only 0.156 MJ $m^{-2}$ $d^{-1}$, which may be viewed as important given that $Q_n$ during November of any study period year was very small.

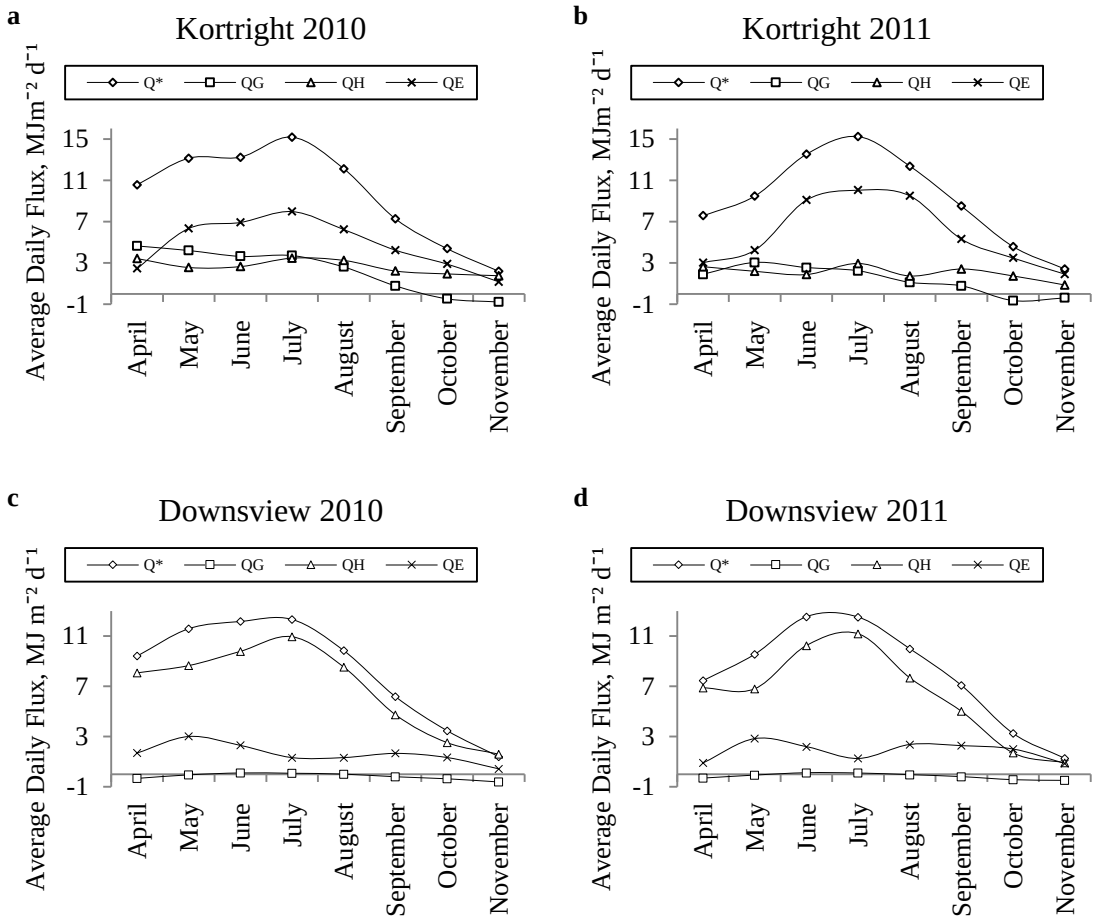


Figure 3.7. Surface energy budget of the field at the Kortright Centre for Conservation from April to November of (a) 2010 and (b) 2011 and of the rooftop of Downsview Park from April to November of (c) 2010 and (d) 2011.

The Bowen ratio energy budget technique provides robust, accurate, and dependable, hourly, daily and seasonal estimates of actual evapotranspiration (Todd et al. 2000). The evaporative fraction, the proportion of $Q^*$ consumed by $Q_{ER}$, was always greater at KC than DP regardless of month or ice-free season, granted comparison is made with respect to similar study period year. Table 3.5 displays the numerical values of the evaporative fraction values for both research sites and study periods.

Table 3.5. Evaporative Fraction at Kortright Centre for Conservation and Downsview Park for 2010 and 2011.

| QER/Q* | Kortright 2010 | Kortright 2011 | Downsview 2010 | Downsview 2011 |
|---|---|---|---|---|
| April | 0.235 | 0.401 | 0.180 | 0.121 |
| May | 0.484 | 0.448 | 0.260 | 0.297 |
| June | 0.524 | 0.673 | 0.189 | 0.175 |
| July | 0.526 | 0.660 | 0.107 | 0.100 |
| August | 0.515 | 0.768 | 0.135 | 0.237 |
| September | 0.585 | 0.625 | 0.269 | 0.322 |
| October | 0.661 | 0.760 | 0.384 | 0.618 |
| November | 0.540 | 0.795 | 0.307 | 0.680 |
| Overall | 0.491 | 0.633 | 0.197 | 0.231 |

## 3.5 Conclusion

Average Bowen ratios differed markedly between the research sites. Downsview experienced seasonal Bowen ratio values between 3.0 and 4.5 and Kortright ranged from 0.3 to 0.6. The net available energy at the Downsview rooftop was consumed by the sensible heat flux whereas at Kortright the latent heat flux was the dominant consumer of the net available energy. Although this conclusion has been hypothesised by other researchers, the magnitude of difference between the energetic fluxes was never empirically identified because those research sites were blended surface cover types and could be identified as experiencing heterogeneous surface structure. This study was able to analyze the surface energy budget of homogenous surface cover types that were within the full adjusted boundary layer.

Kortright evaporated 69% and 77% of precipitation, whereas Downsview generated 24% and 23% of evaporation, in 2010 and 2011 respectively. Although, monthly and daily precipitation events were variable between the two research sites overall study period totals were very comparable suggesting that climate and weather patterns influencing the research sites in the GTA are similar. With respect to water output ratios of water input, the rooftop generated greater runoff ratios on monthly and

during the ice-free study period, averaging 76.5% whereas the field averaged runoff ratios of 27% for the 2010 and 2011 study periods.

The lysimeter deployed on the rooftop, to simulate evaporation-interception, proved useful and allowed for $ET$ flux estimates to be calculated. The success of the lysimeter gives confidence that the urban environment may be outfitted with alternative hydrological instruments to model the evaporation-interception, granted that opportunities exist. The roof gravel experienced a drainage rate of 0.0004 mm $min^{-1}$ which is highly likely not to be the same of the vegetated cover type.

There has never been a study of this magnitude performed in the GTA and thereby has set the baseline for future climatological and hydrological studies for the southern Ontario region. Comparable datasets of this length have never been achieved in the GTA and it is encouraging that the water balance and surface energy budget could be compared of the extreme end points of land development for consecutive years. The uniqueness of the research sites used in this study is rare where prohibited access was granted of a rural and urban land cover types, especially in one of the most populated regions of Canada. There are few urban $ET$ flux studies and will become more important as pressure for urban development increases. The comparison of contrasting land cover types of this magnitude and with comparable climate conditions is the only one of its kind in the world because of the access to these unique research sites. In conclusion, comparison of a rural and urban surface cover has presented that built-up areas are increasing the amount of runoff and reducing evaporative loss of water.

## 3.6 References


Bowen, I. S. 1926. The ratio of heat losses by conduction and by evaporation from any water surface. *Physical Review*, 27, 779 – 787.

Cleugh, H. A. and Oke, T. R. 1986. Suburban-rural energy balance comparisons in summer for Vancouver, B. C. *Boundary-Layer Meteorology*, 36, 351 – 369.

Correa, E., Ruiz, M. A., Canton, A., and Lesino, G. 2012. Thermal comfort in forested urban canyons of low building density – An assessment for the city of Mendoza, Argentina. *Building and Environment*, 58, 219 – 230.

Davies, J. A. 1972. Actual, potential and equilibrium evaporation for a beanfield in southern Ontario. *Agricultural Meteorology*, 10, 331 – 348.

Davies, J. A. and McCaughey, J. H. 1968. Potential evapotranspiration at Simcoe, southern Ontario. *Archiv für Meteorologie, Geophysik und Bioklimatologie Serie B*, 16 (4), 391 – 417.

Denmead, O. T. and McIlroy, I. C. 1970. Measurements of non-potential evaporation from wheat. *Agricultural Meteorology*, 7, 285 – 302.

Elkin, C., Gutiérrez, A. G., Leuzinger, S., Manusch, C., Temperli, C., Rasche, L., and Bugmann, H. 2013. A 2  warmer world is not safe for ecosystem services in the European Alps. *Global Change Biology*, 19, 1827 – 1840.

Fritschen, L. J. 1965. Accuracy of evapotranspiration determinations by the Bowen ratio method. *Hydrological Science Journal*, 10 (2), 38 – 48.

Fuchs, M. and Tanner, C. B. 1970. Error analysis of Bowen ratios measured by differential psychrometry. *Argicultural Meteorology*, 7, 329 – 334.

Fung, F., Lopez, A., and New, M. 2011. Water availability in +2℃ and +4℃ worlds. *Philosophical Transactions of The Royal Society A*, 369, 99 – 116.

Grimmond, C. S. B. and Oke, T. R. 1986. Urban water balance 2. Results from a suburb of Vancouver, British Columbia. *Water Resources Research*, 22 (10), 1404 – 1412.

Grimmond, C. S. B. and Oke, T. R. 1991. An evapotranspiration-interception model for urban areas. *Water Resources Research*, 27 (7), 1739 – 1755.

Grimmond, C. S. B. and Oke, T. R. 1999. Evapotranspiration rates in urban areas. *International Association of Hydrological Sciences*, 259, 235 – 243.

Grimmond, C. S. B., Oke, T. R. and Steyn, D. G. 1986. Urban water balance 1. A model for daily totals. *Water Resources Research*, 22 (10), 1397 – 1403.

Heilman, J. L., Brittin, C. L. and Neale, C. M. U. 1989. Fetch requirements for Bowen ratio measurements of latent and sensible heat fluxes. *Agricultural and Forest Meteorology*, 44, 261 – 273.

Hossen, M. S., Mano, M., Miyata, A., Baten, M. A., and Hiyama, T. 2012. Surface energy partitioning and evapotranspiration over a double-cropping paddy field in Bangladesh. *Hydrological Processes*, 26, 1311 – 1320.

Jacobs, A. F. G., Heusinkveld, B. G. and Holtslag, A. A. M. 2008. Towards closing the surface energy budget of a mid-latitude grassland. *Boundary-Layer Meteorology*, 126, 125 – 136.

Jasechko, S., Sharp, Z. D., Gibson, J. J., Birks, S. J., Yi, Y., and Fawcett, P. J. 2013, Terrestrial water fluxes dominated by transpiration. *Nature*, 496, 347 – 351.

Lockwood, J. G. 1985. World climatic systems. Edward Arnold, London: Great Britain.
Monteith, J. L. and Unsworth, M. H. 1990. *Principles of Environmental Physics*. Oxford: Great Britian, Butterworth-Heinemann.
Monteith, J.L., 1965. Evaporation and environment. In: Fogg, G.E. (Ed.), The State and Movement of Water in Living Organism. Soc. Exp. Biol. Symp. 19, 205–234
Ohmura, A. 1982. Objective criteria for rejecting data for Bowen ratio flux calculations. *Journal of Applied Meteorology*, 21, 595 – 598.
Oke, T. R. 1987. Boundary Layer Climates. 2nd eds. Methuen, London: Great Britain.
Oke, T. R., Spronken-Smith, R. A., Jáuregui, E. and Grimmond, C. S. B. 1999. The energy balance of central Mexico City during the dry season. *Atmospheric Environment*, 33, 3919 – 3930.
Pearlmutter, D., Berliner, P. and Shaviv, E. 2005. Evaluation of urban energy fluxes using an open-air scale model. *Journal of Applied Meteorology*, 44, 532 – 545.
Pearlmutter, D., Krüger, E. L. and Berliner, P. 2009. The role of evaporation in the energy balance of an open-air scaled urban surface. *International Journal of Climatology*, 29, 911 – 920.
Price, R. K. and Vojinovic, Z. 2008. Urban flood disaster management. *Urban water journal*, 5 (3), 259 – 276.
Rutter, A. J., Kershaw, K. A., Robins, P. C. and Morton, A. J. 1971. A predictive model of rainfall interception in forests, 1. Derivation of the model from observations in a plantation of Corsican Pine. *Agricultural Meteorology*, 9, 367 – 384.
Sinclair, T. R., Allen, Jr., L. H. and Lemon, E. R. 1975. An analysis of errors in the calculation of energy flux densities above vegetation by a Bowen-ratio profile method. *Boundary-Layer Meteorology*, 8, 129 – 139.
Todd, R. W., Evett, S. R., and Howell, T. A. 2000. The Bowen ratio-energy balance method for estimating latent heat flux of irrigated alfalfa evaluated in a semi-arid, advective environment. *Agricultural and Forest Meteorology*, 103, 335 – 348.
Trout, K. and Ross, M. 2006. Estimating evapotranspiration in urban environments. *Urban Groundwater Management and Sustainability*, 74, 157 – 168.
Wang, S.-H., Huang, S.-L. and Budd, W. W. 2012. Resilience analysis of the interaction of between typhoons and land use change. *Landscape and Urban Planning*, 106, 303 – 315.

# Chapter 4 Study 2: Better Understanding the Complementary Relationship with use of Bowen Ratio Energy Balance and Class A Pan Evaporation Measurements

## 4.1 Introduction

Bouchet (1963) first proposed the complementary relationship (CR) between actual and potential evapotranspiration. Much theoretical and empirical development of the CR has been put forth since Bouchet (1963) including notable contributions from Morton (1965, 1968, 1969, 1971, 1975, 1976, and 1983) and Brutsaert and Stricker (1979). The models presented by Morton and Brutsaert and Stricker have received sufficient attention but clearly understanding the relationship between actual and potential evapotranspiration has been challenging.

Bouchet (1963) hypothesized that the terrestrial environment would exhibit complementary behaviour between actual and potential evapotranspiration during periods when moisture availability became limited from completely saturated conditions. Bouchet's hypothesis predicted that during times when the landscape experienced wet conditions due to rainfall, dew deposition or irrigation, actual and potential evapotranspiration would be the same amount under the premise of the CR. This unique phemonena was termed the equilibrium wet evaporation rate ($Q_{EP0}$). Models describing $Q_{EP0}$ have been of debate in order to resolve the physically based mechanisms of the CR but no solution has been universally accepted.

This paper provides insight into the CR and interaction between actual and potential evapotranspiration. A Class A evaporation pan (CAEP) was used as a means to obtain potential evaporation values. Simultaneously, a Bowen ratio energy balance system was measuring real evapotranspiration, adjacent to the pan evaporation system. With the environmental monitoring systems in place at the research site, development of a novel resistance framework is proposed for better understanding the CR. The measurement systems were setup in a field of naturalizing ground cover at the Toronto and Region Conservation Authority's (TRCA) Kortright Centre for Conservation (KC), Woodbridge, Ontario, Canada during the summer of 2011. To assist physically characterizing the turbulence at research site, a six level, mechanical wind profile system

was used to estimate the aerodynamic properties and enabled calculations of the resistance framework.

To evaluate differences between the field site and the CAEP, the surface energy budget (SEB) of the pan was compared to the field to determine any energetic differences between the two varying land cover types. Measurements of pan ground heat flux spatial variability was measured to determine any spatial differences in heating from the bottom of the pan into the ground as was pan net radiation and water temperature.

## 4.2 Materials and Methods

### *4.2.1 Materials*

#### *4.2.1.1 Kortright Centre for Conservation*

The research site is representative of a rural land cover type and located in a field at the northern portion of the Kortright Centre for Conservation, KC. KC is located at 9550 Pine Valley Road, between Major Mackenzie Drive and Rutherford Road. It is managed and operated by the TRCA. The coordinate node of the instruments used for modelling the water balance (WB) and SEB at KC were located at 43°50’7” N latitude and 79°35’34” W longitude. The KC study site ranges in elevation from 200 to 215 m above sea level. From a watershed scale, KC is located within the Humber River Watershed.

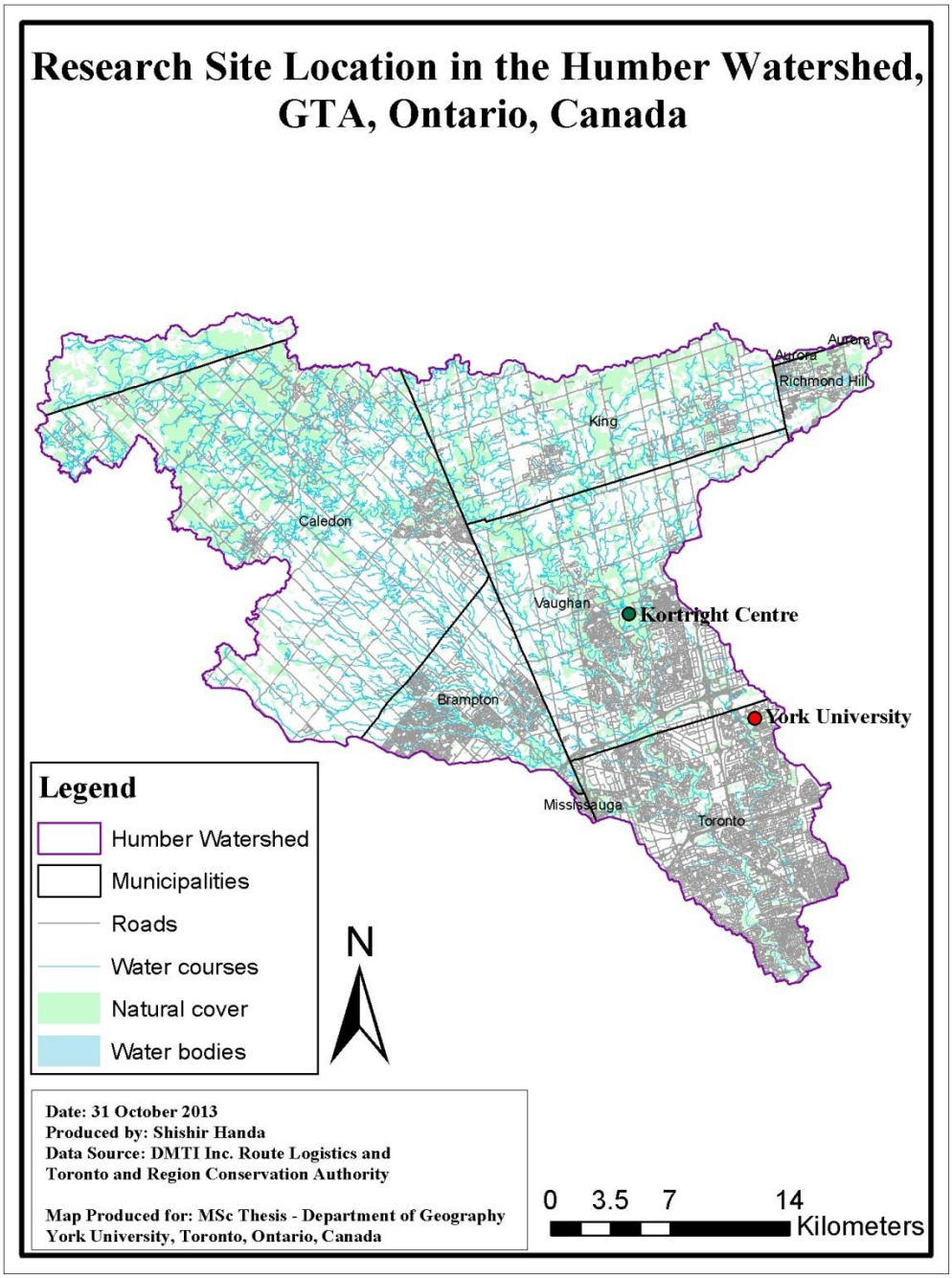


Map 4.1. This map displays the Humber River Watershed and the location of the Kortright Centre for Conservation within the watershed boundary.

The site was chosen with ample fetch to the north, south and east. There is restricted fetch to the west owing to a row of trees mostly comprising of pine. The field is bounded by other similar fields. The plant community at the KC experimental site can be characterised as a mix of herbaceous and woody plant species that is gradually being recolonized by southern Ontario native and naturalised plants such Queen Anne's lace (*Daucus carota*), wild oat grass (*Avena fatua* L), purple vetch (*Vicia americana*), cow vetch (*Vicia cracca*), Canada thistle (*Cirsium arvense*), swamp thistle (*Cirsium muticum*), black-eyed Susan (*Rudbeckia hirta*), red clover (*Trifolium pratense*), New England asters (*Aster novae-angliae*), Canadian goldenrod (*Solidago canadensis*) and tall goldenrod (*Solidago altissima*). The KC study site was a fallow field but previously planted with Timothy grass (*Phleum pratense*) in the late 1990s. The soil matrix has the ability to absorb excess rainfall and plant roots can extract soil moisture during the growing season for transpiration, thereby making KC an oasis surrounded by intensive suburban development.

#### *4.2.1.2 Class A Evaporation Pan*

A National Weather Service Class A evaporation pan was used for this study as a means to determine differences between pan and terrestrial evaporation from the experimental site. The pan (255-200 Evaporation Pan) was purchased by the TRCA from NovaLynx, USA. Change in water level was measured using an analog output evaporation gauge from NovaLynx (255-100 Evaporation Gauge). The energy budget of the pan was determined by measuring the net radiation of the pan ($Q^*_{pan}$) with a Middleton net pyrradiometer (CN1) and the ground heat flux of the pan ($Q_{G_{pan}}$) with four (serial numbers G298, F383, F196 and F669) Middleton soil heat flux plates (CN3). The pan was not supported by wooden slats and was in direct contact with the ground surface below. Four CN3 soil heat flux plates were positioned in the cardinal directions as means to evaluate spatial differences in ground heating of the pan. The CN1 was positioned in the centre of pan approximately 13 cm above the rim to account for a 95%

field of view of the pan water surface. Figure 4.1 shows the various stages of the SEB installation of the pan.

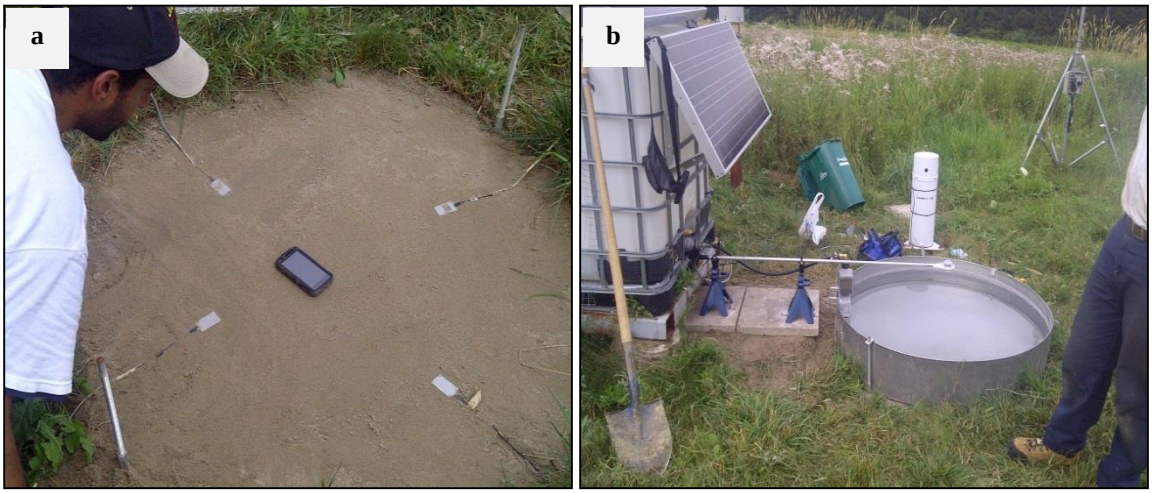

Figure 4.1. (a) displays the placement and calibration of the Middleton Solar soil heat flux plates in the cardinal directions. A digital compass was used to position the heat plates, which was integrated in a smartphone. (b) displays the final installation of the surface energy budget instruments of the Class A evaporation pan.

Data collection of the pan energy budget instruments was semi-automated with a Campbell Scientific CR10x data logger, powered with the 12V batteries connected to the photovoltaic solar panels that were stored in the weather resistant utility box. An additional flux of the pan energy budget had to be accounted because of the column of water. Net radiation of the pan consumed by heating and cooling of the pan water was calculated with a single term of the pan energy budget. The full pan energy budget is given as,

$$Q^*{}_{pan} = Q_{E_{pan}} + Q_{H_{pan}} + Q_{G_{pan}} + Q_W \quad 4.1$$

where $Q_W$ is the amount of net radiation drawn by the water during cooling and heating phases, $Q_{E_{pan}}$ is the latent heat flux of the pan and $Q_{H_{pan}}$ is the sensible heat flux of the pan.

$Q_{E_{pan}}$ was evaluated as,

$$Q_{E_{pan}} = L_v ET_{pan} \quad 4.2$$

where $L_v$ is the latent heat of vaporization of the pan water and $ET_{pan}$ is the decrease of water level (mm) in the pan, associated with pan evaporation and corrected for precipitation by an adjacent tipping bucket rain gauge.

Following Bello and Smith (1990), $Q_W$ was evaluated as,

$$Q_W = c_w(\Delta T/\Delta t)\Delta z \quad 4.3$$

in which $c_w$ is the heat capacity of water, $\Delta T$ is the change in temperature over the time period, $\Delta t$ , and depth is $\Delta z$.

#### *4.2.1.3 Six Level Wind Profile System*

A six level anemometer mast system was deployed in June 2010 at the experimental site to construct wind speed ($u$) profiles of the field. Six Davis Instruments 7911 anemometers and 7914 wind vanes were erected on a 3.81 cm diameter galvanized steel mast at heights of 0.75, 1.00, 1.50, 2.25, 3.00 and 4.00 m above the ground surface, with guy wires to help minimize sway from wind gusts. A Campbell Scientific CR1000 data logger was used to semi-automate $u$ data collection, drawing power from the same power supply as the pan energy budget system.

Profiles of wind speed measurements enabled calculations of the zero-plane displacement height ($d$) and the surface roughness ($z_0$) with use of appropriate stability parameters. The $u$ profile system was ultimately used to calculate the aerodynamic resistance ($r_a$) of the field given as,

$$r_a = \frac{\left[ln\left(\frac{z-d}{z_0}\right) - \Psi_v\right]\left[ln\left(\frac{z-d}{z_0}\right) - \Psi_m\right]}{k^2 u} \quad 4.4$$

where $k$ is the von Kármán constant of 0.41, $\Psi_v$ and $\Psi_m$ are the height integrated stability corrections for water vapour and momentum, respectively (Monteith and Unsworth 1990).

Monteith and Unsworth (1990) state the two best parameters to account for stability of the atmosphere are the bulk (or gradient) form of the Richardson number ($R_i$) and the Monin-Obukhov length ($L$). $R_i$ is calculated from the gradients of temperature ($T$) and $u$ whereas $L$ is determined through fluxes of heat and momentum. $R_i$ is given as,

$$R_i = -\frac{g\delta\theta_v\delta z}{\overline{\theta_v}\delta u^2} \quad 4.5$$

where $g$ is the acceleration due to gravity, $\theta_v$ is the virtual potential temperature, $\delta z$ is the difference between instrument heights and $\delta u$ is the difference in wind speed from the measurement heights. The overbar indicates an averaged value.

The Monin-Obukhov length was determined as,

$$L = \frac{\hat{z}}{Ri} \text{ when } R_i < 0 \quad 4.6$$
$$L = \hat{z}\left(\frac{1}{Ri} - 5\right) \text{ when } R_i > 0$$

where

$$\hat{z} = e^{\left[\frac{(\ln z_1 + \ln z_2)}{2}\right]} \quad 4.7$$

which is the geometric mean height.

The virtual potential temperature ($\theta_v$) was calculated as,

$$\theta_v = \frac{\theta}{1-\frac{e}{p}(0.378)} \quad 4.8$$

where $\theta$ is the potential temperature, $e$ is the vapour pressure and $p$ is the atmospheric pressure. Using the virtual potential temperature accounted for the impact elevation and humidity have on the bouncy and temperature of the atmosphere in the Richardson number.

#### *4.2.1.4 Bowen Ratio Energy Balance System*

Bowen ratio energy balance (BREB) systems use the vertical gradients of $\theta$ ($\Delta\theta$) and $e$ ($\Delta e$) and scales the gradients to local measurements of net available energy ($Q_n$) to calculate the latent heat flux ($Q_{ER}$) or its mass equivalent the evapotranspiration rate ($ET$). Mathematically this is expressed as,

$$Q_{ER} = \frac{Q^* - Q_G}{1+\beta} = \frac{Q_n}{1+\gamma\frac{\Delta\theta}{\Delta e}} \quad 4.9$$

where $\gamma$ is the psychrometric constant and $\beta$ is the Bowen ratio (1926). Net radiation ($Q^*$) was measured with a Middleton CN1 net pyrradiometer aspirated with dry air supplied by an aquarium pump through a desiccant chamber. The ground heat flux ($Q_G$) was measured with a soil heat flux plate (Campbell Scientific Inc., HFT3), buried 2 cm below the soil surface. The air temperature ($T_a$) profile was measured using shielded copper-constantan thermocouples (Omega: special limits of error type T). There are four measurement levels on the KC BREB system at heights of 0.25, 0.75, 1.50 and 3.00 m. At those same levels $e$ was calculated using the LICOR Biosciences' LI-840 infrared gas analyzer (IRGA). Figure 4.2 displays the BREB fully deployed at the experimental field site.

Figure 4.2. This June 2010 image displays the Bowen ratio energy balance system, deployed at the Kortright Centre for Conservation experimental research site used to calculate actual evapotranspiration. In the background the multilevel wind profile system can be seen.

Although Equation 4.9 for calculating $Q_{ER}$ only requires $\theta$ and $e$ to be measured at a minimum of two levels in the atmosphere to determine gradients the multilevel system provided a check of internal consistency of flux estimates. The highest point of the BREB system allows $Q_{ER}$ to be calculated from an area of 300 m radius, with the assumption of 1:100 height to fetch ratio (Heilman et al. 1989). Ambient air was

sequentially drawn through stainless steel mesh insect filters then down from each level through 6.35 mm diameter Bev-A-Line® tubing to minimize gas absorption and diffusion. An aquarium air pump and series of 3 way 12V DC solenoid valves sequentially purged ambient air at a rate of 0.35 $dm^3$ $min^{-1}$ from each level before gas concentrations were sampled. The ambient air was purged for one minute and then sampled for three minutes on each 15 minute cycle. Hourly averages were computed from four 15 minute replicate cycles from each measurement height. Data was stored on a Campbell Scientific CR1000 and retrieved manually on a weekly basis.

The BREB system was initially deployed in August 2008 and several iterations of the photovoltaic solar panel and battery systems have been employed since that time. The solar panels were able to generate 240W to charge the 12V DC marine grade batteries.

#### *4.2.1.5 Toronto and Region Conservation Authority Meteorological Station*

The TRCA meteorological station augmented the BREB, wind profile and pan systems deployed at the research site. Rainfall was measured with a Hydrological Service Ltd. TB3 tipping bucket rain gauge (0.2 mm $tip^{-1}$). Atmospheric pressure was measured with an Onset Barometric Pressure Sensor (S-BPA-CM10). All TRCA meteorological weather station sensors were semi-automated with Onset's HOBO weather station data logger housed in a weather resistant enclosure.

### *4.2.2 Methods*

The methodology employed for the study was based on the measurement systems deployed at the study site during the measurement period of 2011. The basis of this study relied upon the commonly acknowledged surface energy budget (Oke 1987; Bonan 2008) expressed as,

$$Q^* = Q_{ER} + Q_H + Q_G \qquad 4.10$$

The BREB system measures $Q_{ER}$ given by Equation 4.9. The Bowen ratio is expressed as,

$$\beta = \frac{Q_H}{Q_{ER}} \quad 4.11$$

For this research $\beta$ was calculated based on the gradient method as,

$$\beta = \gamma \frac{\Delta\theta}{\Delta e} \quad 4.12$$

The Penman-Monteith (Monteith 1965) combination approach (CA) for the $Q_{ER}$ partitions total $ET$ into three factors responsible for dynamic flux, which are energy availability, atmospheric demand and moisture availability as,

$$Q_{ER} = \frac{\Delta(Q^* - Q_G) + \rho c_p {}^{VPD_z}/_{r_a}}{\Delta + \gamma\left(1 + \frac{r_c}{r_a}\right)} \quad 4.13$$

where $VPD_z$ is the vapour pressure deficit ($VPD$) of the air at height $z$, $\rho$ is the density of air, $c_p$ is the specific heat of air at constant pressure, $\Delta$ is the slope of the saturation vapour pressure-temperature curve and $r_c$ is the canopy or surface resistance. Likewise, $Q_{ER}$ may be partitioned into the three factors responsible for dynamic flux, given after Slayter and McIlroy (1961) as,

$$Q_{ER} = \frac{\Delta}{\Delta + \gamma} Q_n + \frac{\rho c_p}{r_a}(D_z - D_0) \quad 4.14$$

in which $D$ is the wet-bulb depression at the surface (0) and at some height above the surface ($z$). $D$ is determined as the difference of $T$ at varying heights between dry-bulb ($T$) and wet-bulb ($T'$) temperatures.

Equation 4.13 is rearranged to solve for $r_c$ as,

$$r_c = (1 + \beta) r_i + \left(\beta\left(\frac{\Delta}{\gamma}\right) - 1\right) r_a \quad 4.15$$

where $r_i$ is the isothermal or climatological resistance (DeBruin and Holtslag 1982) given as,

$$r_i = \frac{\rho c_p}{\gamma} \frac{VPD_z}{Q_n} \quad 4.16$$

The sensitivity of the $VPD$ in the atmosphere to surface drying will vary with season and air mass type. It is also influenced by $r_i$, which expresses the relative importance of the local energy supply and $VPD$, driving $Q_{ER}$. Aside from $Q_{ER}$ being controlled by $Q_n$ and $VPD$ are the reduced amounts of $Q_{ER}$ resulting from the restriction of moisture available to enter the atmosphere from the surface. Moisture availability is represented by $D_0$, which increases as volumetric soil moisture becomes restricted. During rainfall or dewfall, the surface is considered saturated and $D_0$ should diminish to zero. This indicates the air next to the ground is saturated and allows the expression of the potential latent heat flux in a more simplified form given as,

$$Q_{EP} = \frac{\Delta}{\Delta+\gamma} Q_n + \frac{\rho c_p}{r_a} D_z \quad 4.17$$

The flux computed from Equation 4.17 will always be greater than the flux computed from Equation 4.14 due to the absence of any moisture limitations at the surface. Potential evaporation is controlled by and varies with $Q_n$, $r_a$, and $VPD$ diurnally, seasonally and spatially. It represents the greatest possible $ET$ that may be experienced from the surface of interest if moisture is unrestricted to enter the atmosphere. Equation 4.17 should similarly be applicable to Class A evaporation pans that are consistently filled with water, fulfilling the requirement of unrestricted moisture availability.

Recalling Morton (1969, 1971, 1975, 1976, and 1983) and Brutsaert and Stricker's (1979) investigations of the environmental controls of the wet environment equilibrium evaporation ($Q_{EP0}$) and the issues restricting its definition, clearly defining

the CR has been long withstanding. Brutsaert and Stricker (1979) approached the issue of parameterizing $Q_{EP0}$ by assuming that over a wet surface the atmospheric demand term was a constant proportion of the energy availability term of the CA. The constant was set to an average 27%, which is in close range to the more commonly quoted Priestley-Taylor (1972) value ($\alpha_{PT72}$) of 26% expressed as,

$$Q_{EP0} = 1.27 \frac{\Delta}{\Delta+\gamma} Q_n \qquad 4.18$$

Brutsaert and Stricker (1979) provided substantial evidence that the assumption of Equations 4.18 was valid for three-day estimates of $Q_{ER}$. However, their study was performed during a drought summer in the Netherlands and resulted in undesirable conditions, yielding unrealistic estimates of $Q_{ER}$ during saturated surface conditions. Thus, if Equations 4.17 and 4.18 are substituted into $Q_{ER} = 2Q_{EP0} - Q_{EP}$ we obtain,

$$Q_{ER} = 2\left[1.27 \frac{\Delta}{\Delta+\gamma} Q_n\right] - \left[\frac{\Delta}{\Delta+\gamma} Q_n + \frac{\rho c_p}{r_a} D_z\right] = 1.54 \frac{\Delta}{\Delta+\gamma} Q_n - \frac{\rho c_p}{r_a} D_z \qquad 4.19$$

Priestley and Taylor (1972) demonstrated that non-saturated atmospheric conditions are commonplace over many landscapes with freely available water, both terrestrial and aquatic.

As the ground surface dries the additional humidity deficit in the air created by the reduced local $Q_{ER}$ (enhanced local $Q_H$) will facilitate greater $Q_{E_{pan}}$ resulting in a complementary evaporation described by $D_z = D_{z_A} + D_{z_L}$, in which $D_{z_A}$ is defined as the advective proportion of the humidity deficit and $D_{z_L}$ is defined as the local portion of the humidity deficit. $Q_{ER}$ can therefore be re-expressed as,

$$Q_{ER} = Q_{EQ} + \frac{\rho c_p}{r_a}(D_{z_A} + D_{z_L} - D_0) \qquad 4.20$$

where $Q_{EQ}$ is the equilibrium evaporation given as $\frac{\Delta}{\Delta+\gamma} Q_n$.

There are environments that experience $Q_{EQ}$ and those environments are found when conditions of $D_0 = D_z$ are met. In special cases when $D_0 = D_z = 0$, $Q_{ER}$ is also driven strictly by the energy supply term. In this case, no amount of atmospheric turbulence will influence $Q_{ER}$ when the surface and the overlying air are similarly saturated because eddies transporting water vapour upwards are replaced by eddies with the same amount of water vapour resulting in no net enhancement of vapour exchange. Therefore, the atmospheric demand is neither enhanced nor suppressed at the surface under these conditions. However, if cool moist air is advected over the surface under such conditions then the $VPD$ should decrease with height ($D_0 > D_z$) and convection will ultimately suppress $Q_{ER}$ lower than $Q_{EQ}$. This condition will be termed as sub-equilibrium $ET$ ($Q_{EQ_{sub}}$) because it is lower than $Q_{EQ}$. Conversely, if warmer dry air is advected over the surface then the $VPD$ should increase with height ($D_0 < D_z$) and convection will enhance $Q_{ER}$ greater than $Q_{EQ}$. This observation will be termed as supra-equilibrium $ET$ ($Q_{EQ_{sup}}$) because it is greater than or above $Q_{EQ}$.

$Q_{ER}$ is constant with height within the fully adjusted boundary layer (Oke 1987). Since $Q_{EQ}$ is constant with height the second term in Equation 4.20 should also be constant as well. The aerodynamic resistance increases with height from the surface and sum of the terms in the brackets remains constant with height with respect to the total flux. To the extent that changes with height in $r_a$ are measured or modelled accurately, change with height in the sum of the bracketed terms of Equation 4.20 can be estimated. Important to note, without an *a priori* knowledge of $D_0$ multiple solutions for $D_z$ as a function of $r_a$ can be calculated. Although, in micrometeorological experimental settings where $Q_{ER}$, $r_a$, and $D_z$ are all measured, a unique solution for $D_0$ is achievable by re-arranging the terms in Equation 4.20.

A comparison of how surface drying influences estimates of $Q_{EP}$, using Equation 4.17, allow for better understanding of factors controlling $Q_{ER}$. After Priestley and Taylor (1972), defining the ratio of $Q_{ER}$, Equation 4.14, to $Q_{EQ}$ given by $\alpha_{PT72} = Q_{ER}/Q_{EQ}$ . A

similar ratio of apparent $Q_{EP*}$, using Equation 4.17, to $Q_{EQ}$ given by $\alpha_{PT72*} = Q_{EP*}/Q_{EQ}$ allow better understanding of the processes driving the $Q_{ER}$ process. The proportional error from using Equation 4.17 to estimate $Q_{EP}$ during periods of moisture restriction can be determined with comparison of the newly proposed ratio expressed as,

$$\frac{\alpha_{PT72*}}{\alpha_{PT72}} = 1 + \left(\frac{\gamma}{\gamma+\Delta}\right)\frac{r_c}{r_a} \quad 4.21$$

This indicates that the error associated with using the Penman formula to estimate potential evaporation when it should not be used (when the surface is not wet) is directly related to the canopy resistance and inversely related to the aerodynamic resistance. Errors are largest over dry surfaces under relatively windy conditions or closer to the ground.

The change in temperature as a function of surface drying can be expressed through a series of equations as,

$$\delta T_0 - \delta T_z = (Q_{EP0} - Q_{ER})\frac{r_a}{\rho c_p} \quad 4.22$$

Where $\delta T_z = T_z - T_z'$which are the differences in air temperature when the surface is dry and wet respectively. $\delta T_0 = D_0$ represents surface warming associated with surface drying. Similarly,

$$\delta T_0 = (Q_{EP*} - Q_{ER})\frac{r_a}{\rho c_p} \quad 4.23$$

$$\delta T_z = (Q_{EP*} - Q_{EP0})\frac{r_a}{\rho c_p} \quad 4.24$$

$$D_z = \left(Q_{EP*} - Q_{EQ}\right)\frac{r_a}{\rho c_p} \quad 4.25$$

According to the CR, the expression for reduction of $Q_{ER}$ below $Q_{EP0}$, given by Equation 4.22, is only equivalent to the enhancement of $Q_{EP*}$ above $Q_{EPO}$, given by

Equation 4.24, when surface warming is exactly double air warming, which corresponds to $\delta T_0 = 2\delta T_a$. Except for this unique condition $Q_{EP*}$ does not satisfy $Q_{EP}$, required to meet conditions of the CR. Within the fully adjusted boundary layer, both $Q_{EP0}$ and $Q_{ER}$ are constant with height and $\delta T_0 - \delta T_z$ must increase directly proportional to $r_a$. All changes accompanying $r_a$ must be accommodated by $\delta T_z$ because $\delta T_0 = D_0$ will be invariant with height. With this understanding, a definition of a critical resistance, $r'$ will correspond to a height in the atmosphere above the surface where warming due to surface drying diminishes to zero such that,

$$r' = \frac{\rho c_p D_0}{Q_{EP0} - Q_{ER}} \quad 4.26$$

Equation 4.26 suggests that as surface drying increases, the height in the atmosphere experiencing corresponding gains of $T$ due to moisture reduction will also proportionally increase. During periods of small residuals of $Q_{ER}$ generated by consequences of surface drying, observations at higher heights in the atmosphere must be sought after to register a negligible $T$ change between arid and saturated environmental conditions. For example, $T$ of 288.15 K with $Q_{EPO} - Q_{ER} = 1\ W\ m^{-2}$, $r' = 1200\ D_0$.

Combining Equation 4.22 and 4.26 provides insightful characteristics of $r'$, which follows as,

$$\frac{\delta T_z}{\delta T_0} = 1 - \frac{r_a}{r'} \quad 4.27$$

and describes the relative warming in the atmosphere to that of the surface warming as a function of height via $r_a$.

A solution for $Q_{EPO}$ can be found from Equation 4.26 expressed as,

$$Q_{EP0} - Q_{ER} + Q_{ER} = \frac{\rho c_p}{r'} D_0 + Q_{EQ} + \frac{\rho c_p}{r'} (D_z' - D_0) \Rightarrow Q_{EP0} = Q_{EQ} + \frac{\rho c_p}{r'} D_z' \quad 4.28$$

from which it follows,

$$Q_{EP0} - Q_{EQ} = \frac{\rho c_p}{r'} D_z{}' \Rightarrow D_z{}' = \left(Q_{EP0} - Q_{EQ}\right)\frac{r'}{\rho c_p} \quad 4.29$$

where $D_z{}'$ is the wet-bulb depression at $r'$. By definition, $D_z{}'$ remains unchanged due to surface drying because $\delta T_z$ is zero at $r'$.

Likewise from Equation 4.25,

$$Q_{EP*}{}' - Q_{EQ} = \frac{\rho c_p}{r'} D_z{}' \Rightarrow D_z{}' = \left(Q_{EP*}{}' - Q_{EQ}\right)\frac{r'}{\rho c_p} \quad 4.30$$

Through combination of Equations 4.29 and 4.30, $Q_{EP*}{}' = Q_{EP0}$ at the observed $r'$.

$Q_{EP*}$ will always be larger than $Q_{ER}$ and can thus be easily estimated at a single measurement height , provided $Q_n$ and $u$ are observed. The solution to Equations 4.19 and 4.17 yields,

$$\frac{\alpha_{PT72*}}{\alpha_{PT72}} = \frac{Q_{EP*}}{Q_{ER}} = 1 + \frac{\gamma}{\Delta + \gamma}\frac{r_c}{r_a} \Rightarrow Q_{EP*} = Q_{ER}\left(1 + \frac{\gamma}{\Delta + \gamma}\frac{r_c}{r_a}\right) = Q_{EQ} + \frac{\rho c_p}{r_a} D_z \quad 4.31$$

$Q_{EP*}$ is unique because measurements can be obtained from a single height in the atmosphere through a single measurement of $D_z$ at the same height. The rate of change from $Q_{EP*}$ as $r_a$ increases with height is only predictable provided $r_c$ is known. However, if one instance of $Q_{EP*}$ is measured and it is assumed to be constant with height then a solution for $D_z{}'^*$ of varying values of $r_a$ can be obtained, which preserves flux constancy with height. This hypothetical $T$ profile will always intersect with an actual $T$ profile with the corresponding $r_a$ at the measurement height.

The foregoing advancement of theory introduces new variables, notably a height in the atmosphere where we define a resistance ($r'$) where the influence of surface drying

diminishes to zero. It does not provide an independent method of determining $r'$ from a single micrometeorological measurement level. It also has not provided a micrometeorological method of independently determining $Q_{EP0}$. Nevertheless, if we take evaporation from the pan to represent true potential evaporation, $Q_{EP}$, then for any measurement interval, $Q_{EP0}$ can be determined from the CR equation as $Q_{EP0} = (Q_{EP} + Q_{ER})/2$ where real evaporation is represented by the BREB fluxes. This provides a method of solving for $r'$ using Equation 4.26 and a solution for $\delta T_z$ follows from Equation 4.27 provided $D_0 = \delta T_0$ is available from the P-M formula. Thus the purpose of this experiment is to provide an examination of the behaviour of $r'$ and related parameters using the micrometeorological measurements available at the field site.

For this study, the wet-bulb temperature $T_z'$was not measured directly, however direct measurements of vapour pressure from the infrared gas analyser can be used to calculate $T_z'$ using the iterative process given by Abbott and Tabony (1985).

## 4.3 Results

First we examine the extent to which the net available energy from the pan differs from the surrounding field using data gathered specifically for this purpose. Figure 4.3 displays the spatial variability from 1 August 2013 to 15 August 2013 of $Q_{G_{pan}}$. During days of negative ground heating, the north and south ground heating bias was out competed by the east and west ground heat flux of the pan. On days nine and ten of the experiment, the east side ground heat was negative whereas the other heat flux plates all recorded positive values. This clearly represents the uncertain and variable nature the ground heat flux beneath the pan.

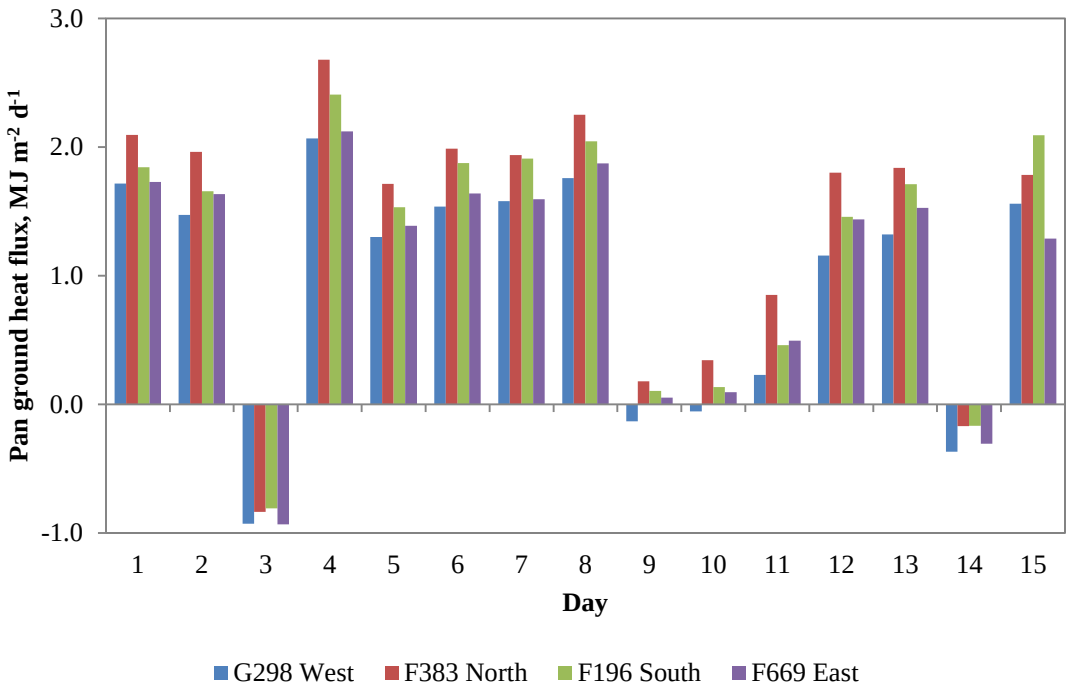


Figure 4.3. Shows the daily amount of spatial variability of the ground heat flux of the Class A evaporation pan used as a source of potential evaporation.

The energy budget of the pan for the 15 day collection period varied with respect to the dominant SEB processes where several days showed much pan evaporation compared to the sensible heat flux of the pan whereas on other days the sensible heat flux of the pan out competed pan evaporation. The fifth day of the study period only showed observations of negative sensible heating of the pan indicating that the air aloft transported more energy than the receipt of pan net radiation and would have enhanced pan evaporation. Similarly, only two days (3$^{rd}$ and 14$^{th}$) displayed overall negative daily average pan ground heat flux measurements. Those days also corresponded to the two days of the study periods with the least receipt of pan net radiation. As seen from Figure 4.4, the energy drawn into the pan water does not display any clear pattern. The flux of energy in the pan water experiences overall daily values that are both negative and positive with close to half the values being positive and the remainder being negative.

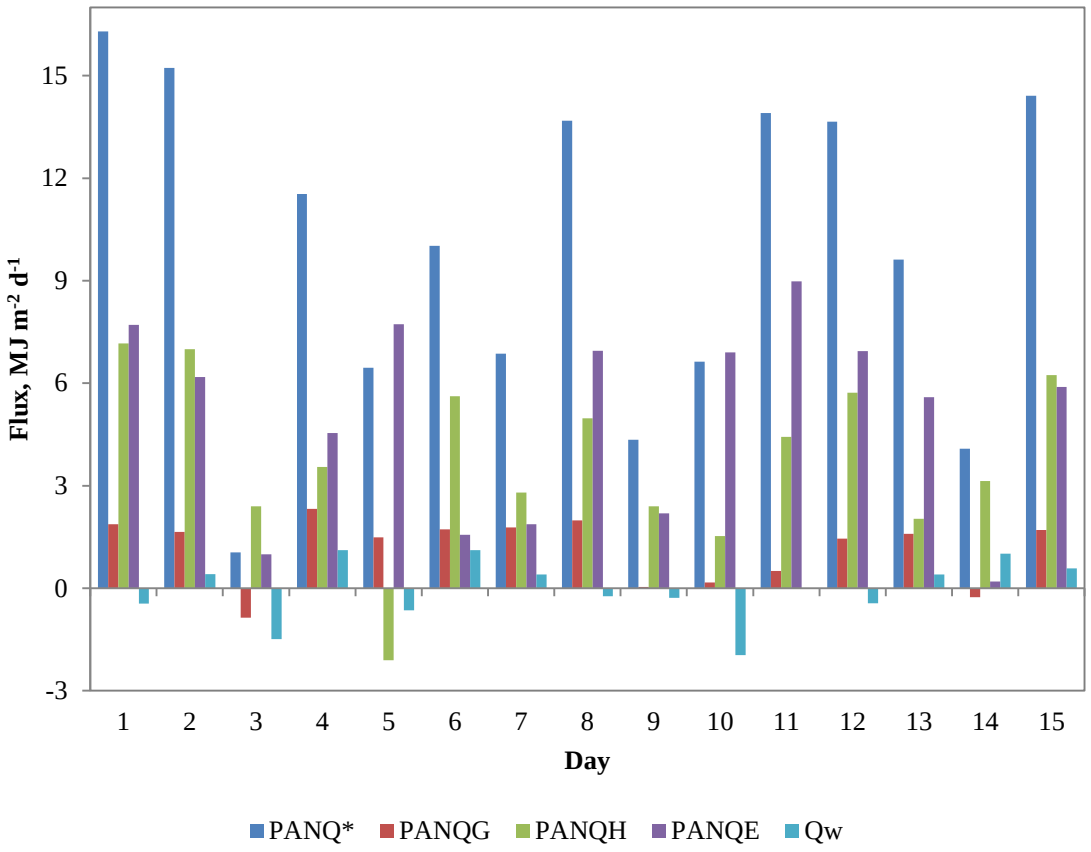


Figure 4.4. The bar chart gives the surface energy budget of the pan for the individual days of the study period.

The surface energy budget processes of the field, from the measurements of the BREB system, are much different than the pan. As noted previously, there were two instances during the measurement period of the pan energy budget where ground heat flux was negative. This was also the case of the field, in which on two days (10$^{th}$ and 11$^{th}$) the ground heat flux of the field experienced overall negative values. However, the two days that the ground heat flux was negative of the field were not the same two days that had negative ground heat fluxes of the pan. This suggests that the ground heating of the pan compared to the ground heating of the field is very different. A consistent trend of the field, as seen from Figure 4.5, is the latent heat flux is the dominant consumer of the net available energy. This signifies that the field was freely allowing water to enter

the atmosphere and much of the net radiation at the field surface was converted into the latent heat energy and released as water vapour.

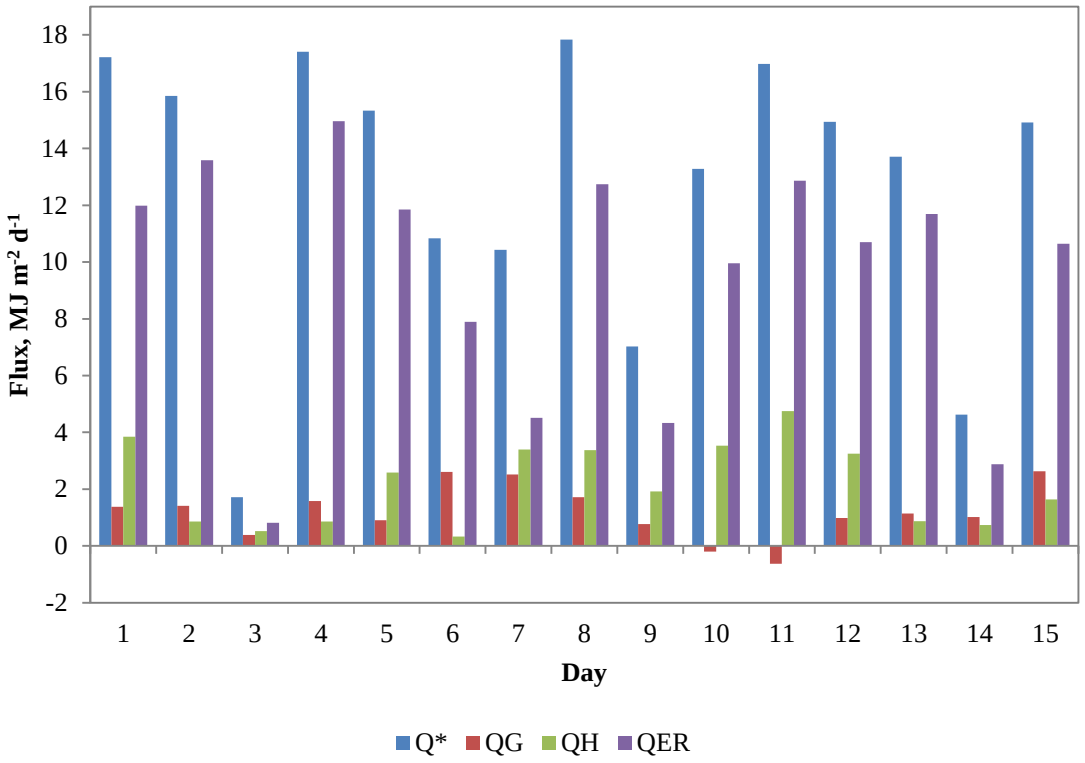


Figure 4.5. The bar graph shows the daily total surface energy budget values of the field measured with the Bowen ratio energy balance system.

One objective for this study was to determine an index between the Priestley-Taylor (1972) alpha values between the pan and the field. Hypothetically, under the CR it is assumed that pan evaporation, as a source of potential evaporation, will either be equal to or greater than real evaporation. The equality of potential or hypothetical potential evaporation to real evaporation is strictly dependent on the aridity of the environment. During completely saturated environmental conditions, both potential and real evaporation must be the same as predicted from traditional theory and Bouchet's hypothesis. It is unreasonable to believe that the alpha value of the pan would be less than the alpha value of the field environment during any given time and that it would be plausible that the alpha value of the pan and the field be equivalent. As seen from figure

4.6b, the slope of the line, set with a y-intercept of zero, between the correlation of the latent heat flux of the field and the equilibrium evaporation of the field is 1.076, which is slightly greater than the line of equality. Figure 4.6a displays the correlation between pan evaporation and equilibrium evaporation of the pan and resulted with a slope of 0.765, indicating that the evaporation of the pan was less than the equilibrium rate. Comparing the linear regression model of Figure 4.6a to 4.6b is questionable. The pan resulted in low alpha values when the field did not reach the accepted evaporation alpha value known to be indicative of freely evaporating surfaces, based on the work of Priestley and Taylor (1972).

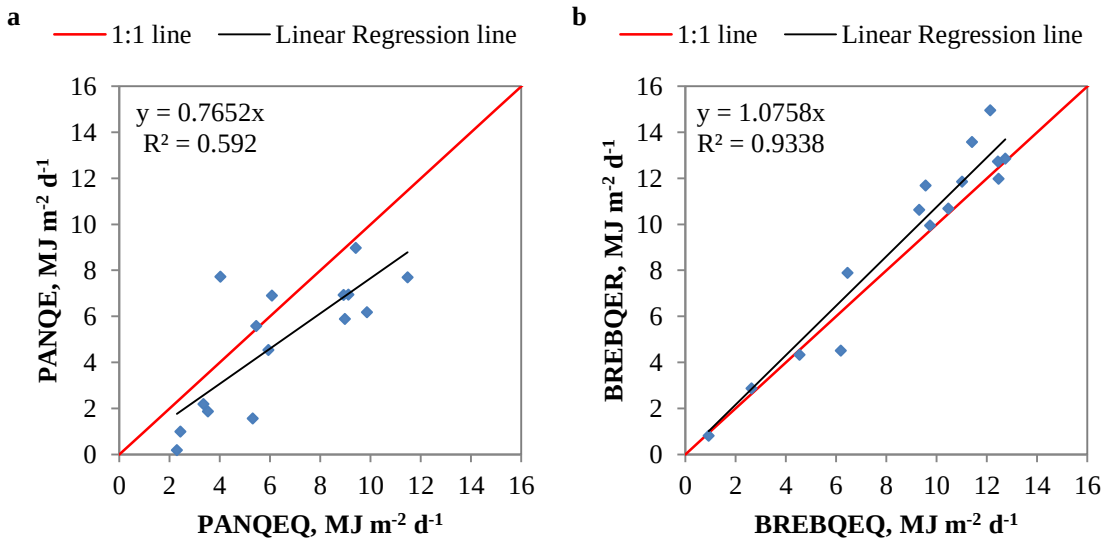


Figure 4.6. (a) displays the correlation between pan evaporation and equilibrium evaporation of the pan. (b) displays the latent heat flux of the field measured with the BREB compared to the equilibrium evaporation of the field.

Similarly, it is expected the pan would have a greater receipt of net radiation. Figure 4.7a displays that the field had greater total receipt of net radiation. This is also the case of the latent heat flux of the pan and the field. As seen from Figure 4.7b, the correlation of pan and field evaporation displays that pan evaporation was almost 50% less than field evaporation. This result does not align with the CR. The expectation would be that pan evaporation should be equal to or greater than terrestrial evaporation.

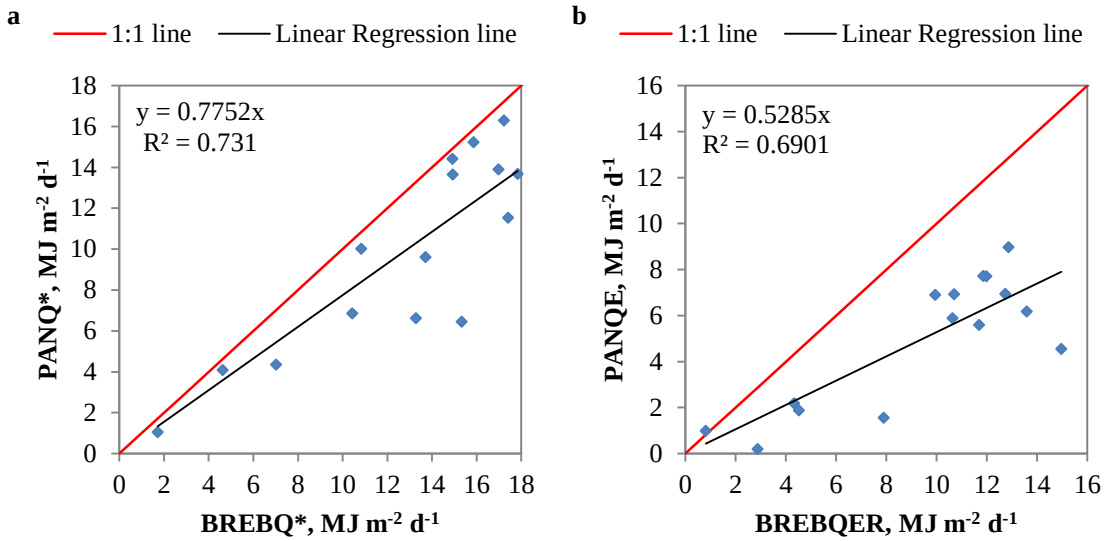


Figure 4.7. (a) displays the correlation of pan net radiation to the BREB net radiation daily total joules. (b) displays the correlation of pan evaporation to BREB evaporation measurements in daily total joules.

Like the net radiation and latent heat flux of the field, the equilibrium evaporation and the net available energy of the field were greater than the equilibrium evaporation and the net available energy of the pan, as can be seen from Figures 4.8a and 4.8b respectively.

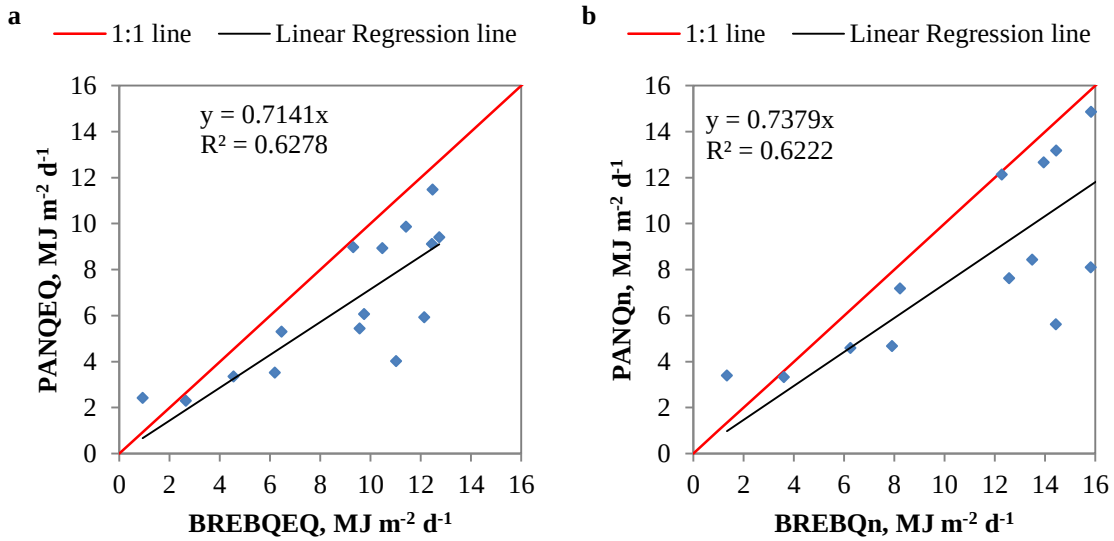


Figure 4.8. (a) displays the correlation of pan equilibrium evaporation to field equilibrium evaporation daily total joules. (b) displays the correlation of pan net available energy to field net available energy measurements in daily total joules.

The averaged values of the spatially distributed ground heat plates of the pan were more than 50% of the time greater than the measured ground heat flux of the field. There are also days that experience dissimilar ground heating between the pan and the field, as can be seen from Figure 4.9.

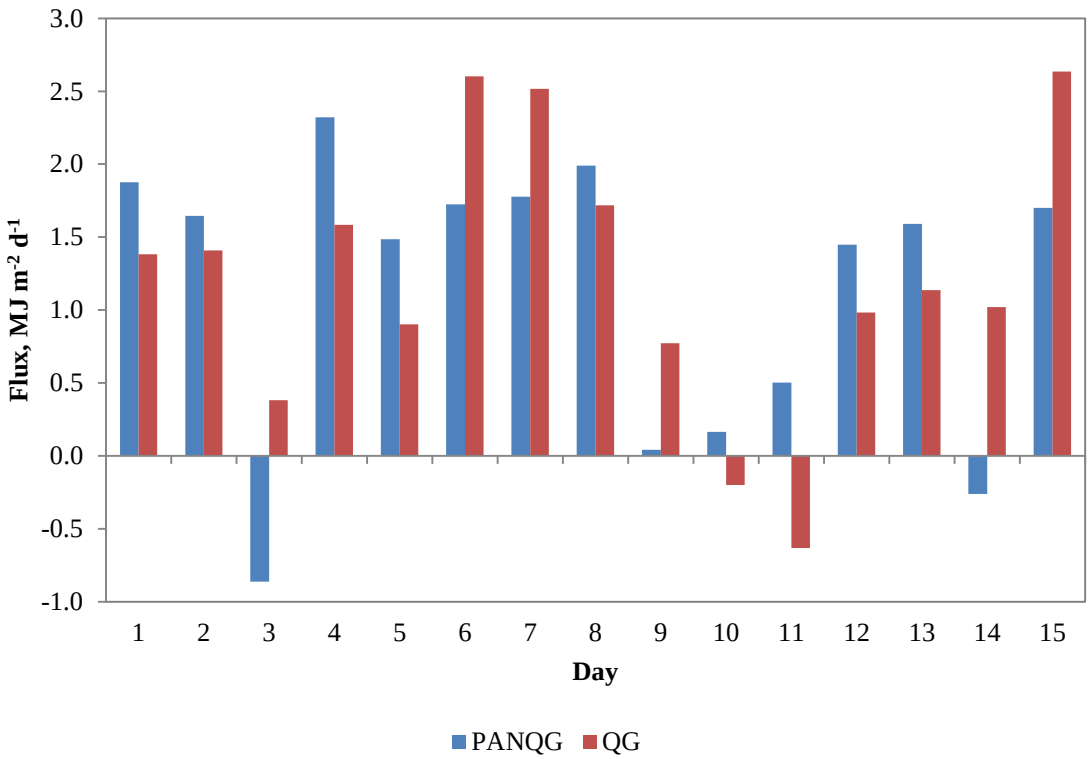


Figure 4.9. This graph depicts the total ground heat fluxes of the field and the pan for each of the study period days.

As noted above, the net available energy of the field was primarily consumed by the latent heat flux. This is also indicative by the daily Bowen ratio values never exceeding 0.9 and the lowest Bowen ratio value of 0.21 occurring on day three of the study period. Day three of the study period also exhibited the lowest income of net radiation to the study site owing to overcast conditions due to a passing storm system.

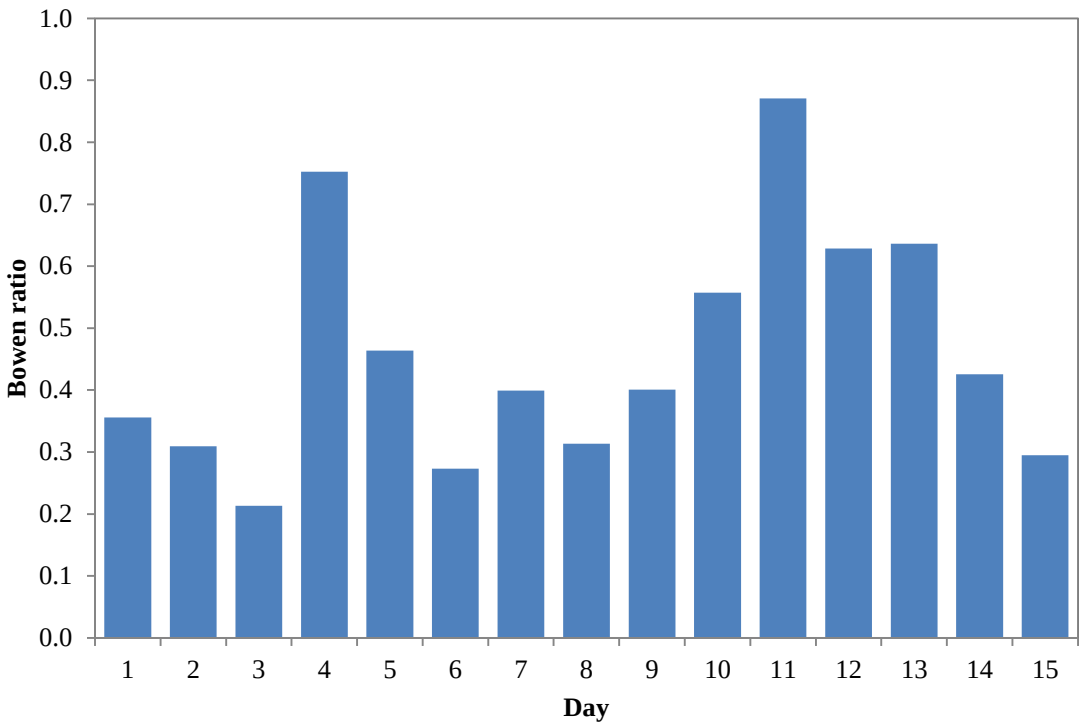


Figure 4.10. Daily Bowen ratio values were calculated based on the gradient measurements of temperature and humidity from the Bowen ratio energy balance system.

During the total study period, an input of 72.8 mm of rainfall was measured with the rain gauge. Total evapotranspiration amounted to 58 mm during the same time period leaving 14.8 mm as runoff (difference between precipitation and evapotranspiration). Out of the 15 days, the total 72.8 mm of rainfall occurred over 10 days but majority of the rainfall at the field site incurred on five individual days. On four of the five days that majority of the precipitation events took place, evapotranspiration was severally suppressed and runoff was the dominant output water balance component. As seen from Figure 4.11, all other days that runoff values were negative and signified that the water table was drawn upon as the source of evaporation from the field. Overall, evapotranspiration consumed 80% of precipitation for the 15 day study period, leaving 20% drawn into runoff. Figure 4.12 displays the graphical distribution of the evaporation and runoff ratios.

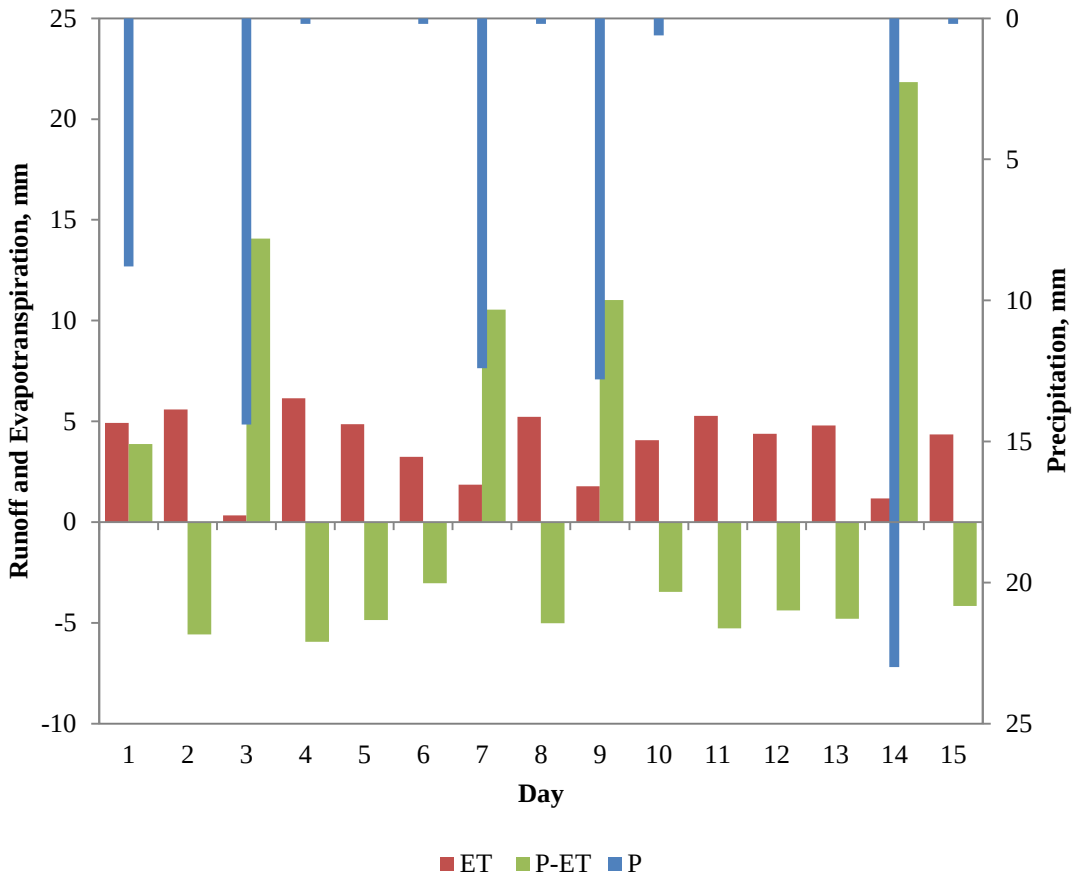


Figure 4.11. The bar graph displays the water balance of the field with daily rainfall, evapotranspiration and runoff.

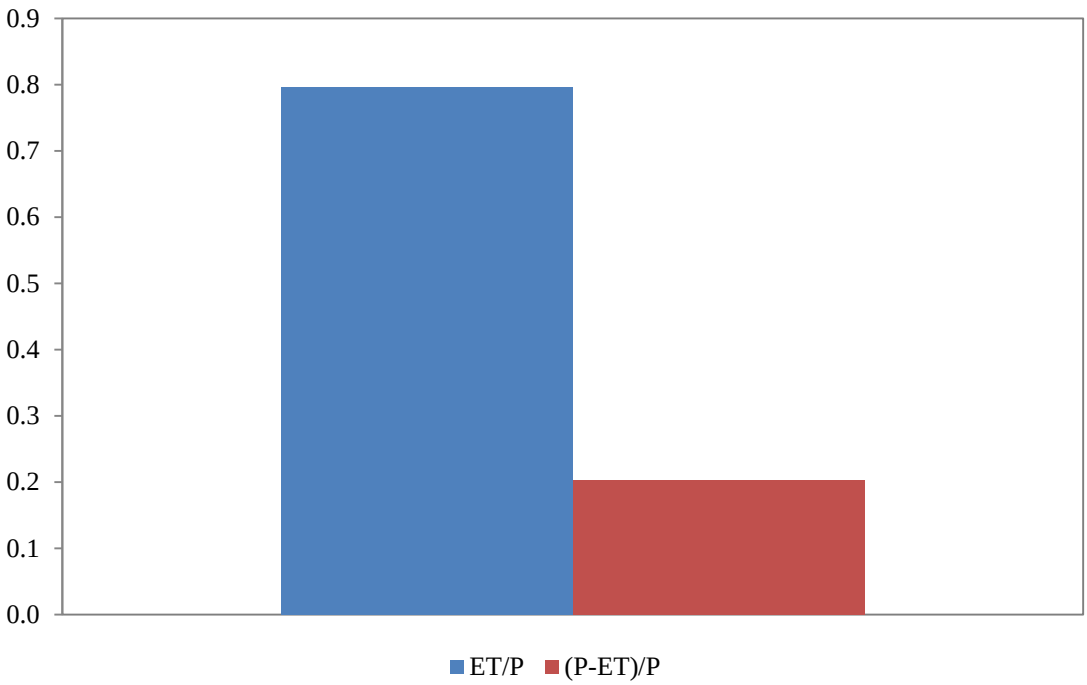


Figure 4.12. Bar graph displaying the proportion of precipitation consumed by evapotranspiration and proportion of precipitation consumed by the difference between evapotranspiration and precipitation.

Figure 4.13 displays the evaporation totals for each day of the study period from the field and the pan. Few days show that pan evaporation exceeded field evaporation. Majority of the total evaporation values from the field for each of the study period days are much greater than the corresponding pan evaporation totals. On several days of the study period, field evaporation is more than double pan evaporation.

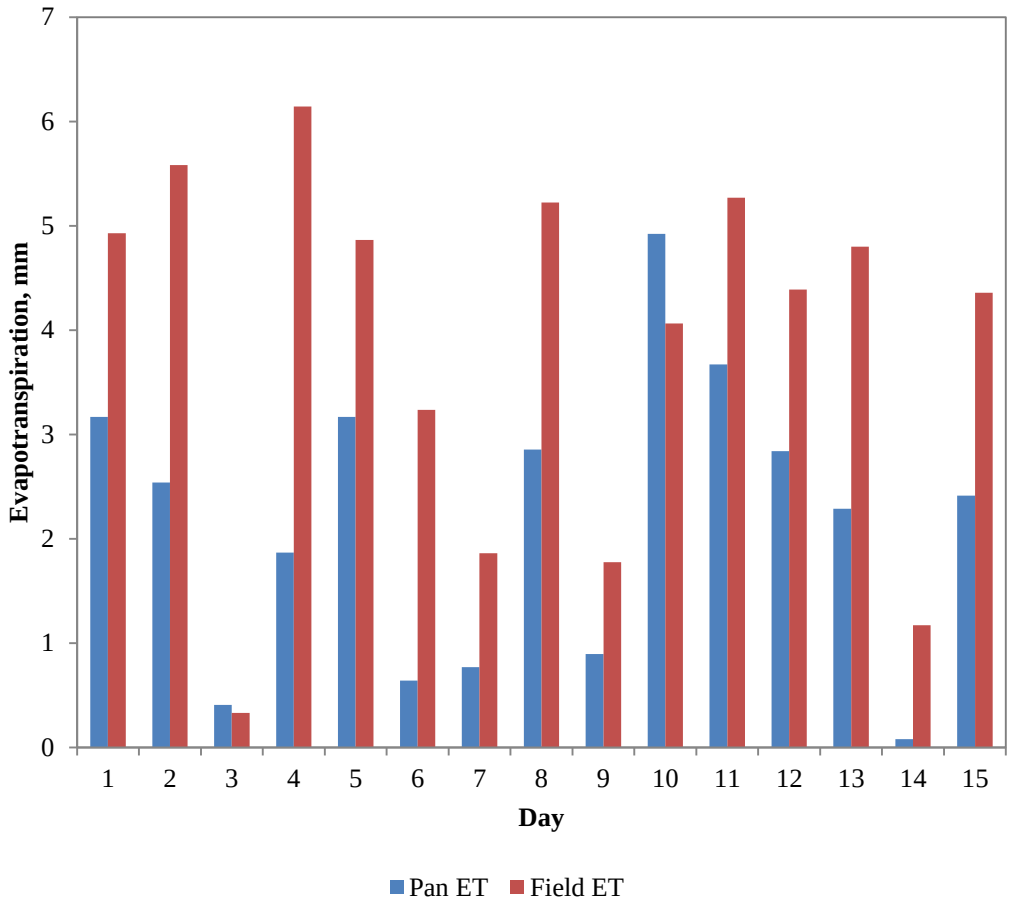


Figure 4.13. Daily evapotranspiration of the field and the pan for the 15 day study period.

Figure 4.14 is a time series graph of the precipitation events during the study period and the change in water level of the pan. For four of the five major rain events, the pan responded immediately to the input of water. On the fifth rain event, the pan lagged with respect to water level rise. The large rain events that were registered with the pan water level gauge were very close numerically to the values collected by the tipping bucket rain gauge. The smaller rain events did not respond as well with the pan water level measurements and went undetected even though the tipping bucket rain gauge indicated deposit of rain.

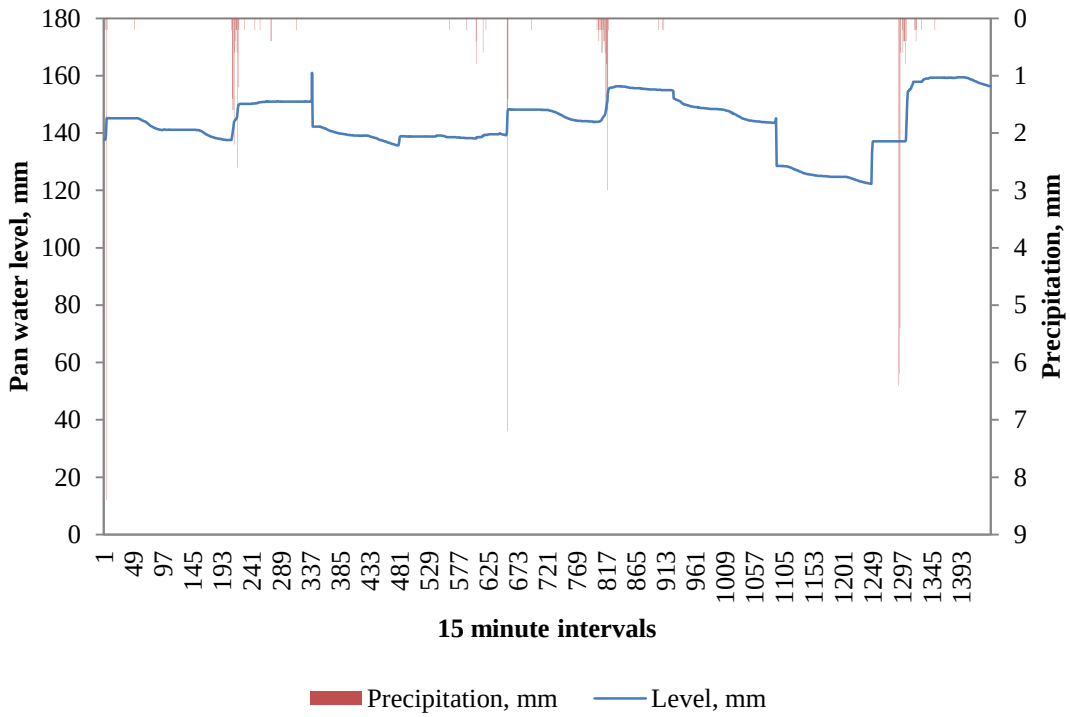


Figure 4.14. The time series graph displays the precipitation and pan water level for the 15 days of the study period. The first 15 minute interval starts at midnight on 1 August 2011.

Daily average daytime aerodynamic resistance for the study period ranged from approximately 100 to slightly above 430 s $m^{-1}$. This can be seen from Figure 4.17 where many of the daily average daytime aerodynamic resistance values are less than 250 s $m^{-1}$. As seen in Figures 4.16a and 4.16b, the displacement height and surface roughness values were found to have a north (+1) and south (-1) wind direction bias (⇌) and were modelled with linear regressions of $d = 0.068 \rightleftharpoons +0.0046$ and $z_0 = -0.0335 \rightleftharpoons +0.0068$ respectively to account for the complexity of the field site. Wind direction bias was isolated by taking the cosine of the vane measurements. The 1.00 m anemometer height wind speed values was found to have the highest coefficient of determination for the relationship with surface roughness and displacement height values that were found when the atmosphere exhibited neutral conditions. For the displacement height correlation, a linear regression line of $d = 0.0707u_2 + 0.4509$ provided the best fit whereas the surface roughness correlation with the 1.00 m wind speed displayed the best

relationship with an exponential regression of $z_0 = 0.2882e^{-0.951u_2}$, which can be seen from Figures 4.15a and 4.15b respectively. With the initial two models between displacement height and wind speed and surface roughness and wind speed, a two variable linear regression model was determined with incorporation of the modelled values based on the north and south wind direction bias. Both, Figures 4.16c and 4.16d, two variable linear regression models displayed coefficient of determination that were slightly less than 80%. The modelled values of the zero plane displacement height and surface roughness allowed the aerodynamic resistance values to be calculated at any desired time but the computed values should be subjected to caution when in use due to uncertainty and variability of results because there are instances that $r_a$ increased with increasing wind speed. This interaction does not align with commonly accepted theory that $r_a$ is inversely related to wind speed (Oke 1987).

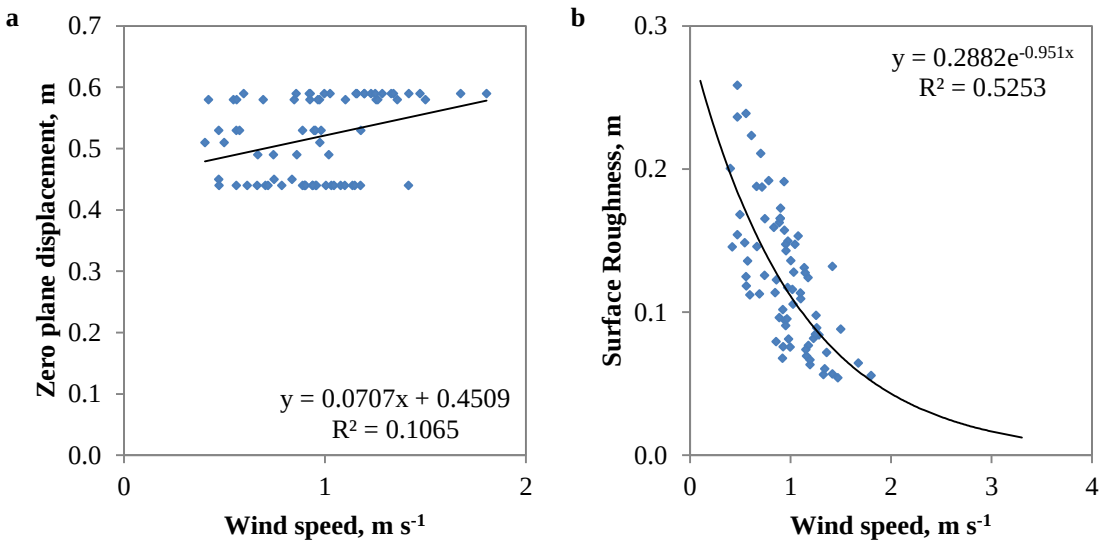


Figure 4.15. Graph (a) displays the correlation between the measured zero plane displacement height with the 1.00 m height anemometer wind speed values, fitted with a linear regression model. Graph (b) displays the correlation between the measured surface roughness values with the 1.00 m height anemometer wind speed values, fitted with an exponential regression model.

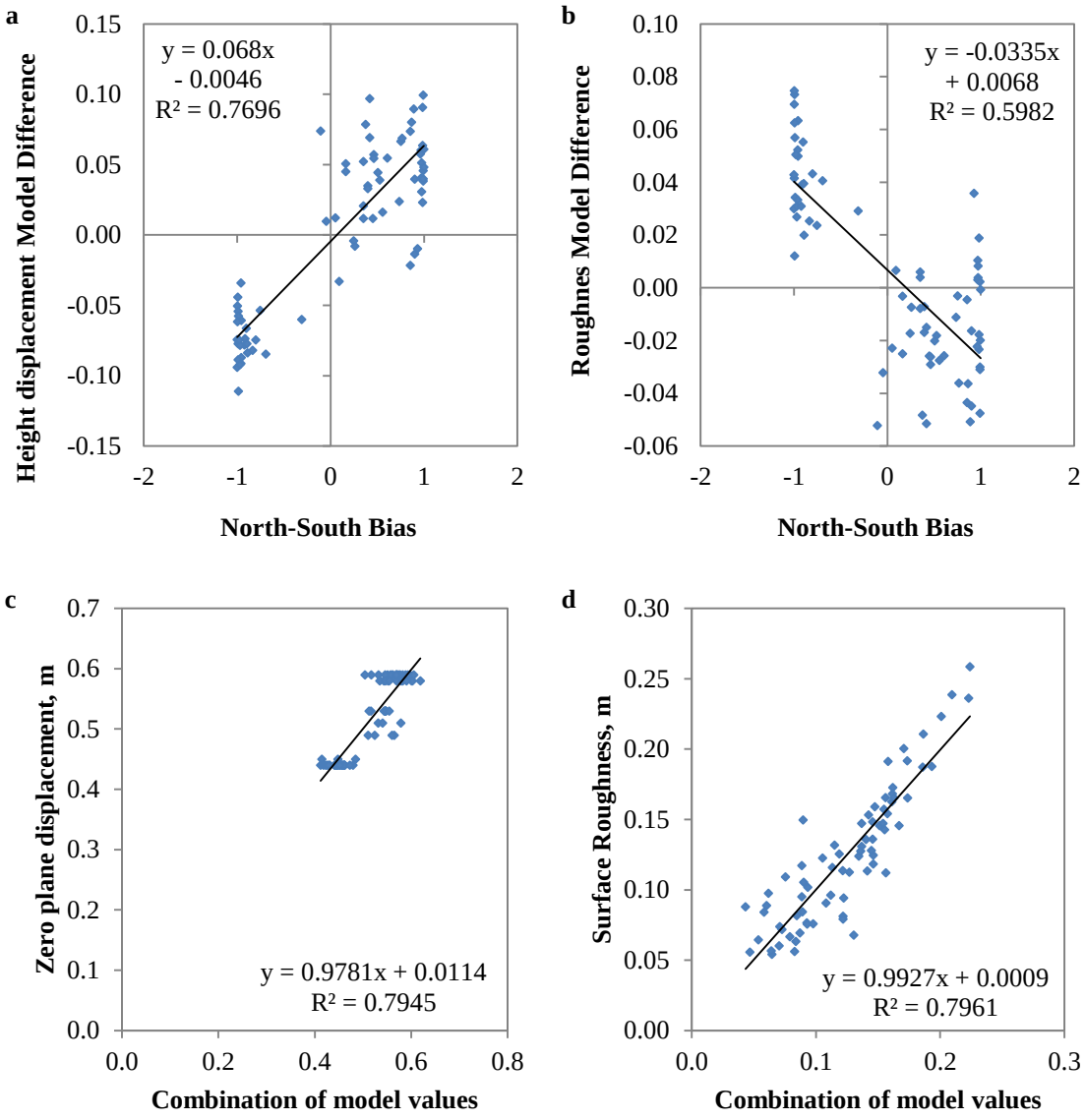


Figure 4.16. Graph (a) displays the correlation of the difference between the modelled zero plane displacement height values and measured displacement height values with the wind direction bias values. Graph (b) displays correlation between the difference of the modelled surface roughness values and measure roughness values to the wind direction bias. Graph (c) displays the correlation between the measured zero plane displacement height value and the combination of the linear regression model of the displacement height with wind speed and the model determined based on the wind direction bias. Graph (d) displays the correlation between the measured surface roughness values and the combination of the exponential regression model of the roughness with the 1.00 m wind speed and the model determined based on the wind direction bias. The linear regression models from (c) and (d) were ultimately used to determine surface roughness and displacement height values at any time during the 15 day study period.

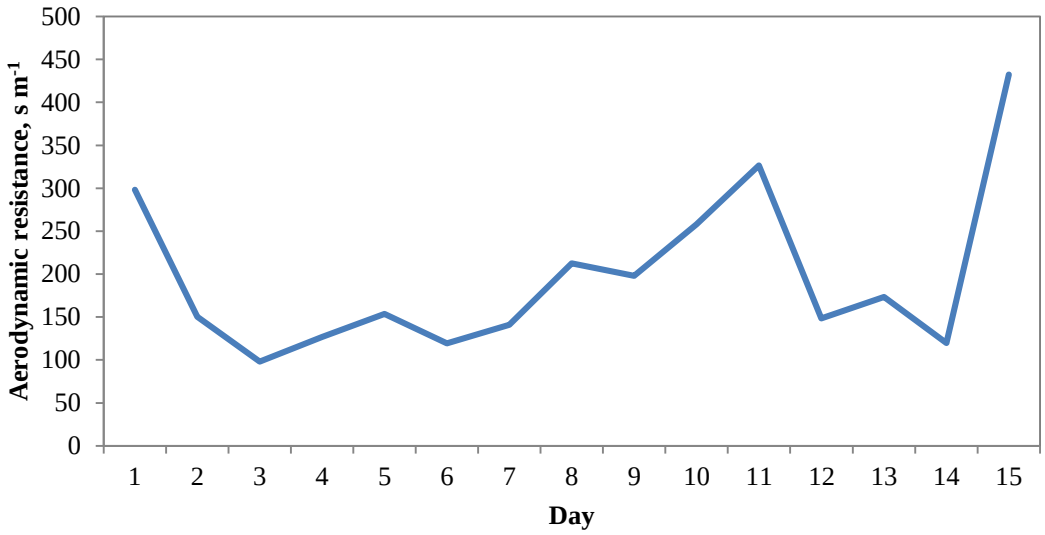


Figure 4.17. Display of the average daily daytime aerodynamic resistance of the field site based on the measurement systems and the modelled values of surface roughness and displacement height.

The isothermal resistance was calculated based on Equation 4.18. Daily average daytime values are plotted in Figure 4.18 and range from approximately 110 to 280 s $m^{-1}$.

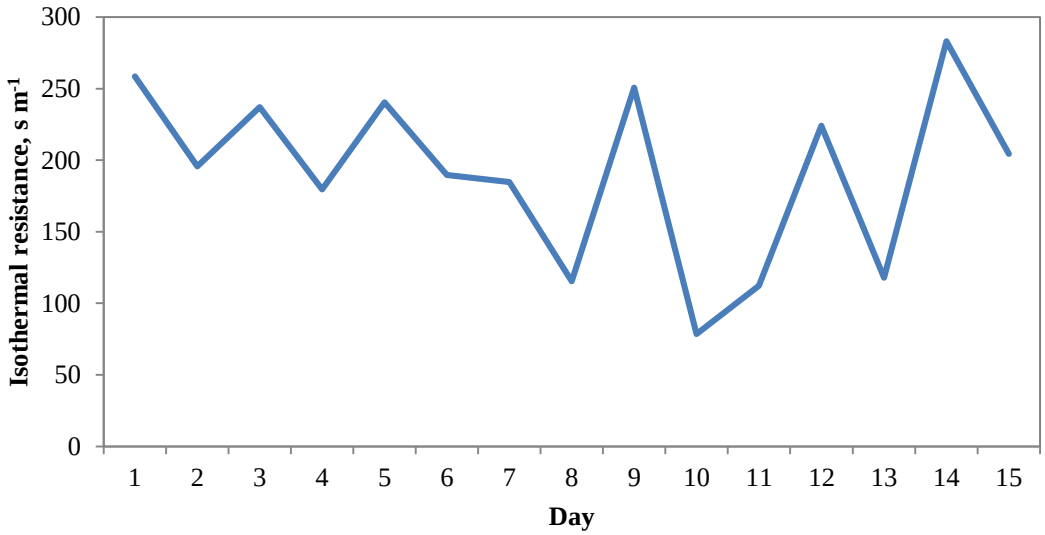


Figure 4.18. Display of the average daily daytime isothermal resistance of the field site.

The canopy resistance was calculated with Equation 4.19 by incorporating the isothermal and aerodynamic resistance values with the Bowen ratio. Daily average

daytime canopy resistance values are plotted in Figure 4.19 and range approximately from 170 to 620 s $m^{-1}$.

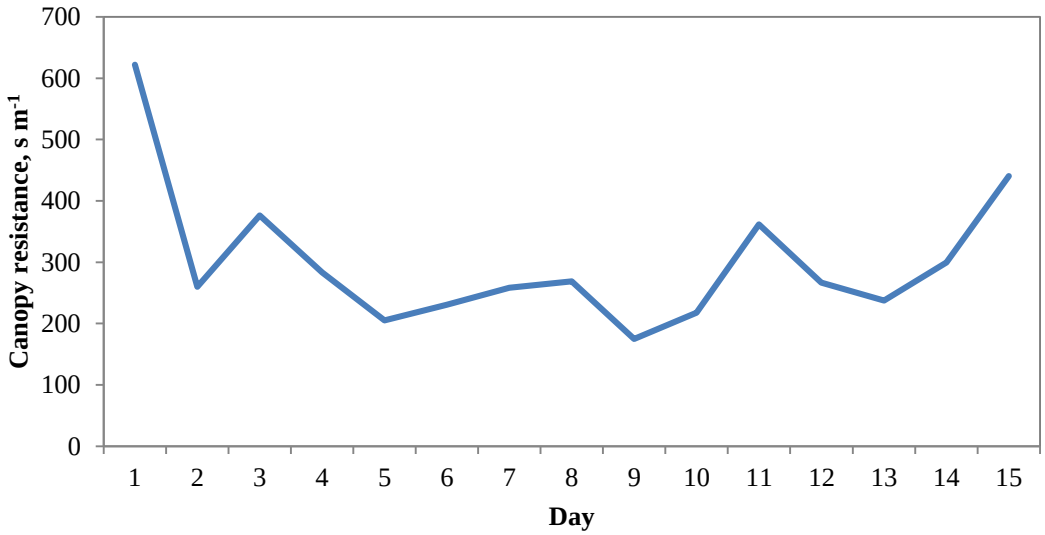


Figure 4.19. Display the average daily daytime values of canopy resistance for the study period at the field site.

Although the methods used to calculate the aerodynamic, isothermal and canopy resistance of the field with the measurement systems has been used by several researchers, many of the values are questionable due to initial values of the aerodynamic resistance not being representative of know interactions with wind speed and normally accepted values of tall grassed land cover. Only three of the 15 days yielded acceptable aerodynamic resistance results that would respond inversely to wind speed measurements. This led to canopy resistance values that could be used to describe the status of the field site and the environmental interactions between the surface and atmosphere. Within the three acceptable days of aerodynamic and canopy resistance values, only several hours of each daytime period could be used for analysis.

Figure 4.20 displays the average hourly surface energy budget fluxes measured with the BREB system on the three acceptable days that the resistance values displayed representative interactions. Two types of energy days can be seen from Figure 4.20, which are low energy and high energy days. On the low energy day (3 August 2011), the

dominant surface energy budget processes consuming the net radiation interchanges with respect to dominance. This is not the same for the high energy days (5 and 12 August 2011) where the latent heat flux is the dominant consumer of the net radiation. Figure 4.20a is the low energy day and that can be attributed to cloudy conditions and a storm event.

Figures 4.20b and 4.20c show the higher energy days and they did not experience any wet weather conditions. There are periods of variable cloud cover as can be seen in Figure 4.20b and persistent cloud cover at the end of the day as seen from Figure 4.20c. Knowing the weather conditions and receipt of net radiation can help to better understand how and why the plant community responds to the environmental conditions of the study site and why water vapour is suppressed or released to the atmosphere. It is expected that the stomates of the plants in the field will allow transpiration to proceed when there is ample sunlight or net radiation. Similarly, the amount of sunlight should influence the environmental temperature and create conditions that would be acceptable or not suitable for the plants to release water vapour to the atmosphere. One limitation of this study to better understand the plant community of the field site was that carbon dioxide concentrations were not used to determine if the plants were assimilating carbon and photosynthesizing.

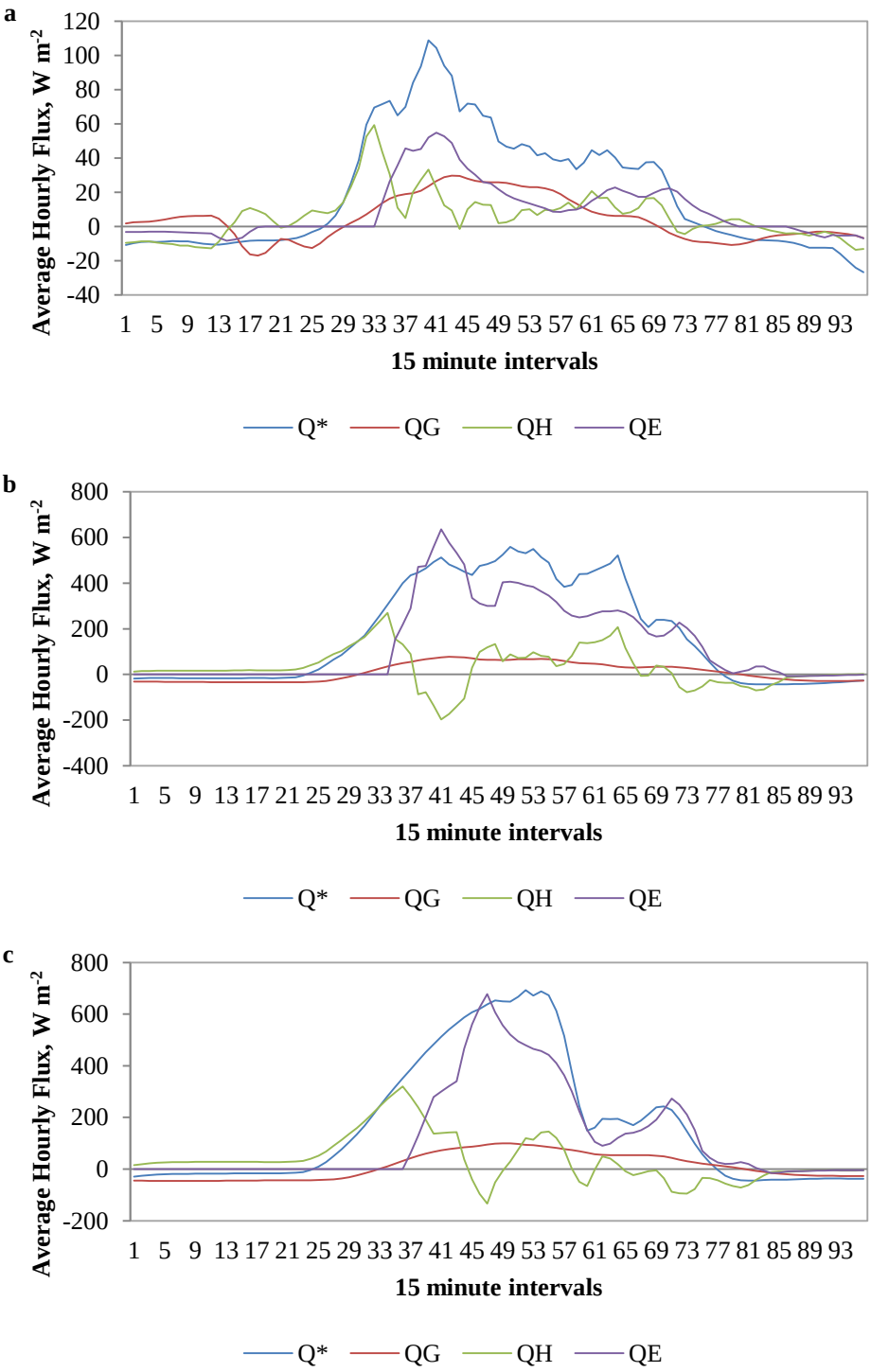


Figure 4.20. These graphs display the hourly average surface energy budget fluxes of the field that were measured with the Bowen ratio energy balance system of the three acceptable days used to better understand the aerodynamic characteristics of the field site.

Due to the displacement height and surface roughness values relying on the 1.00 m height wind speed, few acceptable aerodynamic resistance values could be obtained. The empirical relationships for $z_0$ and $d$ were used to account for the structure of field site because few measurement periods were available to construct actual $z_0$ and $d$ values. Figure 4.20 displays the three days with isolated time periods that the aerodynamic resistance values were responding to the inverse of the 3.00 m height wind speed measurements. In Figure 4.21a the aerodynamic resistance values range from approximately 64 to 82 s $m^{-1}$ with corresponding wind speed values ranging from 0.8 to 1.4 m $s^{-1}$. Figure 4.21a has the largest single day count with 28 quarter hourly measurements. The first measurement interval of Figure 4.21a starts in the morning at 06:45 and ends at 13:30. The calculation of the aerodynamic resistance values begins immediately as the storm event ceases, based on the tipping bucket rain gauge recording its final measurement at 06:45 on 3 August 2011.

Figures 4.21b and 4.21c represent high energy days because close to the noon hour net radiation was at a minimum greater than 550 W $m^{-2}$. During aerodynamic resistance values that were calculated on 5 August 2011, aerodynamic resistance ranged from approximately 70 to just above 160 s $m^{-1}$. Wind speed for the same time period ranged from 0.7 to 1.8 m $s^{-1}$. Likewise, the range of aerodynamic resistance on 12 August 2011 was approximately 70 to 98 s $m^{-1}$ with ranging wind speed measurements between 0.8 and 1.5 m $s^{-1}$. Both 5 and 12 August have very sharp resistance similarities with respect to environmental conditions but there are minor differences between the high energy measurement days.

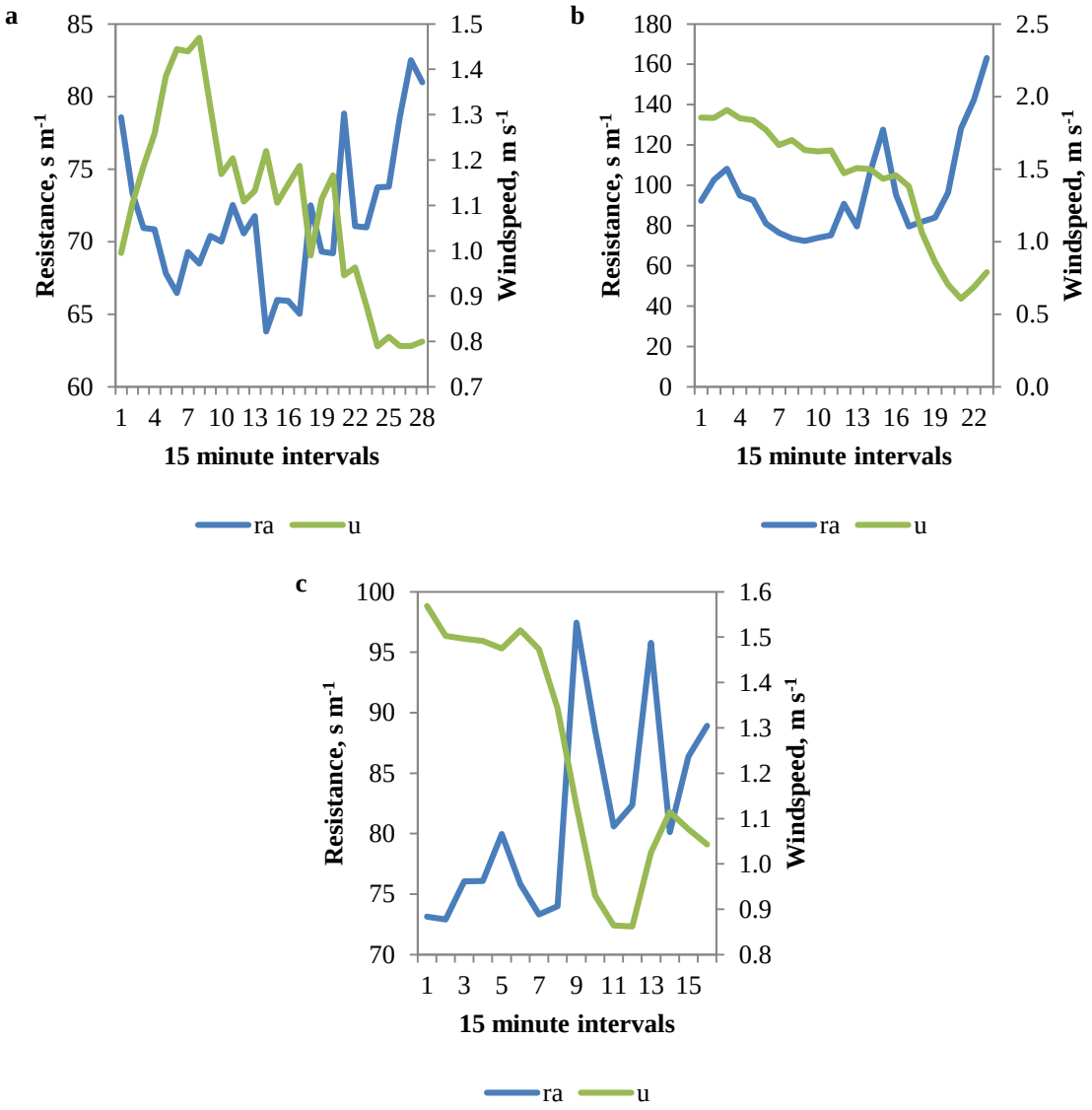


Figure 4.21. These graphs display limited time series of the change of the aerodynamic resistance and wind speed from the three days that were found to respond to the inverse relationship between wind speed and aerodynamic resistance.

Oke (1987) affirmed that five dynamic interactions of an environment allow for plants to photosynthesize and they are sunlight, carbon dioxide, $VPD$, leaf water potential and leaf temperature. One limitation of this study to better understand the plant community physiology was that carbon dioxide was not measured or calculated to be analysed so that relationships could be made with other environmental variables because the CR is based strictly on energetic terms impacting water movement. Leaf water

potential and leaf temperature also were not a primary focus of this study and could not be used to describe the physical nature of the plants. A surrogate for leaf temperature that could be used is air temperature. Net radiation and vapour pressure deficit were measured directly and could be plotted with the canopy resistance to tease out the control mechanisms of transpiration.

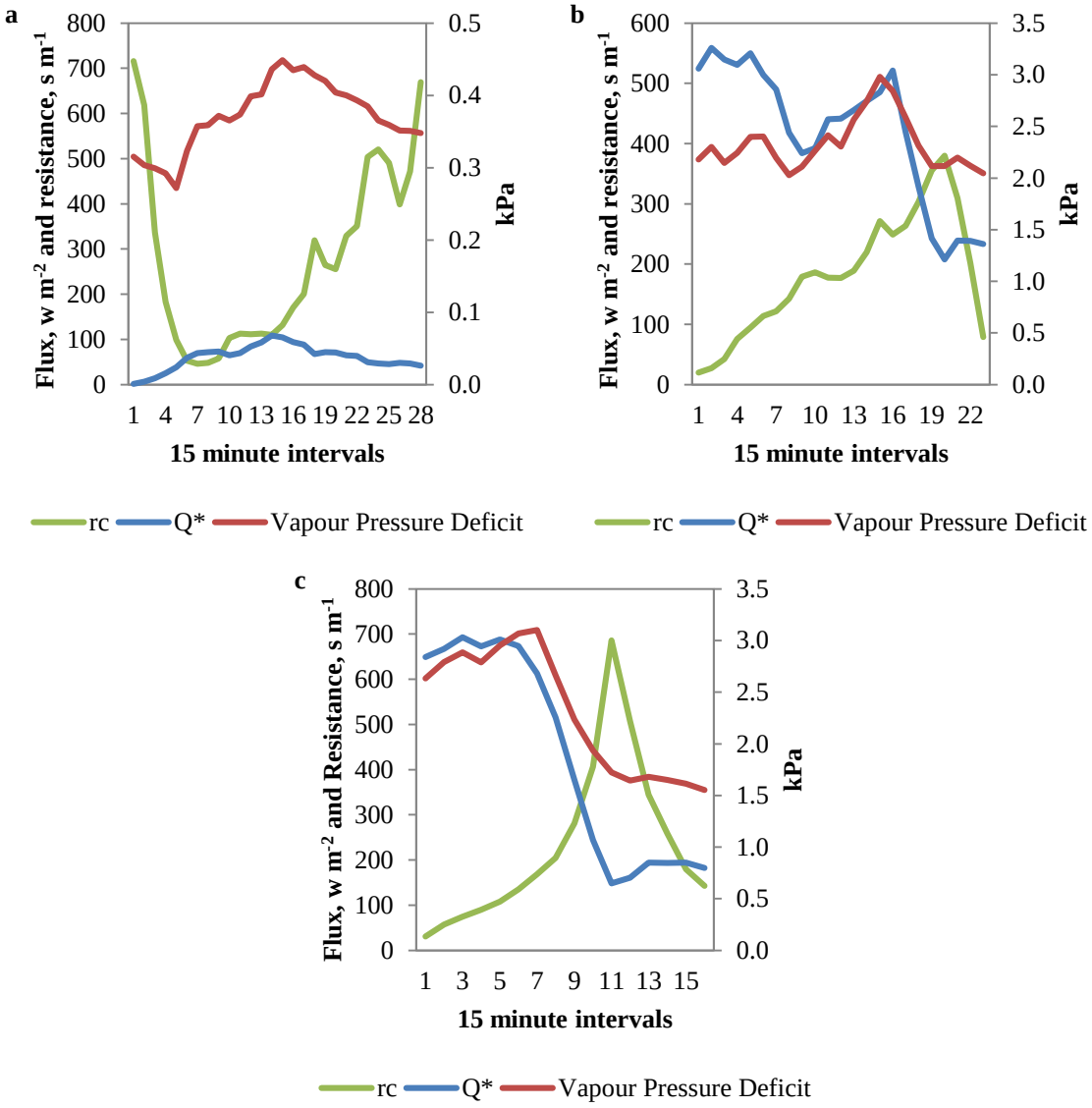


Figure 4.22. These graphs display the time series of net radiation, vapour pressure deficit, and canopy resistance of the three days that were found to be acceptable to better understand the aerodynamic and physiological characteristics of the field site.

The temperature profile measured with the BREB system for the three days that representative resistance values were computed are shown in Figure 4.23. The wet environment day temperature profile ranged from 19.38 to 21.20$^{o}$C thereby being a moderately cool day in August, as can be seen from Figure 4.23a. On the first high energy day, the temperature profile values ranged from 27.44 to 31.40$^{o}$C and were variable during the measurement period as can be seen from Figure 4.23b. The other high energy day temperature profile was not as variable during the measurement period, which can be seen from Figure 4.23c. The temperature profile values were highest at the beginning (31.85$^{o}$C) of the measurement period and decreased towards the end with the lowest value at 25.53$^{o}$C.

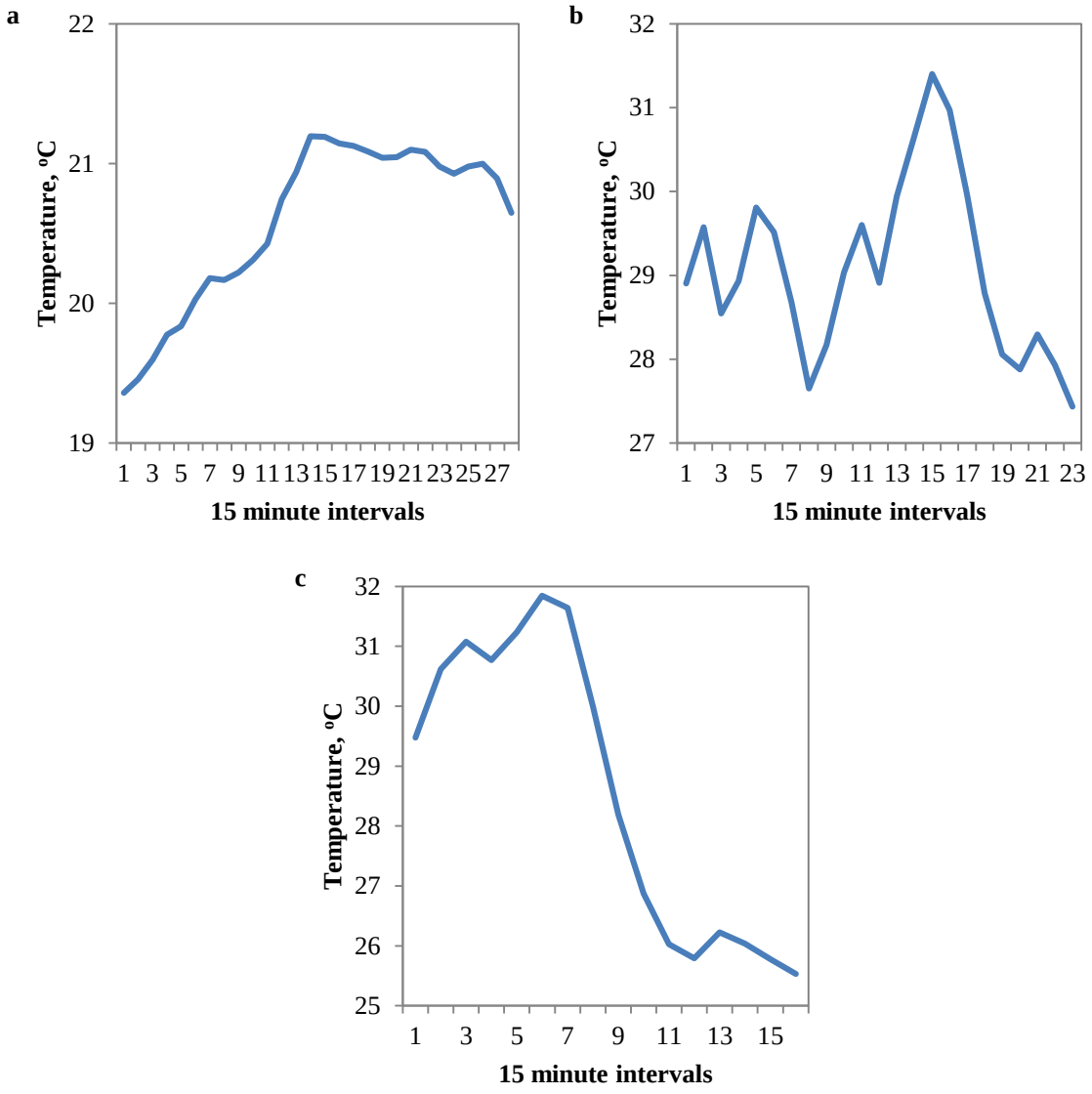


Figure 4.23. These graphs display the average temperature trends that were measured with the Bowen ratio energy balance profile of the three days that were found to be acceptable to better understand the physical characteristics of the field site.

## 4.4 Discussion

From the daily observations of pan ground heat flux, greater amount of energy was drawn into the northern side of the pan. This spatial bias introduces uncertainty, never known prior that within the coverage area of a Class A evaporation pan much spatial variability exists with respect to ground heat flux. Jacobs et al. (1998) did perform

a similar experiment but only used a single soil heat flux plate, positioned in the centre of the pan. They similarly measured the energy budget of their pan.

Total evaporation from the pan for the 15 day study period totaled to 32.5 mm. Total pan evaporation was 56% of the field evaporation based on the ratio of pan evaporation to field evaporation. This value is slightly greater than the potential evaporation that would be experienced in the wet condition of the CR (Morton 1975). The CR dictates that during environmental conditions of complete saturation, potential evaporation will be half the rate in a wet environment compared to an arid environment. During all days, except one, field evaporation was greater than pan evaporation, as seen from Figure 4.13. This result suggests that the pan measurement system was non-functional. It does not resonate with the complementary nature of pan evaporation situated in terrestrial environments.

A very serious deficiency in the design of using the pan to measure potential evaporation can be seen from Figure 4.14 with respect to water level measurement. The results of this study relied on accurate measurement of changes to pan water level due to the theory used based on Bello and Smith (1990). Although pan evaporation seemed to respond to the environmental conditions of the study site, during one specific rain event the pan water level gauge did not respond to increases of water immediately. It is suspect that the instrument seemed to be functioning properly but was not working as desired even though perceived accurate measurements of change in water level were being recorded. There was hope that using a Class A evaporation pan to construct water balance of the field site would be feasible. This was not the case because pan evaporation values were less than field evaporation. Consequently it was not possible to reconstruct $Q_{EP0}$ fluxes with any certainty.

Net radiation, as an indicator of sunlight, showed most trend similarity to canopy resistance. Mainly, as sunlight increased the canopy resistance decreased indicating that evaporation from the experimental site released water into the atmosphere. The $VPD$ did not show clear interactions with the canopy resistance. As the $VPD$ decreased, the ability of the canopy to release water vapour through transpiration should be limited. Also, the

surface should have difficulties evaporating water. It is generally believed that immediately after rainfall has ceased, the canopy resistance should diminish to zero and water should be freely available to enter the atmosphere. The low energy day, which was also the wet environment day, did not experience canopy resistance values that were close to zero. This does cause concern for the computed canopy resistance values being representative of an environment that should have moisture freely available to enter the atmosphere. This issue could be explained by the low receipt of net radiation for the same time period. Another confounding issue is the strong sensitivity of zero plane displacement and surface roughness to wind speed. This sensitivity was so strong the aerodynamic resistance actually increased on several days with higher wind speeds as opposed to what is more universally observed. Because $r_a$ is used in the calculation of $r_c$ a lot of the variability in canopy or stomatal resistance is likely due to this rather than being a real representation of moisture availability.

The calculation of the wet bulb depression at the measurement heights of the BREB temperature profile was determined by the method documented by Abbott and Tabony (1985). The wet bulb depression calculations yielded values that were representative of the environmental conditions. However, due to limitations of the research endeavour, the wet bulb depression at the surface produced values that were not representative and unwieldy. Thus, better understanding the relationship between pan evaporation and the field cannot draw any conclusive results with use of the wet bulb depression values. Due to an incomplete account of the wet bulb depression, the series of equations to help better understand how temperature change influences pan and field evaporation could not be followed through with clear understanding. Similarly, finding the critical resistance with use of the wet bulb depression of the surface could not be achieved.

## 4.5 Conclusions

Due to non-representative pan evaporation values, the comparison of the surface energy budget of the field and the pan could not be analyzed with complete confidence. The surface energy budget of a Class A evaporation pan relies on accurate measurements

of pan water level to calculate the pan latent heat flux and the flux of the pan water due to heating and cooling. The ground heat flux and net radiation of both the field and the pan showed much difference with respect to the surface cover types. Over daily total accumulation of net radiation, the field received a greater flux than the pan. Similarly, the ground heat flux of the pan was very different than the field. It has never been known that the ground heat flux of the pan exhibited as great a bias within a small coverage area. The north and south portion of the pan typically drew more ground heat than the east and west portions of the pan. This highlights the uncertainty and complexity of using a Class A evaporation pan for the purpose of determining evaporation from the landscape.

During the study period measurement, real evaporation was greater than pan evaporation. This result proves inconclusive with respect to previously held beliefs that potential or pan evaporation should always be equal to or greater than real evaporation.

The grassland experimental site is a very complex land cover type. Use of the anemometer mast required savvy solutions to parse out the competing factors governing changes of the aerodynamic and fluid mechanical properties. The surface roughness and zero-plane displacement height were variable and influenced by wind speed and direction. The 1.00 m wind speed height provided the best measurement to model the roughness length and displacement height. Similarly, the north and south wind direction yielded the most influence on roughness and displacement values, as determined from the model.

Only limited time periods from three of the 15 days of the study period garnered acceptable aerodynamic resistance values, which allowed for computed values of the isothermal and canopy resistance. The canopy resistance showed that net radiation is the primary driving force for the surface to release water vapour. Vapour pressure deficit had an influencing role on the canopy resistance but on the high energy days that resistance values were calculated the vapour pressure deficit indicated the atmosphere had the ability to accept water from the surface. Profile temperature averages could prove to be a surrogate for leaf temperature. However, profile temperature values are not the true temperature of the leaf.

Better understanding Bouchet's hypothesis and the relationship between potential and real evaporation is a complex endeavour. The use of the meadow land cover type introduces severe complexity to the analysis and complete understanding of the physical properties of the region. Resolving the complementary relationship and determining the influencing mechanism on the equilibrium wet environment evaporation would be better tested over a surface where surface roughness and zero plane displacement did not change with wind speed (e.g. mowed grass surface) and with a pan which had a reliable water level measurement system.

## 4.6 References


Abbott, P. F. and Tabony, R. C. 1985. The estimation of humidity parameters. *Meteorological Magazine*, 114, 49 – 56.

Bello, R. and Smith, J. D. 1990. The effect of weather variability on the energy balance of a lake in the Hudson Bay Lowlands, Canada. *Arctic and Alpine Research*, 22(1), 98 – 107.

Bonan, G. 2008. Ecological Climatology, Concepts and Applications. 2nd eds. Cambridge University Press: Cambridge, United Kingdom.

Bouchet, R. J. 1963. Évapotranspiration réelle et potentielles significance climatique. *International Association of Scientific Hydrology*, 62, 134 – 142.

Bowen, I. S. 1926. The ratio of heat losses by conduction and by evaporation from any water surface. *Physical Review*, 27, 779 – 787.

Brutsaert, W. and Stricker, H. 1979. An advection-aridity approach to estimate actual regional evapotranspiration. *Water Resources Research*, 15(2), 443 – 450.

DeBruin, H. A. R and Holtslag, A. A. M. 1982. A simple parameterization of the surface fluxes of sensible and latent heat during daytime compared with the Penman-Monteith concept. *Journal of Applied Meteorology*, 21, 1610 – 1621.

Heilman, J. L., Brittin, C. L. and Neale, C. M. U. 1989. Fetch requirements for Bowen ratio measurements of latent and sensible heat fluxes. *Agricultural and Forest Meteorology*, 44, 261 – 273.

Jacobs, A. F. G., Heusinkveld, B. G. and Lucassen, D. C. (1998). Temperature variation in a class A evaporation pan. *Journal of Hydrology*, 206, 75 – 83.

Monteith, J. L. and Unsworth, M. H. 1990. *Principles of Environmental Physics*. Oxford: Great Britian, Butterworth-Heinemann.

Monteith, J.L., 1965. Evaporation and environment. In: Fogg, G.E. (Ed.), The State and Movement of Water in Living Organism. Soc. Exp. Biol. Symp. 19, 205–234

Morton, F. I. 1965. Potential evaporation and river basin evaporation. *Proceedings of American Society of Civil Engineers Journal of Hydraulics Division*, HY6 ,67 – 97.

Morton, F. I. 1968. Evaporation and climate: A study in cause and effect. *Inland Waters Branch Department of Energy, Mines and Resources*, Ottawa, Science Series, 4, 1 – 32.

Morton, F. I. 1969. Potential evaporation as a manifestation of regional evaporation. *Water Resources Research*, 5(6), 1244 – 1255.

Morton, F. I. 1971. Catchment evaporation and potential evaporation further development of a climatological relationship. *Journal of Hydrology*, 12, 81 – 99.

Morton, F. I. 1975. Estimating evaporation and transpiration from climatological observations. *Journal of Applied Meteorology*, 14, 488 – 497.

Morton, F. I. 1976. Climatological estimates of evapotranspiration. *Journal of Hydraulics Division – American Society of Civil Engineers*, 102(3), 275 – 291.

Morton, F. I. 1983. Operational estimates of areal evapotranspiration and their significance to the science and practice of hydrology. *Journal of Hydrology*, 66, 1 – 76.

Oke, T. R. 1987. Boundary Layer Climates. 2nd eds. Methuen, London: Great Britain.

Priestley, C. H. B., and Taylor, R. J. 1972. On the assessment of surface heat flux and evaporation using large-scale parameters. *American Meteorological Society Monthly Weather Review*, 100(2), 81 – 92.
Slayter, R. O. and McIlroy, I. C. 1961. *Practical Microclimatology*. Melbourne: Australia, CSIRO.

# Chapter 5 Conclusions

For this research, evaporation was measured from two sites within the Humber R. watershed over a two year period. At the naturalized site with normal infiltration, hourly estimates of the surface latent heat flux and surface water budget were measured with a four-level Bowen ratio energy balance system. At the urbanized site, with restricted infiltration, the latent heat flux was measured with a combination of a three level BREB system and a weighing lysimeter. At the naturalized site, an ancillary experiment employing a network of soil heat flux plates was conducted to capture the spatial heterogeneity in the ground heat flux and provide more accurate estimates of $Q_G$. Results showed that despite similar rainfall receipt, the naturalized site evaporated 73.0% on average of precipitation back to the atmosphere by drawing on soil moisture passing up through the plant canopy as transpiration. In contrast, the impervious site only evaporated 23.5% of precipitation because the majority of water was routed into the storm water drainage system. The results highlight the implications of urbanization through its effect on the water budget as well as the surface energy balance whereby natural sites have much lower Bowen ratios and where a much larger proportion of the net radiation consumed in latent heating.

The second part of the research explored the theory behind the complementary relationship (CR), based on Bouchet's (1963) hypothesis, between potential and real (or actual) evaporation. It proposed to explore the behavior of a new critical resistance, $r'$ which constitutes a height in the upper atmosphere where the effects of surface drying diminish and vapour pressure deficit is solely a function of regional advection. The experiment occurred at the naturalized flux site using traditional aerodynamic theory supported by wind profile measurements, to derive hourly estimates of canopy and aerodynamic resistances in combination with estimates of true potential evaporation from a Class A evaporation pan in order to examine the behavior of the critical resistance. Ancillary experiments were conducted to evaluate the energy balance of the Class A pan in comparison to the natural environment and showed fair agreement. An assessment of the surface roughness parameter, $z_0$ and the zero plane displacement of the naturalized field showed them to be highly variable on a daily and hourly basis. The variability

owing to changes in the inclination of the grasses under variable winds was modelled as a function of wind speed near the top of the plant canopy. Some of the variability in aerodynamic coefficients was also due to differences in the character of the plant community for different upwind fetches and this was modelled as a function of measured wind direction. The sensitivity of surface roughness to wind speed during the experimental period in August was quite large and often resulted in increases in aerodynamic resistance with increasing wind speed, which was contrary to expectations based on previously published work. Any errors in $r_a$ would be propagated into estimates of $r_c$ and ultimately $r'$. It became apparent that the water level measurement system in the evaporation pan was only working intermittently throughout the entire measurement period which was likely responsible for unrealistically small potential evaporation estimates compared to generally larger values from the field itself. Unfortunately, this precluded any sound conclusions about the complementary relationship from being formed. The theory presented still deserves empirical testing, under more controlled field conditions, as it would potentially allow for the reconstruction of actual evaporation estimates from archived records of pan evaporation, which could prove useful in evaluating historical water balance changes resulting from climate change.

**References**


Abbott, P. F. and Tabony, R. C. 1985. The estimation of humidity parameters. *Meteorological Magazine*, 114, 49 – 56.

Alados, I., Foyo-Moreno, I. and Alados-Arboledas, L. 2012. Estimation of downwelling longwave irradiance under all-sky conditions. *International Journal of Climatology*, 32, 781 – 793.

Baumgartner, A. and Reichel, E. 1975. *World Water Balance: mean annual global, continental and maritime precipitation, evaporation and run-off*, Elsevier Scientific: New York, New York.

Bello, R. and Smith, J. D. 1990. The effect of weather variability on the energy balance of a lake in the Hudson Bay Lowlands, Canada. *Arctic and Alpine Research*, 22(1), 98 – 107.

Bonan, G. 2008. *Ecological Climatology, Concepts and Application: 2nd eds*. Cambridge University Press: Cambridge, United Kingdom.

Bouchet, R. J. 1963. Évapotranspiration réelle et potentielles significance climatique. *International Association of Scientific Hydrology*, 62, 134 – 142.

Bowen, I. S. 1926. The ratio of heat losses by conduction and by evaporation from any water surface. *Physical Review*, 27, 779 – 787.

Brutsaert, W. and Parlange M. B. 1998. Hydrologic cycle explains the evaporation paradox. *Nature*, 396, 30.

Brutsaert, W. and Stricker, H. 1979. An advection-aridity approach to estimate actual regional evapotranspiration. *Water Resources Research*, 15(2), 443 – 450.

Budyko, M.I. 1974. *Climate and Life.* Academic Press: New York, New York.

Christiansen, J. E. 1966. Discussion of potential evaporation and river basin evaporation. *Journal of Hydraulic Engineering*, 92, 225 – 230.

Cleugh, H. A. and Oke, T. R. 1986. Suburban-rural energy balance comparisons in summer for Vancouver, B. C. *Boundary-Layer Meteorology*, 36, 351 – 369.

Correa, E., Ruiz, M. A., Canton, A., and Lesino, G. 2012. Thermal comfort in forested urban canyons of low building density – An assessment for the city of Mendoza, Argentina. *Building and Environment*, 58, 219 – 230.

Davenport, D. C. and Hudson, J. P. 1967. Changes in evaporation rates along a 17-km transect in the Sudan Gezira. *Agricultural Meteorology*, 4, 339 – 352.

Davies, J. A. 1972. Actual, potential and equilibrium evaporation for a beanfield in southern Ontario. *Agricultural Meteorology*, 10, 331 – 348.

Davies, J. A. and McCaughey, J. H. 1968. Potential evapotranspiration at Simcoe, southern Ontario. *Archiv für Meteorologie, Geophysik und Bioklimatologie Serie B*, 16 (4), 391 – 417.

DeBruin, H. A. R and Holtslag, A. A. M. 1982. A simple parameterization of the surface fluxes of sensible and latent heat during daytime compared with the Penman-Monteith concept. *Journal of Applied Meteorology*, 21, 1610 – 1621.

Denmead, O. T. and McIlroy, I. C. 1970. Measurements of non-potential evaporation from wheat. *Agricultural Meteorology*, 7, 285 – 302.

Elkin, C., Gutiérrez, A. G., Leuzinger, S., Manusch, C., Temperli, C., Rasche, L., and Bugmann, H. 2013. A 2  warmer world is not safe for ecosystem services in the European Alps. *Global Change Biology*, 19, 1827 – 1840.

Fairbridge, R. W. (1990). Water deficiency versus water excess: Global management potential. *Greenhouse Effect, Sea Level and Drought*, 325, 185 – 197.

Ferguson, J. 1952. The rate of natural evaporation from shallow ponds. *Australian Journal of Scientific Research*, 5(2), 315 – 330.

Fortin, J. P. and Seguin, B. 1975. Estimation de l'ETR régional à partir de l'ETP local: utilisation de la relation de Bouchet à differentes échelles de temps. *Annales Agronomiques*, 26(5), 537 – 554.

Fritschen, L. J. 1965. Accuracy of evapotranspiration determinations by the Bowen ratio method. *Hydrological Science Journal*, 10 (2), 38 – 48.

Fuchs, M. and Tanner, C. B. 1970. Error analysis of Bowen ratios measured by differential psychrometry. *Argicultural Meteorology*, 7, 329 – 334.

Fung, F., Lopez, A., and New, M. 2011. Water availability in +2℃ and +4℃ worlds. *Philosophical Transactions of The Royal Society A*, 369, 99 – 116.

Granger, R. J. 1989a. A complementary relationship approach for evaporation from nonsaturated surfaces. *Journal of Hydrology*, 11, 31 – 38.

Granger, R. J. 1989b. An examination of the concept of potential evaporation. *Journal of Hydrology*, 11, 9 – 19.

Grimmond, C. S. B. and Oke, T. R. 1986. Urban water balance 2. Results from a suburb of Vancouver, British Columbia. *Water Resources Research*, 22 (10), 1404 – 1412.

Grimmond, C. S. B. and Oke, T. R. 1991. An evapotranspiration-interception model for urban areas. *Water Resources Research*, 27 (7), 1739 – 1755.

Grimmond, C. S. B. and Oke, T. R. 1999. Evapotranspiration rates in urban areas. *International Association of Hydrological Sciences*, 259, 235 – 243.

Grimmond, C. S. B. and Oke, T. R. 1999. Evapotranspiration rates in urban areas. *International Association of Hydrological Sciences*, 259, 235 – 243.

Grimmond, C. S. B., Oke, T. R. and Steyn, D. G. 1986. Urban water balance 1. A model for daily totals. *Water Resources Research*, 22 (10), 1397 – 1403.

Heilman, J. L., Brittin, C. L. and Neale, C. M. U. 1989. Fetch requirements for Bowen ratio measurements of latent and sensible heat fluxes. *Agricultural and Forest Meteorology*, 44, 261 – 273.

Hendriks, M. R. 2010. Introduction to Physical Hydrology. Oxford University Press: New York, New York.

Hobbins, M. T., Ramirez, J. A. and Brown, T. C. 1999. The complementary relationship in regional evapotranspiration: The CRAE model and the advection-aridity approach. *In Proceedings of the Nineteenth Annual AGU Hydrology Days*, 199 – 212.

Hobbins, M. T., Ramirez, J. A. and Brown, T. C. 2001a. The complementary relationship in estimation of regional evapotranspiration: An enhanced advection-aridity model. *Water Resources Research*, 37(5), 1389 – 1403.

Hobbins, M. T., Ramirez, J. A. and Brown, T. C. 2004. Trends in pan evaporation and actual evapotranspiration across the conterminous U.S.: paradoxical or complementary. *Geophysical Research Letters*, 31, 1 – 5.

Hobbins, M. T., Ramirez, J. A., Brown, T. C. and Claessens, L. H. J. M. 2001b. The complementary relationship in estimation of regional evapotranspiration: The complementary relationship areal evapotranspiration and advection-aridity models. *Water Resources Research*, 37(5), 1367 – 1387.

Hossen, M. S., Mano, M., Miyata, A., Baten, M. A., and Hiyama, T. 2012. Surface energy partitioning and evapotranspiration over a double-cropping paddy field in Bangladesh. *Hydrological Processes*, 26, 1311 – 1320.

Huntington, J. L., Szilagyi, J., Tyler, S. W. and Pohll, G. M. 2011. Evaluating the complementary relationship for estimating evapotranspiration from arid shrublands. *Water Resources Research*, 47(5), 1 – 11.

Iruthayaraj, M. R. and Morachan, Y. B. 1978. Relationship between evaporation from different evaporimeters and meteorological parameters. *Agricultural Meteorology*, 19, 93 – 100.

Jacobs, A. F. G., Heusinkveld, B. G. and Holtslag, A. A. M. 2008. Towards closing the surface energy budget of a mid-latitude grassland. *Boundary-Layer Meteorology*, 126, 125 – 136.

Jacobs, A. F. G., Heusinkveld, B. G. and Lucassen, D. C. (1998). Temperature variation in a class A evaporation pan. *Journal of Hydrology*, 206, 75 – 83.

Jasechko, S., Sharp, Z. D., Gibson, J. J., Birks, S. J., Yi, Y., and Fawcett, P. J. 2013, Terrestrial water fluxes dominated by transpiration. *Nature*, 496, 347 – 351.

Kahler, D. M. and Brutsaert, W. 2006. Complementary relationship between daily evaporation in the environment and pan evaporation. *Water Resources Research*, 42, 1 – 9.

Kim, C. P. and Entekhabi, D. 1998. Examination of two methods for estimating regional evaporation using a coupled mixed layer and land surface model. *Water Resource Research*, 33(9), 2109 – 2116.

Kim, C. P. and Entekhabi, D. 1998. Feedbacks in the land-surface and mixed-layer energy budgets. *Boundary Layer Meteorology*, 88(1), 1 – 21.

Kohler, M. A. and Parmele, L. H. 1967. Generalized estimates of free-water evaporation. *Water Resources Research*, 3(4), 996 – 1005.

Korzun, V.I., Sokolov, A.A., Budyko, M.I., Voskrensensky, K.P., Kalinin, G.P., Konoplyantsev, A.A., Korotkevich, E.S. and L'vovich, M.I. 1978. *World Water Balance and Water Resources of the Earth*, UNESCO Press, Paris.

Kovacs, G. 1987. Estimation of average areal evapotranspiration – proposal to modify Morton's model based on the complementary character of actual and potential evapotranspiration. *Journal of Hydrology*, 95, 227 – 240.

Lange, O. L., Lösch, R. and Kappen, L. 1971. Responses of stomata to changes in humidity. *Planta*, 100, 76 – 86.

LeDrew, E. F. 1979. A diagnostic examination of a complementary relationship between actual and potential evapotranspiration. *Journal of Applied Meteorology*, 18, 495 – 501.

Lockwood, J. G. 1985. *World climatic systems*. Edward Arnold, London: Great Britain.
Lvovitch, M. I. 1970. World water balance. In: Symposium on World Water Balance, Vol II. IAH Publ. 93. IAHS Press, Wallingford, UK.
Lvovitch, M. I. 1973. The global water balance. *EOS, Transactions American Geophysical Union*, 54(1), 28 – 53.
Lhomme, J. P. 1997a. A theoretical basis for the Priestley-Taylor coefficient. *Boundary Layer Meteorology*, 82, 179 – 191.
Lhomme, J. P. 1997b. An examination of the Priestley-Taylor equation using a convective boundary layer model. *Water Resources Research*, 33, 2571 – 2578.
Lhomme, J. P. and Guilioni, L. 2010. On the link between potential evaporation and regional evaporation from the CBL perspective. *Theoretical and Applied Climatology*, 101, 143 – 147.
Monteith, J. L. and Unsworth, M. H. 1990. *Principles of Environmental Physics*. Oxford: Great Britian, Butterworth-Heinemann.
Monteith, J.L., 1965. Evaporation and environment. In: Fogg, G.E. (Ed.), The State and Movement of Water in Living Organism. Soc. Exp. Biol. Symp. 19, 205–234
Morton, F. I. 1965. Potential evaporation and river basin evaporation. *Proceedings of American Society of Civil Engineers Journal of Hydraulics Division*, HY6 ,67 – 97.
Morton, F. I. 1968. Evaporation and climate: A study in cause and effect. *Inland Waters Branch Department of Energy, Mines and Resources*, Ottawa, Science Series, 4, 1 – 32.
Morton, F. I. 1969. Potential evaporation as a manifestation of regional evaporation. *Water Resources Research*, 5(6), 1244 – 1255.
Morton, F. I. 1971. Catchment evaporation and potential evaporation further development of a climatological relationship. *Journal of Hydrology*, 12, 81 – 99.
Morton, F. I. 1975. Estimating evaporation and transpiration from climatological observations. *Journal of Applied Meteorology*, 14, 488 – 497.
Morton, F. I. 1976. Climatological estimates of evapotranspiration. *Journal of Hydraulics Division – American Society of Civil Engineers*, 102(3), 275 – 291.
Morton, F. I. 1978. Estimating evapotranspiration from potential evaporation: practicality of an iconoclastic approach. *Journal of Hydrology*, 38, 1 – 32.
Morton, F. I. 1983. Operational estimates of areal evapotranspiration and their significance to the science and practice of hydrology. *Journal of Hydrology*, 66, 1 – 76.
Morton, F. I., Ricard, F. and Fogarasi, S. 1985. Operational estimates of areal evapotranspiration and lake evaporation – Program WREVAP. *Environment Canada – National Hydrology Research Institute*, 24, 1 – 15.
Mukammal, E. I. and Neumann, H. H. 1977. Application of the Priestley-Taylor evaporation model to assess the influence of soil moisture on the evaporation from a large weighing lysimeter and class A pan. *Boundary Layer Meteorology*, 12, 243 – 256.
Nakagawa, S. 1984. Study on evapotranspiration from pasture. Environmental Resource Centre Papers University of Tsukuba, No. 4.

Nash, J. E. 1989. Potential evaporation and the complementary relationship. *Journal of Hydrology*, 111, 1 – 7.

Niedzialek, J. M. and Ogden, F. L. 2012. First-order catchment mass balance during the wet season in the Panama Canal Watershed. *Journal of Hydrology*, 462 – 463, 77 – 86.

Ohmura, A. 1982. Objective criteria for rejecting data for Bowen ratio flux calculations. *Journal of Applied Meteorology*, 21, 595 – 598.

Oke, T. R. 1987. Boundary Layer Climates. 2nd eds. Methuen, London: Great Britain.

Oke, T. R., Spronken-Smith, R. A., Jáuregui, E. and Grimmond, C. S. B. 1999. The energy balance of central Mexico City during the dry season. *Atmospheric Environment*, 33, 3919 – 3930.

Parlange, M. B. and Katul, G. G. 1992. An advection-aridity evaporation model. *Water Resources Research*, 28(1), 127 – 132.

Pearlmutter, D., Berliner, P. and Shaviv, E. 2005. Evaluation of urban energy fluxes using an open-air scale model. *Journal of Applied Meteorology*, 44, 532 – 545.

Pearlmutter, D., Krüger, E. L. and Berliner, P. 2009. The role of evaporation in the energy balance of an open-air scaled urban surface. *International Journal of Climatology*, 29, 911 – 920.

Peck, A. M., Bowering, E. A., and Simonovic, S. P. 2013. A flood risk assessment to municipal infrastructure due to changing climate part II: case study. *Urban Water Journal*, 1 – 13.

Peck, A. M., Bowering, E. A., and Simonovic, S. P. 2013. A flood risk assessment to municipal infrastructure due to changing climate part I: methodology. *Urban Water Journal*, 1 – 12.

Penman, H. L. 1948. Natural evaporation from open water, bare soil and grass. *Proceedings of the Royal Society of London – Series A, Mathematical and Physical Sciences*, 193(1032), 120 – 145.

Pettijohn, J. C. and Salvucci, G. D. 2006. Impact of an unstressed canopy conductance on the Bouchet-Morton complementary relationship. *Water Resources Research*, 42(9), 1 – 9.

Philipona, R. 2013. Greenhouse warming and solar brightening in and around the Alps. *International Journal of Climatology*, 33, 1530 – 1537.

Price, R. K. and Vojinovic, Z. 2008. Urban flood disaster management. *Urban water journal*, 5 (3), 259 – 276.

Priestley, C. H. B., and Taylor, R. J. 1972. On the assessment of surface heat flux and evaporation using large-scale parameters. *American Meteorological Society Monthly Weather Review*, 100(2), 81 – 92.

Ramirez, J. A., Hobbins, M, T. and Brown, T. C. 2005. Observational evidence of the complementary relationship in regional evaporation lends strong support for Bouchet's hypothesis. *Geophysical Research Letters*, 32,

Rutter, A. J., Kershaw, K. A., Robins, P. C. and Morton, A. J. 1971. A predictive model of rainfall interception in forests, 1. Derivation of the model from observations in a plantation of Corsican Pine. *Agricultural Meteorology*, 9, 367 – 384.

Seguin, B. 1975. Influence de l'evapotranspiration regionale sur la mesure locale d'evapotranspiration potentielle. *Agricultural Meteorology*, 15, 355 – 370.
Sinclair, T. R., Allen, Jr., L. H. and Lemon, E. R. 1975. An analysis of errors in the calculation of energy flux densities above vegetation by a Bowen-ratio profile method. *Boundary-Layer Meteorology*, 8, 129 – 139.
Slayter, R. O. and McIlroy, I. C. 1961. *Practical Microclimatology*. Melbourne: Australia, CSIRO.
Solomon, S. 1966. Potential evaporation and river basin evaporation. *Journal of Hydraulic Engineering*, 92, 219 – 225.
Solomon, S. 1967. Relationship between precipitation, evaporation and runoff in tropical-equatorial regions. *Water Resources Research*, 3(1), 163 – 173.
Szilagyi, J. 2001a. On Bouchet's complementary hypothesis. *Journal of Hydrology*, 246, 155 – 158.
Szilagyi, J. 2001b. Modeled areal evaporation trends over the conterminous United States. *Journal of Irrigation and Drainage Engineering*, 127(4), 196 – 200.
Szilagyi, J. 2007. On the inherent asymmetric nature of the complementary relationship of evaporation. *Geophysical Research Letters*, 34, 1 – 6.
Szilagyi, J. and Jozsa, J. 2008. New findings about the complementary relationship-based evaporation estimation methods. *Journal of Hydrology*, 354, 171 – 186.
Szilagyi, J. and Jozsa, J. 2009. Analytical solution of the coupled 2-D turbulent heat and vapour transport equations and the complementary relationship of evaporation. *Journal of Hydrology*, 372, 61 – 67.
Szilagyi, J., Katul, G. G. and Parlange, M. B. 2001. Evapotranspiration intensifies over the conterminous United States. *Journal of Water Resources Planning and Management*, 127(6), 354 – 362.
Todd, R. W., Evett, S. R., and Howell, T. A. 2000. The Bowen ratio-energy balance method for estimating latent heat flux of irrigated alfalfa evaluated in a semi-arid, advective environment. *Agricultural and Forest Meteorology*, 103, 335 – 348.
Trout, K. and Ross, M. 2006. Estimating evapotranspiration in urban environments. *Urban Groundwater Management and Sustainability*, 74, 157 – 168.
Wang, S.-H., Huang, S.-L. and Budd, W. W. 2012. Resilience analysis of the interaction of between typhoons and land use change. *Landscape and Urban Planning*, 106, 303 – 315.
Wessel, D. A. and Rouse, W. R. 1994. Modelling evaporation from a wetland tundra. *Boundary Layer Meteorology*, 68, 109 – 130.
Whitfield, P. H. 2012. Floods in future climates: A review. *Journal of Flood Risk Management*, 5[4], 336 – 365.
Ye, X., Liu, J. and Zhang, Q. 2011. A modeling study of hydrological response to landuse changes based on hypothetical scenarios for the Poyang lake catchment. *2011 International Symposium on Water Resource and Environmental Protection*, 1, 550 – 553.